Monitoring and modeling nearshore morphodynamic behaviour on storm time scales

Master of Science thesis report

Master of Science student:
S.T.J. van Son

Monitoring and modeling nearshore morphodynamic behaviour on storm time scales

Master of Science thesis author
S.T.J. van Son

Graduation committee	**Section**
Prof.dr.ir. M.J.F. Stive	Hydraulic Engineering, TU Delft
Prof.dr.ir. W.S.J. Uijttewaal	Environmental fluid mechanics, TU Delft
Dr. A.J.F. van der Spek	Hydraulic Engineering, TU Delft, Deltares
Ir. D.J.R. Walstra	Hydraulic Engineering, TU Delft, Deltares
Dr. R.C. Lindenbergh	Optical and laser remote sensing, TU Delft
Ir. S. de Vries	Hydraulic Engineering, TU Delft
Ir. M.A. de Schipper	Hydraulic Engineering, TU Delft

Date
May 2009

Cover picture source: www.kustfoto.nl

Preface

This report presents the Master thesis work performed from September 2008 until May 2009. The thesis is part of the Master of Science program at the Faculty of Civil Engineering and Geosciences, Delft University of Technology.
The report describes the monitoring and modeling of the morphodynamic behaviour of the shoreface near Ter Heijde on a time scale of storms.

Cooperation with the Geomatics Synthesis Project team proved very valuable for a rapid start of the thesis work. This led to an opportunity to present my first results on the symposium called "Novel Techniques for Coastal Monitoring" on the Aerospace Engineering Faculty.

Between September and January several bathymetric surveys have been carried out on the Dutch North Sea near Ter Heijde together with Sierd de Vries and Matthieu de Schipper. Not only from inside the TUDelft, but also outside the university several parties showed interest in this new monitoring technique. This has led to the idea of using the Jetski for more commercial research.

Last but not least I would like to thank my graduation committee, office mates, friends and family for their support.

Bas van Son

Delft, May 2009

Table of contents

Summary

The project objective
The main objective of this study is to describe the dynamic morphological behaviour of the shoreface of the straight sandy Holland coast near Ter Heijde on the time scale of storms. A Jetski is used as a platform for bathymetric surveys and computations are made with the numerical model Delft3D.

The physical system of a straight sandy coast such as the Holland coast should be understood at a high level such that existing or future coastal problems (i.e. erosion and sedimentation) can be assessed properly and that mitigating measures (e.g. nourishments) can be evaluated on their effectiveness.

Coastal monitoring
An area of 1200m by 800m of the shoreface near Ter Heijde in the Netherlands has been monitored using a Jetski equipped with instruments for performing bathymetric surveys. A Single Beam Echo Sounder (SBES) for depth measurements and accurate GPS for positioning (RTK-GPS).
The local morphology as a result of the field surveys shows a longshore subtidal bar that is aligned parallel to the shore. The position of the bar is monitored on several moments in time, within weeks before and after storm events between September and December 2008. This bar is situated between 500m and 600m seaward of the coastline and its crest lies around –4m NAP. On the Southside of the project area the bar is somewhat steeper and higher than on the North side of the area.
The bar has migrated approximately 10m onshore during a calm weather period (mid September until the end of October 2008). In the stormy month November the bar migrated between 25 and 30m offshore.

An assessment of the quality of the Jetski as a platform for bathymetric surveys has been performed. It turns out that the Jetski is applicable for bathymetric surveys at sea. The vertical (depth) accuracy is of order 0.1m and the horizontal position accuracy is of order 0.5m. The vertical accuracy could be improved to about half of this value by means of the following actions:

- Install a motion sensor and filter outliers from the dataset;
- Measure the speed of sound in water accurately;
- Improve the quality of the Single Beam Echo Sounder;
- Only sail tracks in landward direction;
- Only include depth measurements while sailing in a straight line.

The horizontal accuracy can also be reduced considerably by installing the motion sensor. Besides, it is recommended to compare the Jetski measurement with other survey platforms for extra reference data.

Coastal modeling
The numerical area model Delft3D is set up to simulate storm events and to reproduce the morphological changes as monitored in the field using wave conditions from the offshore Europlatform buoy. After the simulation of a storm on the North Sea, the model results show offshore bar migration and some flattening of the bar crest. This flattening becomes more pronounced for model runs of more than a few days of storm.

Analysis of the wave propagation inside the survey area shows that the breaker function (dissipation of wave energy) of the subtidal sandbar greatly depends on the water level during storm. The higher the water level is, the lower the dissipation of wave energy above the bar.
Results about currents show that storms from the Southwest strongly enhance the flood currents to the North, but reduce the ebb currents to the South. On the other hand storms from the Northwest enhance the ebb currents to the South. Longshore and cross-shore flow velocities are higher in the South side of the project area, where the bar is higher than in the North side. The same holds for the sediment transport: the higher the bar, the more sediment is transported in cross-shore direction during a storm event.
The morphological behaviour of the foreshore is highly changeable, but indicates clearly where erosion and where sedimentation has taken place. During a storm, erosion is mainly observed around the groins whereas sedimentation takes place further seawards.

Synthesis
Existing theory and observations from literature are compared with field measurements and numerical model results.
Theory and observations described in literature as well as the Ter Heijde field observations show that the bar migrates onshore during fair weather conditions, whereas it moves offshore during storm conditions. The main onshore driving component is wave asymmetry whereas the main offshore driving component is undertow.
The sedimentation and erosion patterns from a simulated storm look very similar to the resulting patterns from the field measurements. This applies for the shoreface as well as for the foreshore behaviour.
Above the monitored and the modeled bar the most sediment transport takes place on the Southside of the survey area. This is where the subtidal bar as well as flow velocities are higher than on the North side.
One dissimilarity, however, is that the degree of flattening of the bar crest during storm is stronger than it should be considering the observations in the field.

Bar-migration monitored on a yearly interval by JARKUS (Jaarlijkse Kustmetingen) could be of the same order as changes monitored on a storm time scale. These annual trends can be analyzed relative to monthly trends using the Jetski measurements on a storm time scale.
It is therefore recommended to appoint some representative locations along the Dutch coast and monitor the inter-annual morphological trends on a storm time scale (e.g. monthly).

List of abbreviations

BKL	Basal Coastline
ETRS89	European Terrestrial Reference System 1989
GPS	Global Positioning System
IMU	Inertial Measurement Unit
JARKUS	JAarlijkse KUStmetingen
NAP	Normaal Amsterdams Peil
ppm	Parts per million
ppt	Parts per thousand
Q3D	Quasi 3-Dimensional
RD	Rijksdriehoeksmeting
RSP	RijksStrandPalen
RTK	Real Time Kinematic
SBES	Single Beam Echo Sounder
UTC	Coordinated Universal Time
WGS84	World Geodetic System 1984

List of symbols

Roman symbols

Symbol	*Designation*
a	Van Rijn reference height [m]
c	Wave celerity [m/s]
$c_{Mackenzie}$	Speed of sound in water [m/s]
d	Water depth [m]
D_{50}	Median sediment diameter [m]
d_{GPS}	Depth of sea floor below GPS antenna [m]
d_{NAP}	Depth of sea floor below chart datum [m]
d_{SBES}	Depth of sea floor below SBES transducer [m]
H_s	Significant wave height [m]
H_m	Mean wave height [m]
h_{GPS}	Height of GPS antenna above the reference ellipsoid [m]
h_{NAP}	Height of chart datum above reference ellipsoid [m]
L	Measures of length of Jetski equipment [m]
Offset	Height difference between GPS and SBES transducer [m]
R_{xy}	Correlation function [-]
S	Salinity [ppt]
T_m	Mean wave period [s]
T_p	Peak period [s]
T	Temperature [°C]
t	Time [s]
V_{error}	Total vertical error [m]
H_{error}	Total horizontal error [m]
v	Sailing speed [m/s]
$x_{seafloor}$	Horizontal x-coordinate of the seafloor in RD [m]
$y_{seafloor}$	Horizontal y-coordinate of the seafloor in RD [m]
$z_{seafloor}$	Vertical z-coordinate of the seafloor in NAP [m]
z_{GPS}	Height of GPS antenna above chart datum [m]

Greek symbols

Symbol	*Designation*
α	Shoreline angle [°North]
Δd	Vertical error contribution [m]
Δt	Computational time step [s]
Δxy	Horizontal error contribution [m]
θ	Beam width of echo sounder [°]
ρ	Water density [kg/m^3]
σ	Standard deviation [m]
τ	Latency / time offset [s]
φ	Roll / pitch angle [°]

1 Introduction

The coastal environment is probably the most dynamic of any ocean domain. The endless sequence of storms and calms causes beach changes that vary from severe erosion with expensive property loss to the accretion of acres of new beachfront. With increasing population pressure on the coasts and themes like 'building with nature' being very relevant within the field of civil engineering, the development of a fundamental understanding of the dynamic behaviour of the coastal system is imperative.

The physical system of a straight sandy coast such as the Holland coast should be understood at a high level such that existing or future coastal problems (i.e. erosion and sedimentation) can be assessed properly and that mitigating measures (e.g. nourishments) can be evaluated on their effectiveness.

1.1 Background

Rijkswaterstaat performs surveys of the cross-shore bathymetry: once per year and with a mutual distance of 250m (JARKUS, explained in appendix G). These intervals however are longer in time and larger in space than many morphological processes. Small-scale characteristics of the shoreface dynamics such as storm impact on a subtidal bar cannot be derived from these measurements. Performing more detailed surveys just before and after storm events is necessary to monitor the rapidly changing morphology.
In this study, data about small scale morphological characteristics was obtained using a Jetski as a survey platform. Bathymetric surveys were carried out on the shoreface of the North Sea near Ter Heijde. This could be achieved due to the flexible availability and the ability to survey within the surf zone.

An earlier experiment on the short-term behaviour of the Dutch coastal system is the COAST3D-Egmond project [van Rijn et al., 2002]. Bathymetric changes and processes like wave heights and flow velocities within the project area were monitored on site for several weeks. This experiment produced valuable datasets and knowledge about the dynamics of the coastal zone near Egmond.
In this study a different location (Ter Heijde, more South on the Holland coast) is monitored by performing bathymetric field surveys. Wave heights and flow velocities were obtained by Rijkswaterstaat or by means of model computations. A second difference between Ter Heijde and Egmond is that in Ter Heijde only one subtidal shore-parallel bar is present whereas at Egmond there are two subtidal shore-parallel bars.

1.2 Relevance

In 1990 a new national coastal policy was adopted aiming both at safety against flooding and at sustainable preservation of the values of dunes and beaches. In order to achieve this, the coastline must be maintained within certain margins. This so-called 'Dynamic Preservation' policy intends to maintain the seaward boundary of the Netherlands at its 1990 position and to preserve natural dynamics of the coastal zone as much as possible. The coastal state indicator is called the Basal Coast Line (BKL). It represents the desired state that is used for the actual management of the coastline and has been defined as the average position of the coastline in 1990.

The main method applied to counteract structural erosion is sand nourishment in the coastal zone. Beach nourishments as well as shoreface nourishments have been performed for 35 years, more extensively since 1990. The effect of beach nourishments is limited, and has a rather short lifetime of about 1 to 2 years [WL|Delft Hydraulics, 2006]. Nowadays, nourishment of sand in deeper water is a promising method to counteract structural erosion [Van Rijn et al., 2002].

1.3 Research objective

The main objective of this study is to describe the dynamic morphological behaviour of the shoreface of the straight sandy Holland coast near Ter Heijde on the time scale of storms using a Jetski as a survey platform.

Sub-objectives derived from this main aim are as follows:

- Assess the quality and applicability of the TUDelft Jetski as a platform for bathymetric surveys in the coastal zone of the North Sea.
- Assess the two and three-dimensional morphological behaviour of the nearshore bar system in relation to the characteristics of the incoming wave and flow field.
- Test whether the numerical area model Delft3D can predict the evolution of the seabed topography in the wave-current field as it is monitored in the field.
- Describe the underlying processes (e.g. wave and flow field) that drive the morphological changes as measured in the field and computed with the model.

1.4 Methodology

For the achievement of the overall objectives the following route has been followed:

- Analyze existing theory and observation on short-term morphodynamic processes in the coastal zone.
- Perform process research by repeatedly executing bathymetric surveys in the field.
- Analyze the obtained field data from the surveys and interpret the differences in bottom topography.
- Perform a numerical modeling study using Delft3D and assess its ability to reproduce the morphological changes as observed in the field. On the other hand use the model to quantify and qualify processes that have not been measured in the field (i.e. wave heights and flow velocities).
- Relate existing theory and observations from literature to the field surveys and to the numerical model results in a synthesis.

1.5 Reader

The layout of the report is as follows. First, in chapter 2, a description is given of the characteristics of the Dutch coastal system. In chapter 3 the field surveys are treated, data is processed, and the quality of the Jetski as a platform for bathymetric surveying is assessed. Finally the change of bottom topography between surveys is discussed. The numerical area model Delft3D is set up in chapter 4 to quantify and qualify the processes that are the basis of the measured coastal changes. Besides, an attempt is made to reproduce the monitored changes as observed in the field. Chapter 5 is the synthesis and brings together results from literature, from field measurements and from model computations; a comparison is made between them. Finally conclusions are drawn and recommendations are given in chapter 6.

2 Coastal characteristics

2.1 Introduction

The Holland coast is situated in the central part of the Dutch coast between Den Helder in the North and Hoek van Holland in the South. The coastal stretch of the Holland coast is about 120km long and mainly consists of sandy beaches and multiple barred nearshore zones [TAW, 1995]. The project location Ter Heijde is located on this Holland coast, in between the harbor moles of Hoek van Holland and Scheveningen (figure 2-1a). In figure 2-1b the project area (later called: survey area) is shown within an aerial photo together with three JARKUS transects crossing the area.

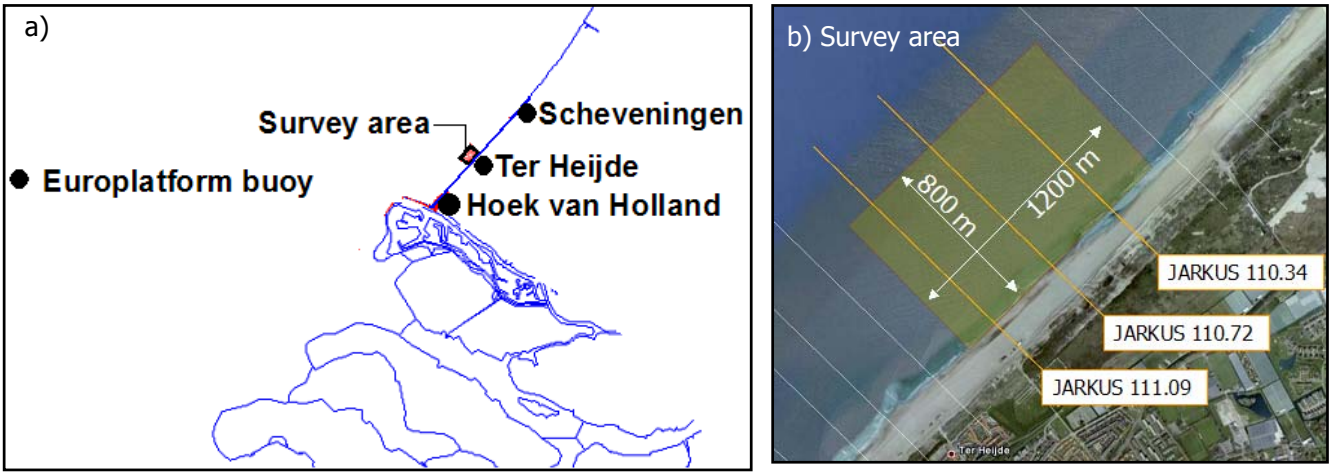

Figure 2-1: Project location a) Survey area along Holland coast b) Survey area with JARKUS transects

A description of the project area along the Dutch coast and its hydrodynamic and morphodynamic characteristics is given in this chapter. Characteristics are defined for the project area itself and for the environment influencing the area. The characteristics have different impact on different scales; therefore the scales dealt with in this report are defined. Not only nature influences the processes that are present in the coastal area. Also human interventions have their impact on the coastal system. Recent sand nourishments in the project area and their evolution in the past few years are shown. For the sake of a clear terminology in this report figure 2-2 is given. This figure shows a schematic overview of the coastal zone together with corresponding coastal engineering terms.

2.2 The project area

Geomorphology
At Ter Heijde, the general coastline orientation is 49° North (topographic). The local morphology shows a longshore subtidal bar that is aligned parallel to the shore. JARKUS data shows that at least 1km North and South of Ter Heijde the same subtidal bar is observed.

Sand nourishments
In figure 2-3 one of the JARKUS transects that lies within the survey area (JARKUS 110.34) is plotted for year 2005 until 2008. Table 2-1 shows where sand nourishments have recently been carried out. The figure clearly shows one subtidal bar in 2005 (blue line in figure 2-3). One year later, the 2005-shoreface nourishment appears on the seaside of the bar (green line in figure 2-3). In the years after, this nourishment fuses together with the bar and in 2008 one single bar is observed.

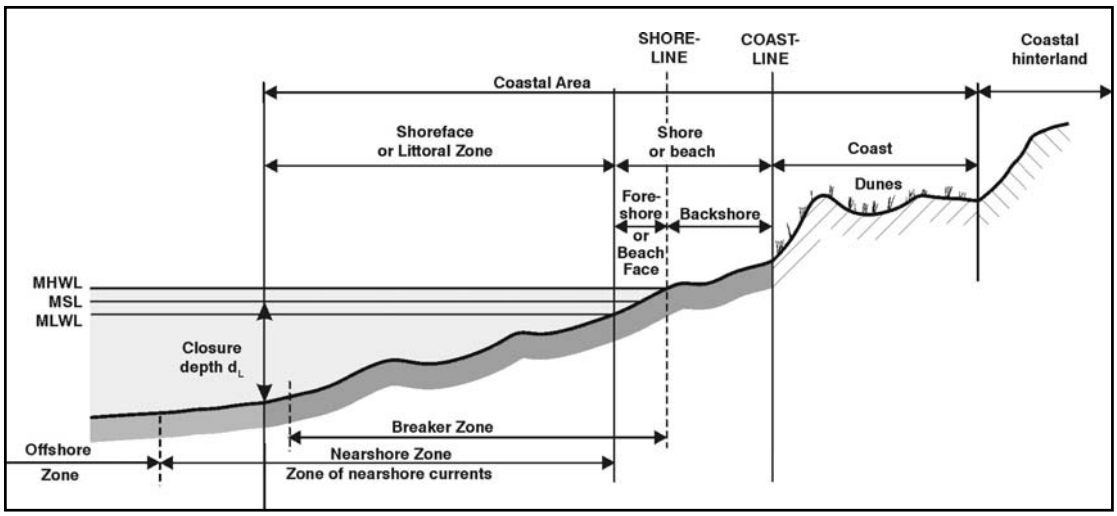

Figure 2-2: Definition of coastal terms (source: CERC, 1984)

Table 2-1: Nourishments at or near Ter Heijde from 2000 until 2008 [Source: Rijkswaterstaat]

Year	Transect start	Transect end	Transect length	Nourishment type
2001	107.40	112.50	5100	Shoreface
2001	108.00	112.00	4000	Beach
2003	107.73	113.19	5460	Beach
2004	107.73	113.19	5460	Beach
2005	108.00	113.00	5000	Shoreface

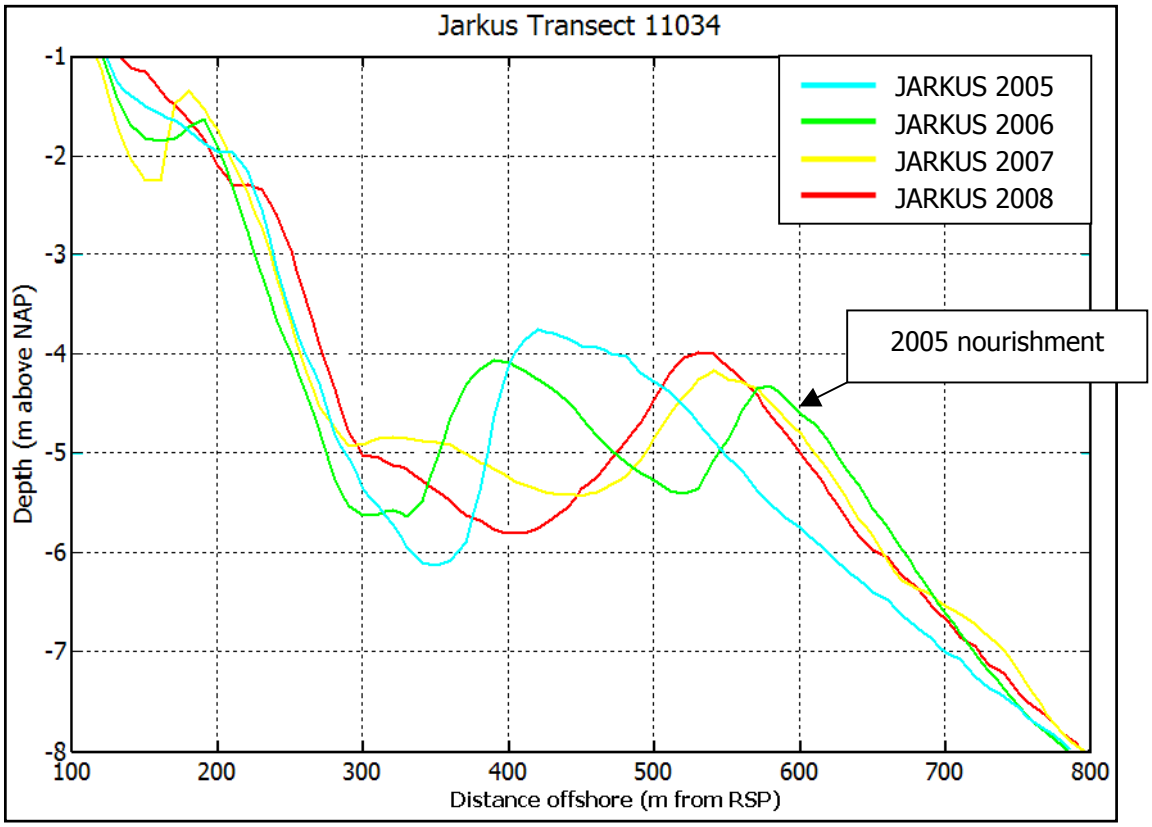

Figure 2-3: JARKUS transect 110.34 from 2005 until 2008

Coastal classification

Sandy coasts can be classified into three types [van Rijn et al., 2002]:

- 2-dimensional, uniform in alongshore direction;
- 2.5-dimensional, as 2D, but with natural non-uniformities such as rip-channels and crescentic bars;
- 3-dimensional, with irregular features such as headlands and tidal inlets.

The Ter Heijde coast can be classified as a 2.5-dimensional coast. The outer bar shows non-uniformities since its crest height is not constant in longshore direction. The nearshore area is highly non-uniform due to the presence of the groins.

Grain size

The median sand grain size (D_{50}) in the area is around 300µm. This value is derived from measurements performed by Medusa[1] on the shoreface near Ter Heijde on 16th September 2008.

2.3 Temporal and spatial scales

The shape of a coastal profile is the result of cyclic behaviour. On different time scales different behaviour can be considered. In coastal engineering practice the following spatial scales are considered [Stive et al., 2006]:

- Micro-scale or process-scale level: concerns the constituent processes of waves, currents and sediment transport and the smallest-scale morphological phenomena; ripple and dune formation.
- Meso-scale or dynamic-scale level: concerns the principal morphodynamic behaviour, due to interaction of the constituent processes and the bed topography. The principal forcings are seasonal and inter-annual variations in the tide, weather conditions and human interactions.
- Macro-scale or trend-scale level: slow trends at scales much larger than those of the primary morphodynamic behaviour. The principal forcings are the longer-term cycles in the tide, decadal scale variations in the wave climate, consistently repeated human interference activities.
- Mega-scale level: the level at which the principal elements of the entire system interact. The principal forcings are mean sea level rise, climatic change, long-term tidal variation and subsidence.

Mutual interactions exist between different temporal and spatial scales [Stive et al., 2006]. Since morphological behaviour is being monitored on the short-time scale of storms, this thesis deals with the micro- and meso-scale hydrodynamic and morphodynamic processes.

[1] During the Geomatics Synthesis Project mid-September 2008 the company Medusa used a radioactive probe to classify the grain size off the Ter Heijde coast.

2.4 Coastal processes

The Holland coast only forms part of the Dutch coastline. Some specific hydrodynamic and morphodynamic features are applicable to the coastal zone in which the survey area is situated. These features are the domain boundaries that are responsible for changes in the bottom topography (figure 2-4). A description of the relevant processes is therefore given in this section.

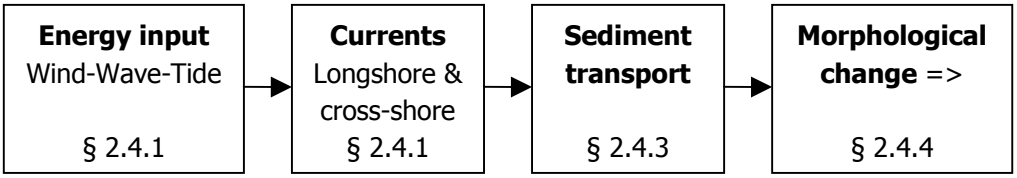

Figure 2-4: Hydrodynamic and morphodynamic processes

More detail about the coastal morphology and processes concerning waves and currents is given in appendix A. The processes that are discussed are refraction, shoaling, wave breaking, radiation stress, wave set-up and wave set-down, longshore current, cross-shore current and sediment transport.

2.4.1 Energy input

Wind and waves

The Holland coast is a mixed-energy coast, according to the classification scheme of Davis and Hayes [1984]. A mixed-energy coast implies that both wind waves and tides act on the sandy sediments and induce the morphological responses. Most of the winds along the Holland coast come from the North Sea. The prevailing wind direction is Southwest (23%), followed by West (16%), East (13%) and Northwest (12%) [Stolk, 1989]. The storm winds causing the largest wind set-up along the coast are coming from the Northwest [Sistermans, 2007].

The governing wind climate causes a yearly mean wave height (H_m) of about 1.2m and a yearly mean period (T_m) of about 5s. Wijnberg [1995] published Rijkswaterstaat-data of the wave climate from different stations off the Holland coast for different wave classes. Waves mainly approach the coast from Southwesterly and North-Northwesterly directions.

During fair-weather conditions (H_m<1m) waves approach the coast most often from Northwesterly directions. During conditions with H_m between 1.5 and 3.5m, waves approach the coast most often from Southwesterly directions. The largest storm waves, with H_m>4.5m, are incident from the West to the Northwest. The seasonal variation in the storminess of the wind climate is clearly reflected in the wave climate. In the stormy winter months (November-January) the monthly mean wave height is about 1.7m, while in the summer months (April-August) the mean monthly wave height is just about 1m.

Magnitude, duration and frequency of storms are interesting features concerning the monitoring of morphological changes on the time scale of storms. Storm statistics on the North Sea were published by Augustijn et al. [1990] and [1996] over a total time span of 42 years (1964-1996). A storm is defined as a period of wind speeds above 20m/s. The average total storm duration is 500 hrs/year, 90 hrs/year during summer months (April – August), 410 hours during winter months (September – March). The variation in the amount of storms is large: 13 storms in 1989, 48 storms in 1970. On average one storm occurs every month in summer months and five storms during winter months, the average frequency of storms is 35 per year.

Wave induced currents
Waves that break when entering shallow water transport momentum (the phenomenon called radiation stress, appendix A). For waves approaching perpendicular to the shore this leads to a slight decrease of the mean water level outside the breaker zone; inside the breaker zone it leads to a rise in the mean water level in shoreward direction (wave setup). This formed gradient drives an undertow in seaward direction that compensates the mass transport in the crest of the breaker. Waves approaching the shore under an angle also transfer momentum in longshore direction and will generate longshore current (Figure 2.5).

Tidal currents
The mean semi-diurnal tidal range at Scheveningen is 1.48m (neap tide) and 1.98m (spring tide) [Waternormalen, 2008].
The tidal currents in the nearshore zone are Northward directed during flood period and Southward directed during ebb period. The semi-diurnal tidal curve is asymmetrical with a rising tide of 7 to 8 hours and a falling tide of 4 to 5 hours at the tidal station in Scheveningen (8 km North of Ter Heijde along the straight coast). Due to the tidal asymmetry the flood current has a maximum value of 0.8m/s whereas the maximum ebb currents have maximum values of about 0.7m/s (along the Holland coast). This results in residual current velocities of the order of 0.1m/s to the North [van Rijn, 1997].

2.4.2 Sediment transport

Wave motion over an erodible sand bed can stir up sediment with large near-bed concentrations, as shown by laboratory and field measurements. Mean currents such as tide-, wind- and density-driven currents carry the sediments in the direction of the main flow; this type of transport usually is termed the current-related transport. On the other hand wave-induced transport processes are related to the oscillating and mean currents generated in the wave boundary layer by high-frequency waves [Van Rijn, 1997].

2.4.3 Morphological change → bar behaviour

Bar migration
Many natural sandy coasts exhibit one or more longshore-aligned bars near shore that act as natural breakwaters. The dissipation of wave energy due to depth-limited wave breaking over these shoals reduces wave energy reaching the shore. From observations it is evident that cross-shore migration of these bars is strongly related to the attendant wave conditions [Carter and Balsillie, 1983]. Field experience over a long period of time in the coastal zone has led to the notion that storm waves cause sediment to move offshore while fair-weather waves and swell return the sediment shoreward [Van Rijn, 1998].

Cross-shore transport
Net offshore transport generally is dominant when significant wave breaking over a bar crest is observed. Net onshore transport due to wave asymmetry is generally dominant in non-breaking wave conditions outside the surf zone. The major transport components contributing to the wave-induced transport processes are given below [Van Rijn, 1997]:

Offshore:
- Net offshore-directed transport due to the generation of a net return current (undertow, figure 2-5) in the near-bed layers balancing the onshore mass flux between the crest and trough of breaking waves.

Onshore:
- Net onshore-directed transport (bed load and intermittent suspended load) due to asymmetry of the near-bed orbital velocities with relatively large onshore peak

velocities under the wave crests and relatively small offshore peak velocities under the wave troughs.

- Net onshore-directed transport due to the generation of a quasi-steady weak current (Longuet-Higgins streaming) in the wave boundary layer.

Gravity-induced transport components related to bed slopes could result in both on- and offshore transport.

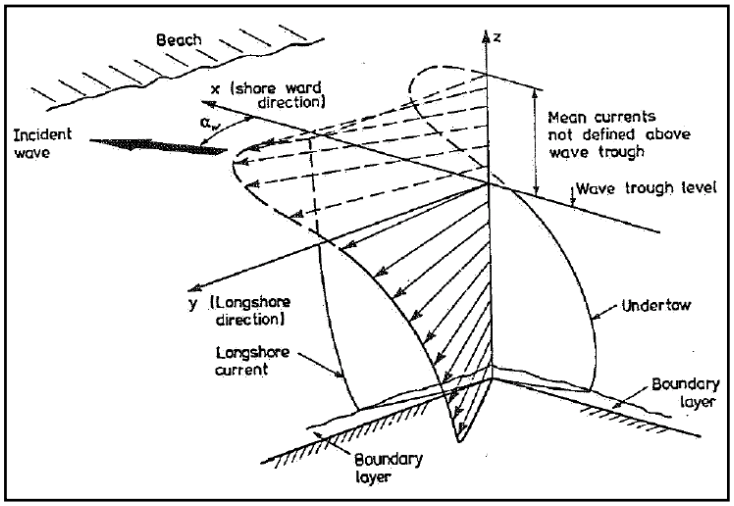

Figure 2-5: Impression of the horizontal and vertical structure of the nearshore current velocity field consisting of a longshore current and a cross-shore undertow [Van Dongeren et al., 1995].

Longshore transport

Longshore-directed transport is due to the generation of longshore wave-driven currents due to breaking waves [Van Rijn, 1997] as well as tidal currents. Waves break in the surf zone and under certain conditions over the offshore subtidal bar developing a longshore current.

Morphological behaviour in the foreshore

TAW [1995] describes the effect of groins along the Dutch coast: In the foreshore of Ter Heijde there are tide driven currents and waves approach under different angles. Around low water, the currents and thus the sediment transport will be blocked due to the presence of the groins. Besides, the flow is pushed in seaward direction and seaward-directed rip currents along the groins can develop.

Around high water the groins are completely submerged. In comparison with a situation without groins the flow resistance is now increased, thereby decreasing the flow velocities.

Most important aspects of the coastal characteristics

The project area is situated on the Holland coast and contains a longshore subtidal bar that is aligned parallel to the shore. The morphological behaviour is dealt with on the micro- and meso-scale of storms. The interaction with the domain boundaries causes changes in bottom topography. An important issue is the cross-shore transport of the subtidal bar. According to existing theory and observations, storm waves cause sediment to move offshore whereas fair-weather conditions return the sediment shoreward.

3 Coastal monitoring

3.1 Introduction

The aim of the coastal monitoring process is to obtain bathymetric maps of the shoreface on different moments in time. The process describes all steps between the actual survey in the field and the resulting products that are used for morphological interpretation in the end of this chapter. In figure 3-1 the actual products are displayed in frames. Between the frames, the actions performed to create these products are given. Besides the data obtained during the monitoring campaign, also hydrodynamic and meteorological data from Rijkswaterstaat is collected.
Note: the resulting morphological changes are treated in chapter 3.7. If those are of special interest to the reader, then paragraph 3.2 to 3.6 could be skipped.

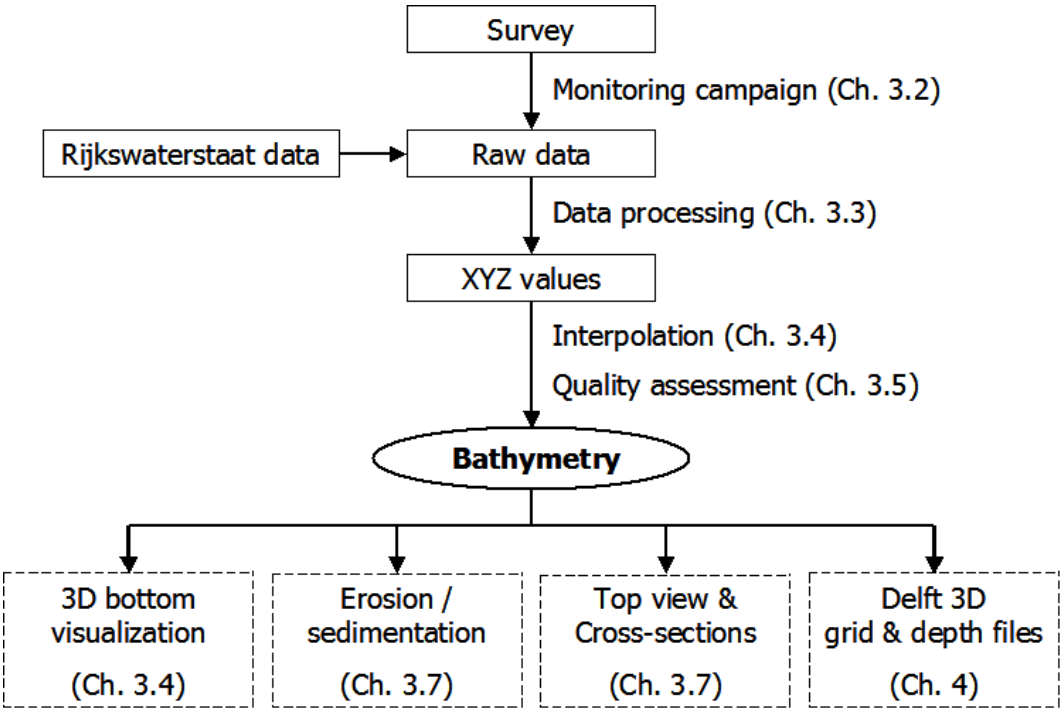

Figure 3-1: Monitoring flow diagram

3.2 Monitoring campaign

3.2.1 Time and location

The monitoring campaign has taken place from the 15th of September until the 12th of December on the shoreface near Monster-Ter Heijde. On the map in figure 3-2 the location of the 1200m x 800m survey area is indicated. Within the four-month period the environmental conditions were followed closely and surveys were performed whenever possible before and after storm periods.
Five surveys provided valuable data, the features of these surveys are given in table 3-1 and the sailed tracks are visualized in figure 3-3.

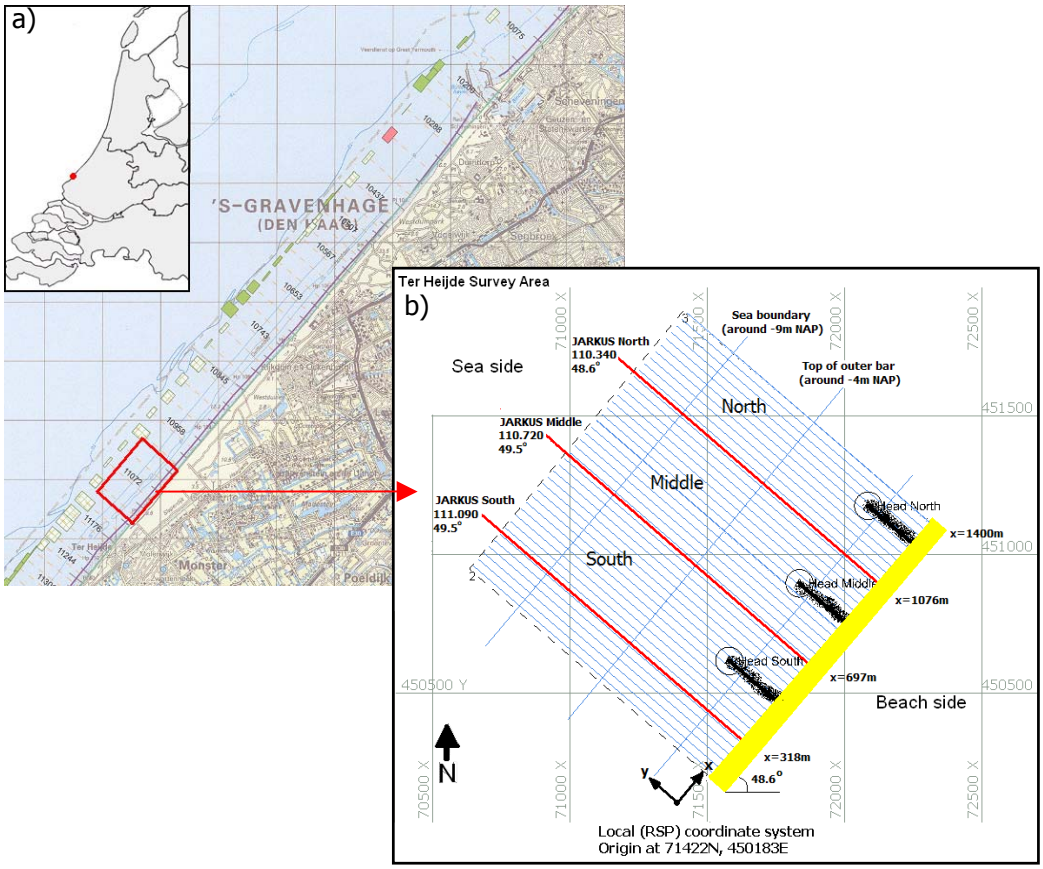

Figure 3-2:a) Map of the Netherlands and the Delfland coast b) Map of the survey area

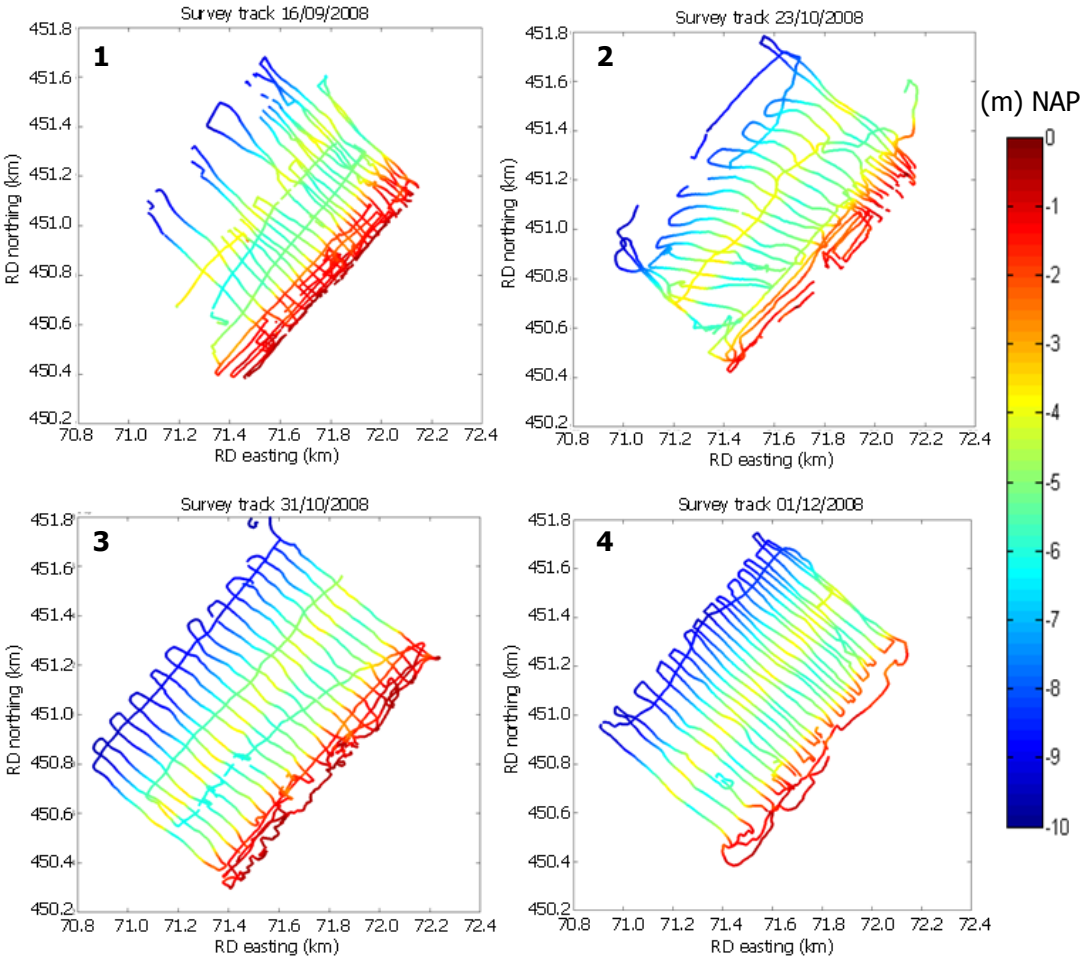

Figure 3-3: Sailed tracks during surveys on four different days

3.2.2 Survey platform

The monitoring campaign focuses on morphological changes in near shore areas on a storm time scale, therefore the survey platform needs to be able to cope with specific requirements. The survey platform used is a Yamaha VX Jetski (figure 3-4). This platform has several advantages over conventional survey vessels:

Figure 3-4: TU Delft Jetski

- The Jetski has a large power-to-weight ratio, providing great acceleration for surveying safely between breaking waves in the surf zone.
- It has the ability to sail in very shallow water (depth<1m) due to pump-drive propulsion.
- It is relatively light and can thus be launched from places that may not be accessible for other surveying platforms.
- As the crew is flexible, decisions about a survey can be taken up to hours before the real survey. This is very advantageous in situations depending on environmental conditions as well as for monitoring short-term morphological changes.

The Jetski is equipped with several survey instruments, visualized in figure 3-5. A Hydrobox Hydrographic Single Beam Echo Sounder (SBES) [2008] is mounted, as well as a Global Positioning System (GPS) receiver and a laptop, which logs all the measurements. Hydrographic software [Hypack, 2008] combines the echo soundings with GPS data. Geo-referencing of all sounding data is done using Real Time Kinematic GPS positioning (RTK-GPS). Differential corrections are received every second via a mobile Internet connection from a reference station in Hoek van Holland [LNR]. In this manner an accurate position of the GPS antenna is recorded once per second. Real time output such as position, depth and speed are provided on a display screen for the driver.

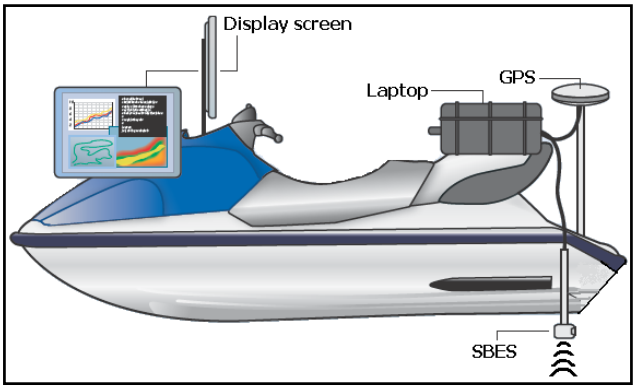

Figure 3-5: Jetski equipment (by Dean Alberga)

3.2.3 Survey conditions

The exact dates of the surveys are indicated in table 3-1 together with the environmental conditions during the surveys. The aim of the first four surveys was to monitor the morphological changes of the outer bar as well as variations in the intertidal area. The 5th survey, on the 12th of December, was of a different type. The aim of this measurement was to provide information about the reproducibility of the measurements. During this survey the JARKUS-transects were surveyed multiple times with varying sailing speeds.

Table 3-1: Survey conditions and details, wave data source: Rijkswaterstaat

Survey	**1**	**2**	**3**	**4**	**5**
Date	16/09/2008	23/10/2008	31/10/2008	01/12/2008	12/12/2008
Wave height (H_s)	0.5m	1.5m	0.8m	0.7m	1.5m
Mean wave period (T_p)	3.6s	4.2s	4.0s	4.2s	4.2s
Mean wave direction	Northeast	Southeast	North-northeast	North	South
Wind speed & direction	2 Bft, Northeast	3-4 Bft, South	2-3 Bft, East-Northeast	1-2 Bft, North	3 Bft, South
Water temperature	18°C	14°C	13°C	9°C	7°C
Salinity	28.5ppt	28.5ppt	28.5ppt	28.5ppt	28.5ppt (see appendix D)
Speed of sound	1508m/s	1496m/s	1492m/s	1478m/s	1470m/s
Mutual track distance	30m	50m	55m	45m	~0m (see footnote[2])
Surveying time	3 hrs 5 min	3 hrs 50 min	3 hrs 10 min	2 hrs 5 min	2 hrs 35 min

3.2.4 Surveying in practice

Performing measurements in the field means a great dependence on environmental conditions. Many aspects have to be taken into account for a successful survey; those concerning the environmental conditions are listed below.

- Wave height: The lower the waves the better the measurements. On a day on which the survey was cancelled while being on site, the significant wave height was 1.7m and the mean period 5.5s (as recorded at the Europlatform buoy). Generally wave heights below 1.2m are good for performing surveys.
- Wave period: Short local wind driven waves (Period<3s) influence the Jetski motion much more than longer period waves or swells (Period>7s). In the surf zone, however, surveying between breaking swells is more difficult than amongst short breaking waves. Breaking swells also generate many air bubbles in the water that may contribute to the SBES signal distortion.
- Wind direction: Especially days with offshore wind are suitable for surveys because of the short wind fetch (Fetch is the distance over which a wind acts to produce waves). Experience learns that surveys are most successful for offshore winds up to 4 Beaufort, onshore winds should remain below 3 Beaufort.
- Temperature: The coldest survey has been on the 12th of December. The water temperature was 7° C and the air temperature 2° C. Surveying on days with temperatures below 0° C would require more protective clothing than the existing equipment.

[2] During this on survey 12-12-2008 only the JARKUS transects were sailed many times, therefore the mutual track distance is 0m.

- Tidal level: The tidal level is not of any importance for shoreface measurements. For measurements within the intertidal area a period around high tide is required. A minimum water depth of 1.2m is required for proper SBES measurements. Therefore, during neap tide no good measurements can be performed within the inter-tidal area.
- Daylight hours: Daylight hours restrict the time available for a survey since sailing in the dark is forbidden and dangerous.

Other practical aspects are battery capacity, safety, planning and flexibility of the crew.

3.2.5 Wave conditions in periods between surveys

The environmental conditions between the field surveys in September – December 2008 are represented by parameters describing the offshore wave field. The offshore significant wave height, offshore wave period and offshore direction characterize the offshore wave field. The term 'offshore' means that the wave conditions are recorded in 30m water depth by the Europlatform Waverider buoy, which is situated on the North Sea, west of Hoek van Holland (see map in figure 2-1a).

The experimental period has been split up into three sub-periods A, B and C. Surveys have been performed before and after each period, as indicated by the vertical red lines in figure 3-6. In period A moderate wave conditions are observed with a short period of high-energy wave conditions. Severe storm is observed in period C with a peak storm having an offshore wave height of 5.5m.

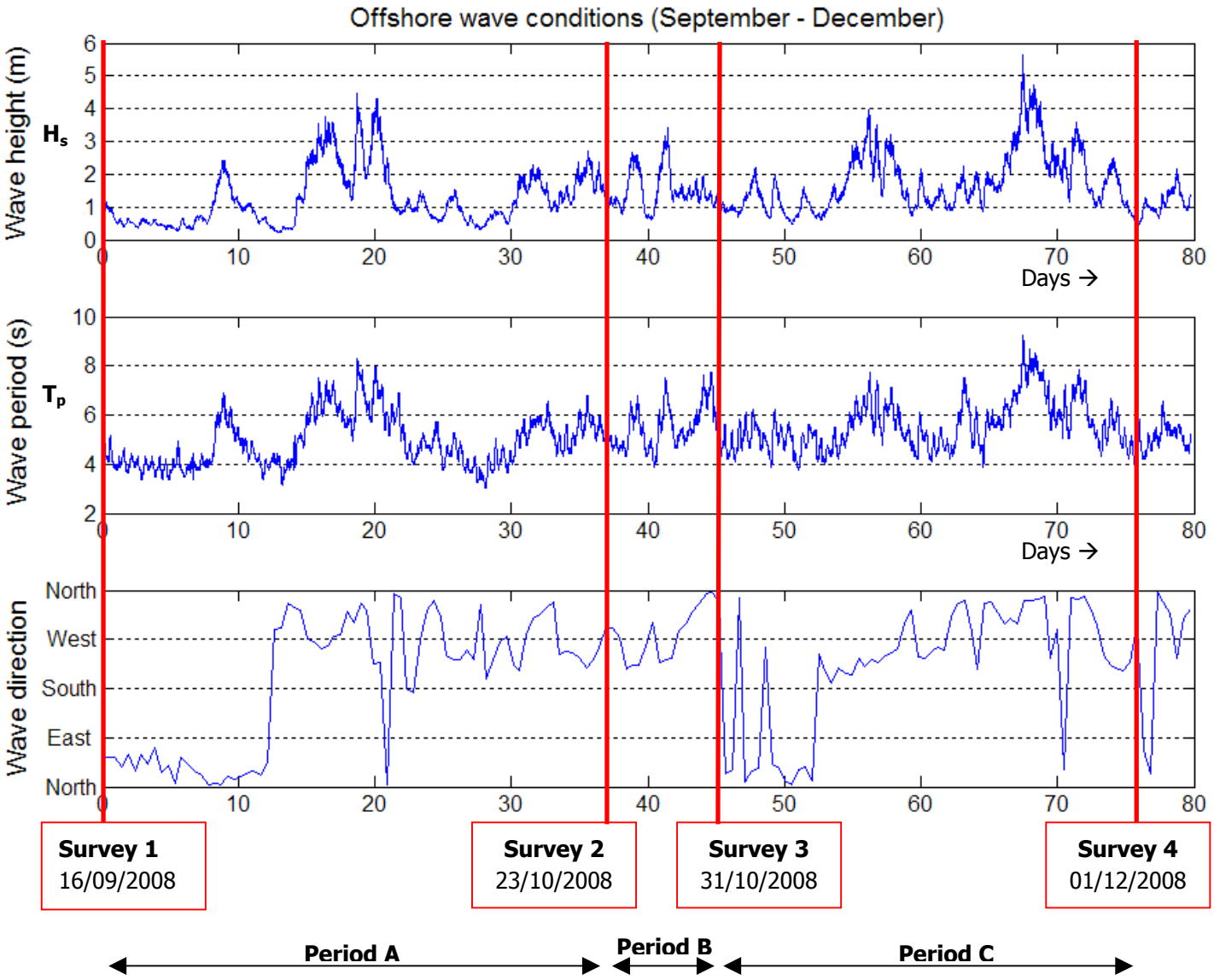

Figure 3-6: Offshore wave conditions within the experimental period. Source: Rijkswaterstaat

3.3 Data processing

The data processing consists of a number of actions that are performed to process raw data from the field surveys. The main objective of the data processing is to derive meaningful information about the bottom topography from the measurements.

3.3.1 Processing raw data

Both the GPS antenna and the SBES transducer separately log data in their specific temporal and spatial reference system. The following actions are performed to translate these raw data files into a meaningful file consisting of depth values at specific locations.

1. Transform GPS data into the RD and NAP coordinate system
2. Correct for the speed of sound in water
3. Correct for the offset between SBES transducer and GPS antenna
4. Correct for the latency between SBES time and GPS time
5. Filtering spikes in the SBES data using a moving average filter
6. Couple and match the GPS signal to the SBES signal by temporal interpolation
7. Calculate the depth for specified locations
8. Smoothen the sea floor observations using a moving average filter

All eight actions are explained and worked out in more detail in the following section. Many symbols are used; therefore figure 3-7 gives an overview of the meaning of the relevant symbols as well as four important reference levels.

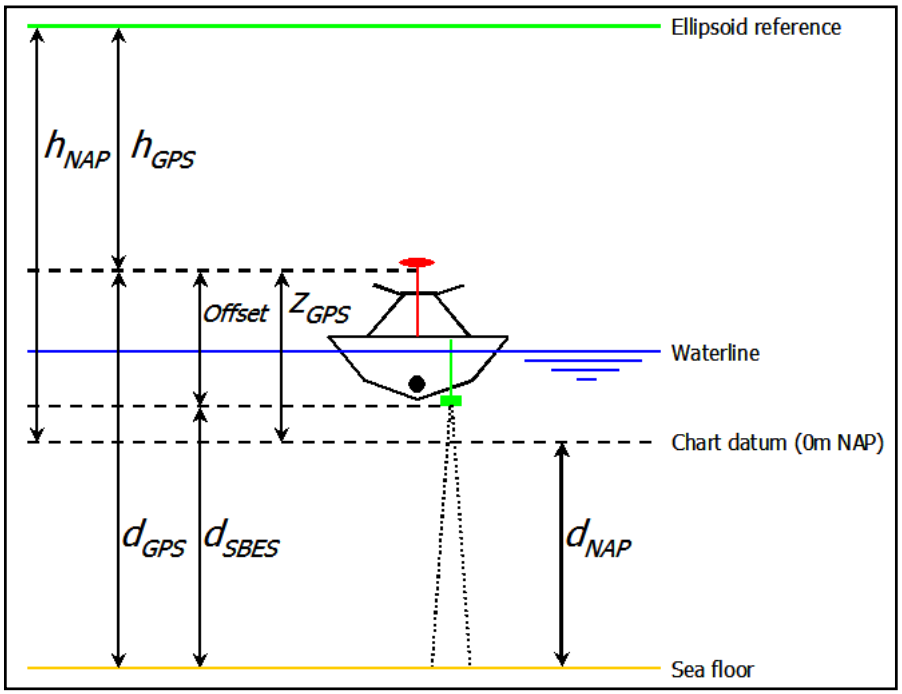

Figure 3-7: Depths, height and vertical reference levels relative to the SBES and GPS

Step 1. Coordinate system

Raw data from the GPS receiver are given in degrees latitude and longitude and meters height above the reference ellipsoid (Bessel1841) indicated as h_{GPS} in figure 3-7. The coordinate system is called ETRS89 (European Terrestrial Reference System, 1989). All horizontal coordinate components are transformed into RD (Rijksdriehoeksmeting) and the vertical component into NAP (Normaal Amsterdams Peil) [Dutch Cadastre, 2008].
Raw SBES data files on the other hand are given in meters below the transducer, indicated as d_{SBES} in figure 3-7.

Step 2. Speed of sound in water

A set of sound signals (a ping) is emitted towards the sea floor. The time it takes for a signal to travel to the sea floor and back is used to determine the depth of the point of reflection on the sea floor. Hence the speed of sound in water is a required input parameter. This parameter has not been measured in the field; instead it is calculated using the empirical relation of Mackenzie [1981]. The speed of sound depends on the depth, salinity and temperature (equation 3-1).

$$c_{Mackenzie}(d,S,T) = 1448.96 + 4.591T - 5.304\cdot10^{-2}T^2 + 2.374\cdot10^{-4}T^3 + 1.340\cdot(S-35) + 1.630\cdot10^{-2}d + 1.675\cdot10^{-7}d^2 - 1.025\cdot10^{-2}T(S-35) - 7.139\cdot10^{-13}Td^3 \quad (3\text{-}1)$$

Where d is the water depth in meter (m), S is the salinity in parts per thousand (ppt) and T is the water temperature in degrees Celsius (°C).
Two alternative ways to obtain this speed of sound in water are:

1. Perform a bar-check: at the survey location a bar could be lowered some known distance beneath the surface. The measured depth of the bar is compared to the measured SBES depth.
2. Use a probe that measures the speed of sound in water directly. A probe is very expensive and has not been available for the surveys performed.

Equation 3-2 shows the correction that is applied to each survey dataset separately. The value 1500 refers to the default value for the speed of sound in water (1500m/s) used in the SBES receiver [Hydrobox, 2008].

$$d_{SBES} = d'_{SBES}\cdot\left(\frac{c_{Mackenzie}}{1500}\right) \quad (3\text{-}2)$$

Where d'_{SBES} is the uncorrected depth in meters below the SBES transducer.

Step 3. Offset between SBES transducer and GPS antenna

On the Jetski the GPS antenna is mounted on a steel bar at the rear side. The SBES transducer is located underneath the Jetski (see figure 3-5). A correction is applied by simply adding the vertical offset to every measured echo sounder value.
The offset correction is calculated as shown in equation 3-3. Inaccuracies resulting from the application of equation 3-2 and 3-3 are further analyzed and discussed in paragraph 3.4.

$$d_{GPS} = d_{SBES} + Offset \quad (3\text{-}3)$$

Herein d_{GPS} is the depth in meters below the GPS antenna, d_{SBES} is the depth below the SBES transducer after it is corrected for the speed of sound in water. *Offset* is the height difference between the GPS and the SBES transducer, (*Offset* = 1.136m). Figure 3-7 clearly showed the interrelation between different parameters used here.

Step 4. Latency between SBES time and GPS time

Both the SBES and the GPS work in their specific time frame; the Hypack software combines both signals in the UTC (Coordinated Universal Time) time frame. By combining both signals some latency (time offset) may be introduced. Since the fluctuating heave motion caused by the waves on the North Sea is present in both the SBES signal and the GPS signal a cross-correlation can be performed to determine the magnitude of this time offset. A cross-correlation is a measure of similarity of two signals as a function of a time lag applied to one of them [Orfanidis, 1996].

In order to find the latency value, the correlation function (equation 3-4) is applied to both the GPS and the SBES signal. The highest correlation gives the most likely time latency. The resulting latency is +0.4 seconds and applies to all surveys. This time offset is corrected for by adding 0.4 seconds to the SBES time.

$$R_{x(t_0)y(t_0+\tau)} = \frac{\overline{xy}(t_0;\tau)}{\left[\overline{x^2(t_0)}\,\overline{y^2(t_0+\tau)}\right]^{0.5}} \qquad (3\text{-}4)$$

R_{xy} = Correlation function

x = GPS signal (vector)

y = SBES signal (vector)

τ = Time offset / latency

Step 5. Moving average filter

In figure 3-8 the measured SBES values are shown (see the blue asterisk, *). The signal shows high frequency fluctuations of order 0.1s in time (zoomed area in the figure 3-8 shows more detail) corresponding to 0.3m horizontal distance (for a sailing speed of 3m/s) and order 0.1m in depth. The exact nature of this fluctuation is unknown, but their cause may originate from the following factors:

- The algorithm within the SBES transducer that is used to detect the sea floor [Hydrobox, 2008];
- Interference with other electrical devices on the Jetski [Hydrobox, 2008];
- Signal distortion caused by particles or bubbles in the water column;
- Vibration of the SBES: The SBES transducer is fixed on a steel frame and moves through the water column. Turbulent water motion around the transducer may cause some fluctuations of the device;
- Jetski vibration: high frequency vibrations are caused by the engine of the Jetski and by the bouncing of the Jetski on the water surface. Figure E-1 in Appendix E shows this high frequency signal (order <0.5s) in the motion sensor signal.

Real Jetski motions (roll and pitch) are not the cause since the period of the natural movement of the Jetski on the sea waves is in the order of seconds. Bottom features are not likely to contribute to these high frequency fluctuations either. If these fluctuations were real, ripples would have a length of 30cm and a height of 10cm. When comparing the intertidal area it is visibly flat during low tide, during high tide, when the same area is monitored with the Jetski, the short period fluctuations are still present in the dataset. The spikes are most likely artifacts and not bathymetric features.

A moving average filter with a window of (0.5s) is applied to smoothen the SBES signal and remove spikes. The mathematical form of this filter is given in equation 3-5. The blue asterisk (*) in figure 3-8 show the raw SBES values, the red line shows the filtered SBES signal.

$$d_n = (d_{n-2} + d_{n-1} + d_n + d_{n+1} + d_{n+2}) / 5$$
$$d = d_{GPS} \text{ (depth below GPS antenna)} \qquad (3\text{-}5)$$

In which n is the number of a point along the sailing track. The filter is applied to the measured and calculated depth relative to the GPS antenna, meaning that d_n corresponds to d_{GPS}.

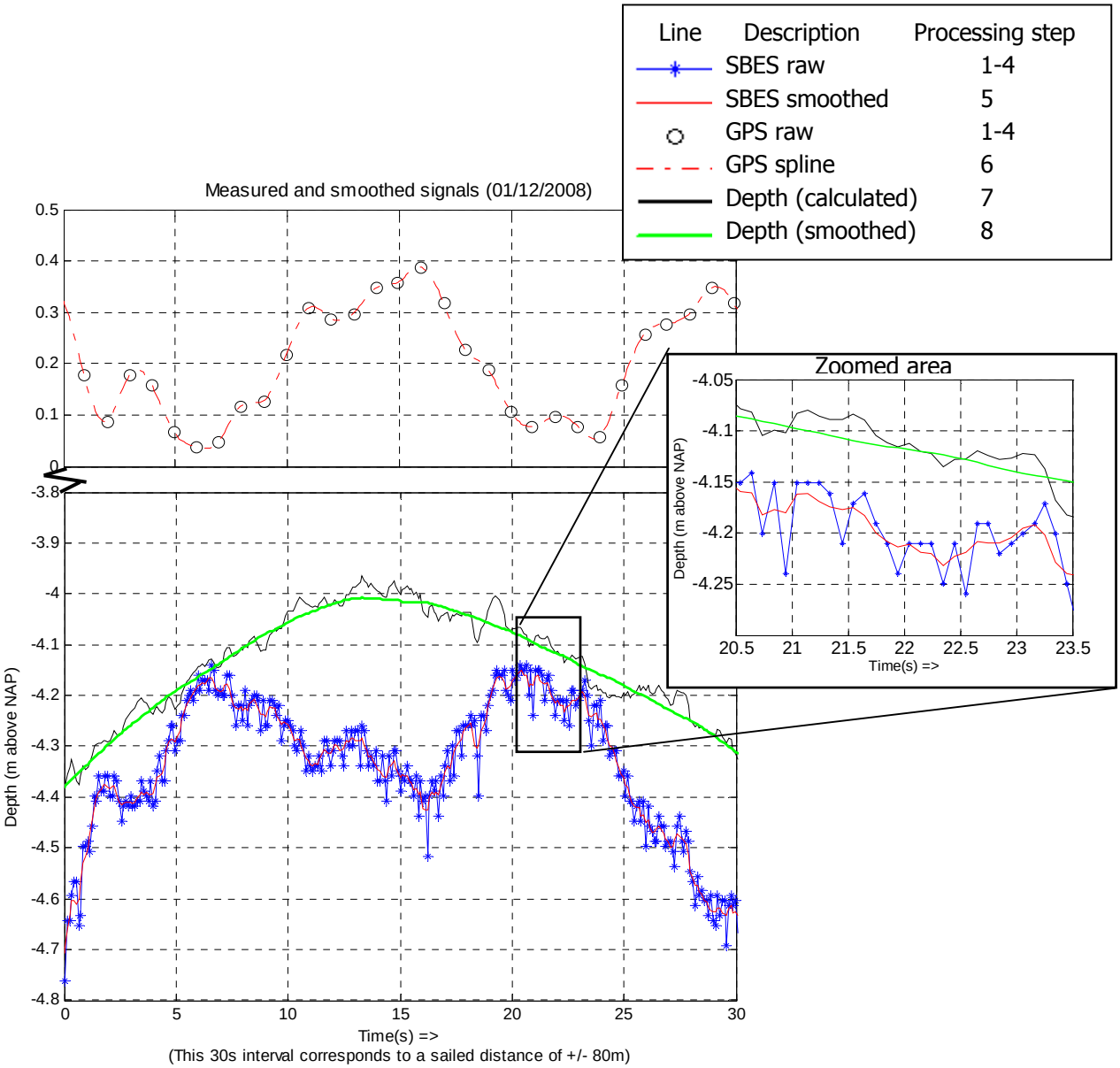

Figure 3-8: GPS, SBES and bottom signal on 01/12/2008

Step 6. Cubic spline interpolation of the GPS signal

The GPS positions are logged every second, where the SBES logs a value 10 times per second. In order to determine a position for each SBES measurement the GPS positions (marked as 'o' in figure 3-8) are interpolated to the times of the SBES measurements using cubic spline interpolation (given by the red dash-dotted line in figure 3-8).
Cubic spline interpolation is a piecewise continuous curve, passing through each of the given values [MathWorks, 2005]. In this way valuable data obtained by the SBES transducer is not left out. For a sailing speed of 3m/s this means that every 0.3m a seafloor position is logged instead of every 3m.

Step 7. Depth calculation

Applying all previous steps results in GPS locations in RD and NAP with corresponding depth values below the GPS antenna. Both signals are in the same time reference system (UTC). Every 1/10s a point on the seafloor (relative to NAP, chart datum) is calculated from a GPS location and its corresponding depth below the GPS antenna as shown in equation 3-6.

$$\begin{aligned} x_{seafloor} &= x_{GPS} \\ y_{seafloor} &= y_{GPS} \\ z_{seafloor} &= d_{NAP} = d_{GPS} - z_{GPS} \end{aligned} \tag{3-6}$$

x, y = Horizontal position (in RD), z = Vertical position (in NAP)

Step 8. Smoothen the (along track) sea floor observations using a moving average filter

The accurate GPS positioning gives good information about the heave motion of the Jetski while sailing on waves. Errors due to roll and pitch motions however are not corrected for since no motion sensor data was available. These motions cause errors in the calculated depth values (discussed in paragraph 3.4). The aim of the sea floor smoothing with a central moving average filter is to filter out the topographic artifacts due to the roll and pitch motions. For the construction of this filter some considerations must be made:
On one hand the number of points used for smoothing (smoothing window) must be a few times larger than the period of the fluctuations in the data that need to be filtered out. On the other hand the smoothing window should not be so large that important morphological features are being filtered out.
The central moving average filter is given in equation 3-7.

$$\begin{aligned} d_n = (&d_{n-33} + d_{n-30} + d_{n-27} + \ldots + d_{n-6} + d_{n-3} + d_n \\ &+ d_{n+3} + d_{n+6} + \ldots + d_{n+27} + d_{n+30} + d_{n+33}) / 23 \end{aligned} \tag{3-7}$$

In which n is the number of a point in time along the sailing track. The filter is applied to the bottom depth value as calculated in step 7, meaning that d_n corresponds to d_{NAP}.
The smoothing window contains 33 points on both sides of the calculated depth value d (along the sailed track). This corresponds to a total period of 6.6s over which the depth is averaged. For a sailing speed of 3m/s the smoothing window is approximately 20m. This smoothing window of 6.6s could be modified for different wave periods, sailing speeds and sailing direction (seawards / shoreward). This has not been done to keep calculations simple. Moreover, after the installation of a motion sensor this smoothing should not be necessary anymore.
Finally the resulting bottom used for further calculations is the green line in figure 3-8. More figures showing signals from different survey conditions can be found in appendix D.

Note that there is a 3-point step size; this is chosen to save computational time. Moreover the filtering of the SBES signal in processing step 5 already filters the two intermediate points (that smoothing window contained 5 points).

3.4 Bathymetric depth interpolation

Depth values along sailed track lines need to be transformed into a bathymetric map containing depth values on a pre-defined rectangular 3x3m grid. Therefore depth values are interpolated towards the grid points.

3.4.1 Ordinary Kriging

The interpolation method used for creating bathymetric maps of the surveyed area is Ordinary Kriging. This method can be used for interpolation to estimate values in a regular grid using irregularly spaced data.
The Kriging method has two advantages; it takes the error of the observations into account and it uses the spatial correlation derived from the data itself [Wackernagel, 2003].

Ordinary Kriging serves to estimate a value at a point in a region for which a variogram is known. To do Kriging, a variogram needs to be constructed. This is done by first calculating the average cross-shore profile, i.e. summing the height values in the longshore direction. Next, this profile is subtracted from the measured heights, resulting in a dataset of residuals. From this new dataset, dissimilarities between pairs of points are calculated. These dissimilarities are grouped by their distance, and the average of each group is computed (red dots in figure 3-9).

Once the experimental variogram is constructed, a variogram model is fitted to it (figure 3-9). The exponential model is found to give the best fit to the variogram, resulting in a nugget value of $0.02m^2$ and a range of about 100m at which the dissimilarity becomes constant. The nugget gives valuable information about the standard deviation of the measurements, which is worked out later in this chapter (in figure 3-17). A more thorough description of Ordinary Kriging can be found in appendix B.

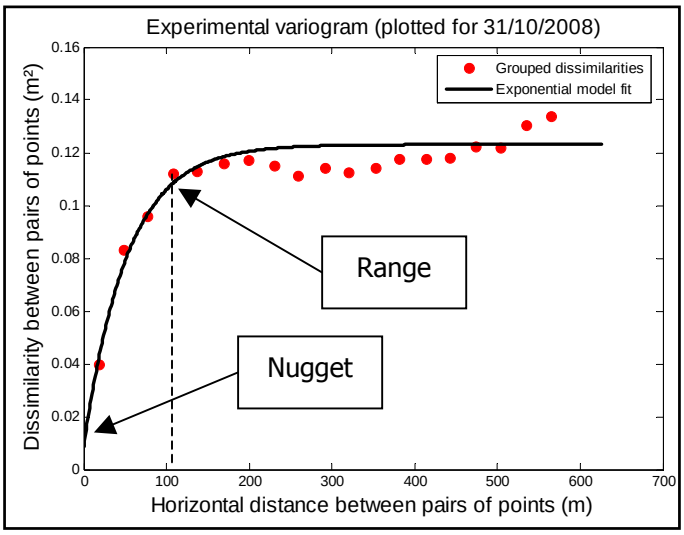

Figure 3-9: Experimental variogram

Now the variogram is known, it can be converted into a covariance function, after which the Ordinary Kriging system can be constructed. Solving this system for the nearest 500 points in a 3 by 3 meter grid results in a bathymetric map. This result will later be used as an input file in the numerical model Delft3D (chapter 4). In Delft3D the grid size is increased to a 10 by 10 meter grid, the main reason being the computational time saving. Besides Delft3D computations, the bathymetries from different surveys are compared in cross-sections and erosion-sedimentation plots as shown later on in this chapter.

3.4.2 Bathymetric map

Figure 3-10 and figure 3-11 show the bathymetric map of the survey area. These maps are the result of the interpolation of data obtained during the survey on the 1st of December. For obtaining this bathymetry almost 30 tracks were sailed from the landside to the seaside and back as shown in the beginning of this chapter, figure 3-3. The longshore distance covered by those tracks and visible in figure 3-11 is 1200m.

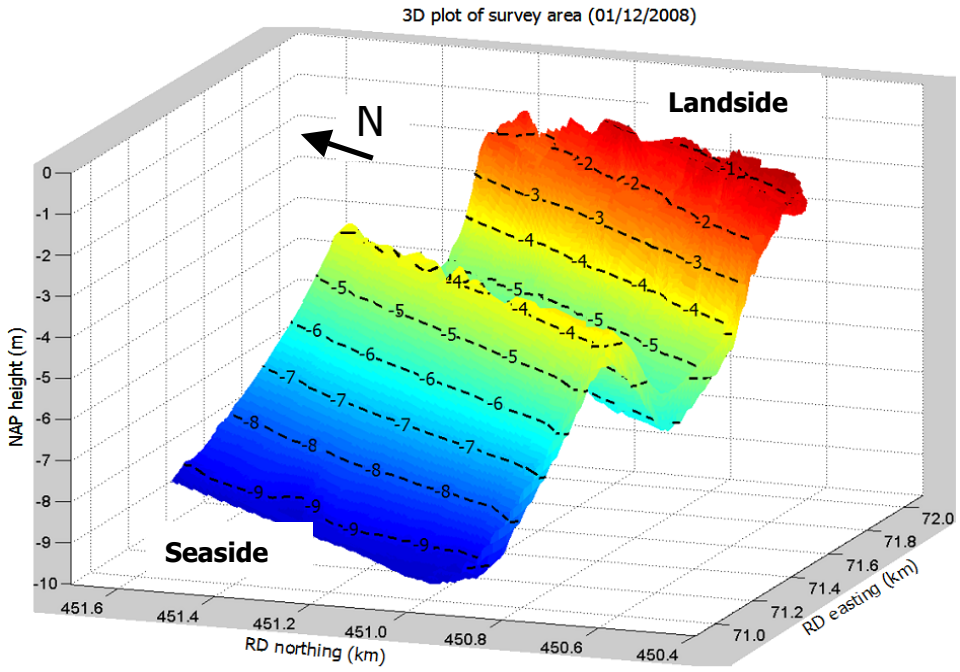

Figure 3-10: Bird eye view of bathymetry of survey area including depth contour lines

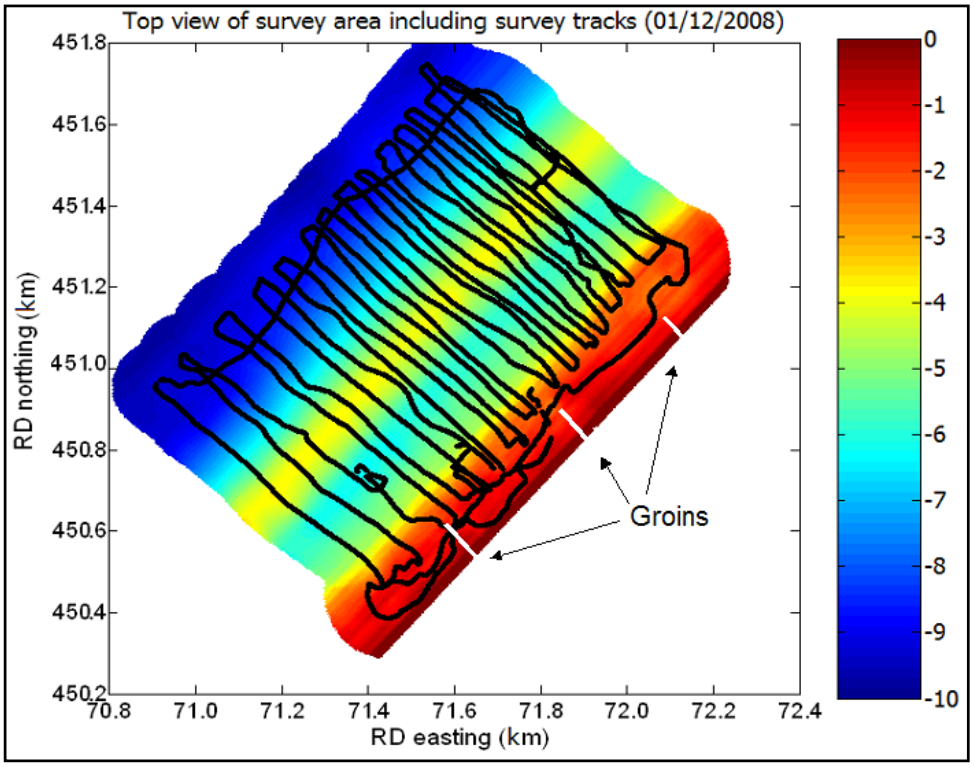

Figure 3-11: Top view of bathymetric of survey area including survey tracks (01/12/2008)

3.5 Quality assessment

The Jetski is developing towards a useful survey platform for bathymetric surveys, in particularly in the coastal zone of the North Sea. The quality of the Jetski as a platform for bathymetric surveys is therefore assessed. Some data is lost during surveys as described in the beginning of this section. The measured depth values deviate somehow from the true depth due to measurement errors. All error sources are defined and the theoretical error is determined for every separate contribution. Besides the theoretical error, the empirical error is derived from the datasets that are obtained in the field. Finally the empirically obtained errors and theoretically calculated errors are compared to each other.

3.5.1 Loss of data

In figure 3-3 some survey tracks show gaps in the measurements. A number of factors play a part in this loss of data, the first three factors are due to the echo sounder, the last one concerns the GPS:

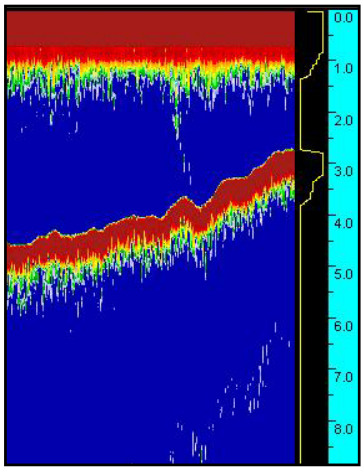

Figure 3-12: SBES output (depth below SBES in m)

1. The sailing speed of the Jetski is too high (v>3m/s). The deeper the water, the lower the maximum speed may be before the signal is lost. MacMahan [2001] gives a relation for the maximum sailing speed before signal dropouts occur. According to that relation no loss of data should occur when sailing speeds remain below 5m/s. Analyses of the speed during data dropouts shows that for the TUDelft Jetski in practice the survey speed limit is approximately 4m/s.
2. For shallow-water settings in Hydrobox [2008] the SBES values will only be recorded up to 10m water depth. For deeper water measurements the settings have to be adjusted.
3. A blanking distance causes loss of data in shallow water (i.e. less than about 1.2m). A short time fraction after the emission of a sound pulse the SBES cannot receive any reflected signal. In figure 3-12 a graphical image of the SBES output is given. The numbers on the right hand side indicate the measured water depth. The upper red band is the blanking distance; the depth is derived from the topside of the lower red band. One can imagine that in shallow water the two red bands cannot be distinguished from each other anymore, so no depth value can be defined below approximately 1.2m of water depth.
4. SBES data is recorded, but no GPS position is available. Either too few satellites are in view or there is a short loss of connection with the GPS reference station. These SBES data are filtered out to make sure no GPS positions are extrapolated in the further processing.

3.5.2 Theoretical error

Platform motion (pitch and roll)

The GPS and SBES are rigidly fixed on the Jekski. Since no motion sensor is applied the roll and pitch motions will cause errors in the measurements.

Two factors play a role in the error contribution due to the Jetski motions: The SBES signal that is sent to the bottom and the offset between the GPS and SBES. Both contributions are worked out in the following section.

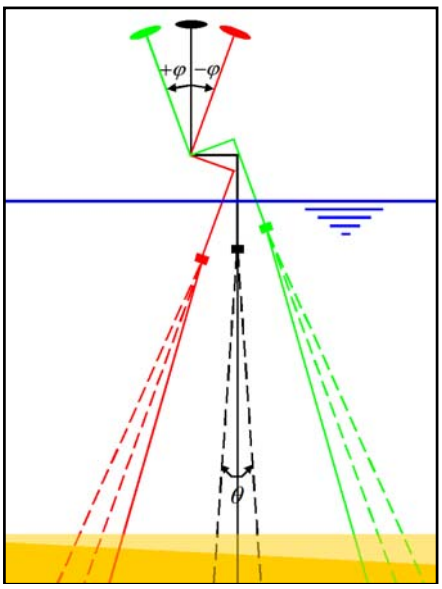

Figure 3-13: Rear view of SBES and GPS roll motions (Green = +20°, Red = -20°)

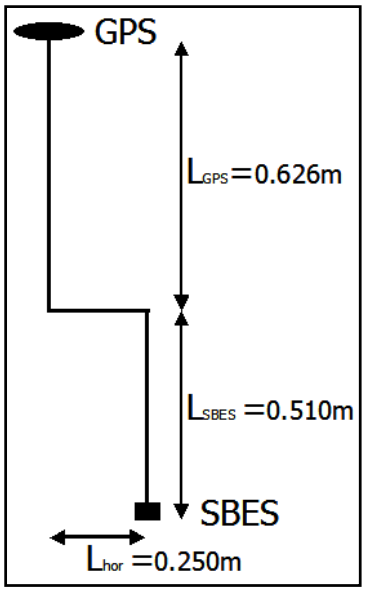

Figure 3-14: Schematic rear view of SBES and GPS

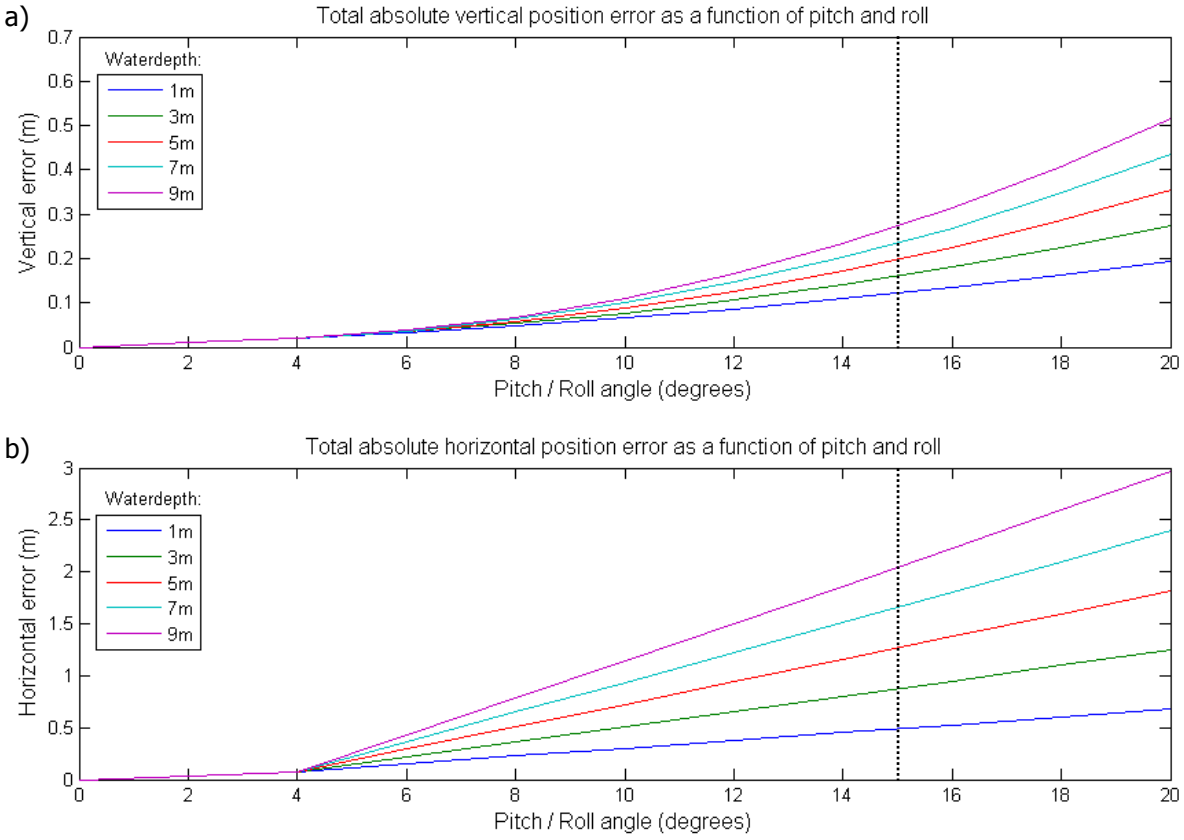

Figure 3-15: Error due to Jetski motions a) Vertical error b) Horizontal error

SBES signal error

The SBES has a beam width of 8°. It records the earliest return from its transmission (i.e. the echo having traveled the shortest distance). Figure 3-13 shows that the water depth will be overestimated when the attitude angle of the Jetski exceeds half the opening angle. This error contribution applies to an assumed flat bottom and can be calculated by equation 3-7 and 3-8. These equations are derived from MacMahan [2001] and adapted for this particular case:

$$\text{Vertical error:} \quad \Delta d_{SBES} = \begin{cases} 0 & \text{for } \varphi \le 0.5\theta \text{ , } \theta = 8^{\circ} \\ \dfrac{d}{\cos(\varphi - 0.5\theta)} - d & \text{otherwise} \end{cases} \tag{3-7}$$

$$\text{Horizontal error:} \quad \Delta xy_{SBES} = \begin{cases} 0 & \text{for } \varphi \le 0.5\theta \text{ , } \theta = 8^{\circ} \\ d \cdot \tan(\varphi - 0.5\theta) & \text{otherwise} \end{cases} \tag{3-8}$$

Where:

φ = Roll or pitch angle of the Jetski

θ = Beam width of the emitted SBES pulse

Offset error

As mentioned before the vertical offset between the GPS antenna and the SBES transducer is corrected for by simply subtracting the offset from the GPS height. In case of roll and pitch motion this assumption causes the theoretical error as given in equation 3-9. The meaning of the symbols used in the equations can be found in figure 3-14.

$$\begin{aligned} \Delta d_{offset} &= \sin\varphi \cdot L_{GPS} + \sin\varphi \cdot L_{SBES} \\ \Delta xy_{offset} &= L_{GPS} + L_{SBES} - (\cos\varphi \cdot L_{GPS} + \sin\varphi \cdot L_{hor} + \cos\varphi \cdot L_{SBES}) \end{aligned} \tag{3-9}$$

The total horizontal and vertical error due to platform motion is calculated by summing the separate contributions:

$$\begin{aligned} V_{error} &= \Delta d_{SBES} + \Delta d_{offset} \\ H_{error} &= \Delta xy_{SBES} + \Delta xy_{offset} \end{aligned} \tag{3-10}$$

In the above only the error of a motion in positive φ-direction (green in figure 3-13) is calculated with these equations. The error due to a negative rotation (red in figure 3-13) causes nearly the same, but a slightly smaller error; therefore it is not further discussed here.

The resulting plots of equation 3-10 in figure 3-15 present the theoretical horizontal and vertical error due to the platform motions (roll and pitch). For varying angles the resulting errors are plotted, each line corresponds to a different water depth. The 20º angle indicates the upper boundary, because a motion above that magnitude would almost make the Jetski roll over. The important question remains how much motion the Jetski faces during specific wave conditions. Appendix E shows that the roll motion is higher than the pitch motions, but both of them remain within the 4º boundaries on a very calm day (H_s<0.3m).

Echo sounder

Theoretically the echo sounder has a vertical accuracy of 0.01m [Hydrobox, 2008]. However, spikes are present in the data and may increase the inaccuracy. Here the maximum error is assumed to increase with the water depth, starting with 0.01m in 1m water depth and

increasing to 0.05m in 9m water depth. The filtering and removal of these spikes in the SBES signal was discussed in processing step 5 in chapter 3.3.

Platform motion (heave)
By applying RTK-GPS the vertical position of the Jetski (heave) can be defined. Waves cause a heave motion in the order of seconds whereas the heave due to the vertical tide is in the order of hours. The application of cubic spline interpolation, however, between successive GPS measurements introduces some error. Within a 1-second interval the Jetski may have moved slightly different on the waves than the interpolated spline motion. A consequence may be that the GPS does not record the full range of motion. The magnitude will be of order 0.01m; this error becomes more pronounced at higher sailing speeds and rougher seas.

Squat
Squat is a rotation of the vessel caused by the application of power. In case of squat the rear side of the Jetski moves down. This vertical displacement is measured accurately by the RTK-GPS. The SBES moves along with the GPS (because they are mounted so close to each other) and thus the effect of squat on the error in the measurements is negligible. Squat results in some pitch of the platform, the pitch due to waves however is much larger, this error contribution has been treated in the previous and shown in figure 3-15a.

GPS accuracy
The GPS method used for the surveys is Real Time Kinematic GPS (RTK-GPS). This method requires simultaneous observations at two locations. On one side the receiver with its antenna at a fixed reference point (i.e. Hoek van Holland reference station). On the other side the mobile antenna on the Jetski, whose antenna position is to be determined.
A minimum of five satellites must be tracked. The baseline accuracy can be expected to be 1cm+1ppm (parts-per-million of the distance between the base station and moving GPS-receiver) for the horizontal position and 2cm+2ppm for height [Leica, 2001].
With a distance of approximately 7km between Hoek van Holland and the survey area near Ter Heijde the expected theoretical standard deviation (being a random error) for the GPS measurements is 3.4cm in the vertical and 1.7cm in the horizontal direction.

Shape of seafloor
In two ways the shape of the sea floor can contribute to the measurement uncertainty: A sloping bottom and ripples on the seafloor.
The beam width of the SBES is very small (4º angle) and the maximum bottom slope in the survey area is only 2.5º (at the land side of the outer bar). In figure 3-16a a graphical representation of the situation is given. With a simple geometric analysis the vertical error contribution is found to be less than 0.01m at 5m water depth. The horizontal error is found to be of order 0.1m in a water depth of 5m (where bottom slopes are at their maximum).

Small-scale morphological features like ripples with length scale in the order of a meter on the seafloor may introduce some systematic bias in the signal. Figure 3-16b shows that the top of the ripples causes the earliest return of the SBES pulse. The computed seafloor position will then be somewhat higher than the real seafloor.

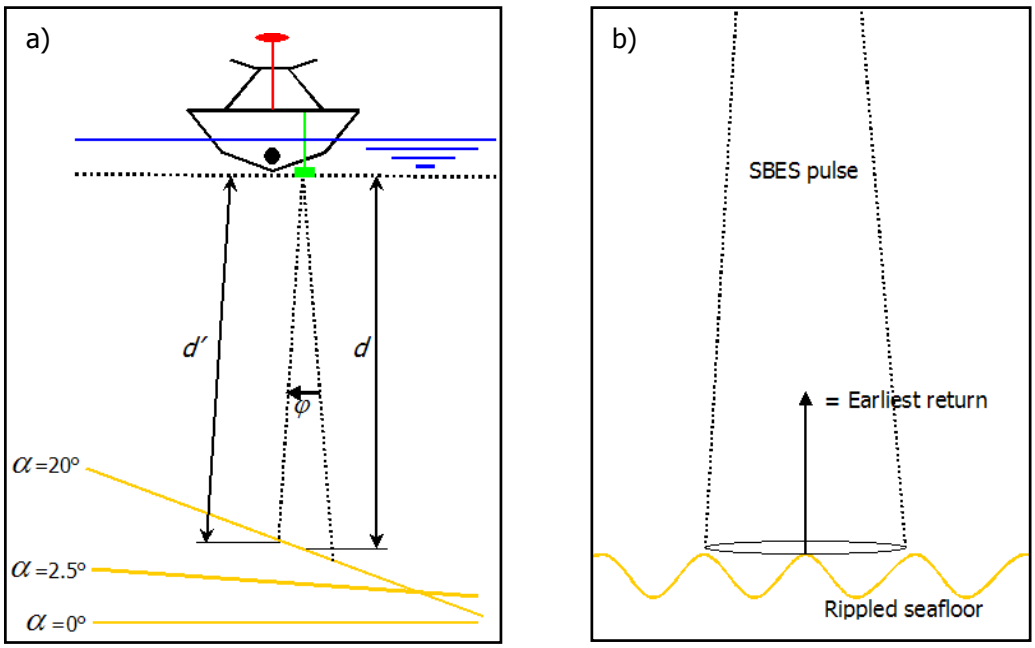

Figure 3-16: Error contribution due to the shape of the seafloor.
a) Bottom slope effect, b) Influence of ripples on reflected signal

Error as a result of interpolation

The variogram function from section 3.4 provides valuable information for the estimation of the standard deviation corresponding to the Ordinary Kriging interpolation. In more detail, the dissimilarity value (vertical axis of the variogram function) corresponds to the variance of the depth values, and thus the standard deviation is the square root of the dissimilarity. For every distance from a measurement point one can compute the average depth variance. If we assume the nugget value to be 0 (i.e. two measurements of the same point have exactly the same value) then an assessment can be made of the precision of the bathymetric map.

The standard deviation is shown in figure 3-17 for two survey days. Great gaps are visible between the tracks sailed on 16/09/2008. On 31/10/2008 a maximum mutual distance of 55m has been maintained, by doing so the standard deviation of the depth values between separate tracks stays below 15cm.

Good coverage of the area is thus obtained when tracks are sailed within approximately 60m from each other. When also some longshore tracks are sailed, creating a block pattern, the maximum standard deviation of the interpolated depth values can be maintained below 15cm for the whole area.
When the distance between sailed tracks is more than 60m the standard deviation will grow rapidly. In such cases it is advised to compare the same surveyed tracks on different days with each other and not interpolate towards an area map.

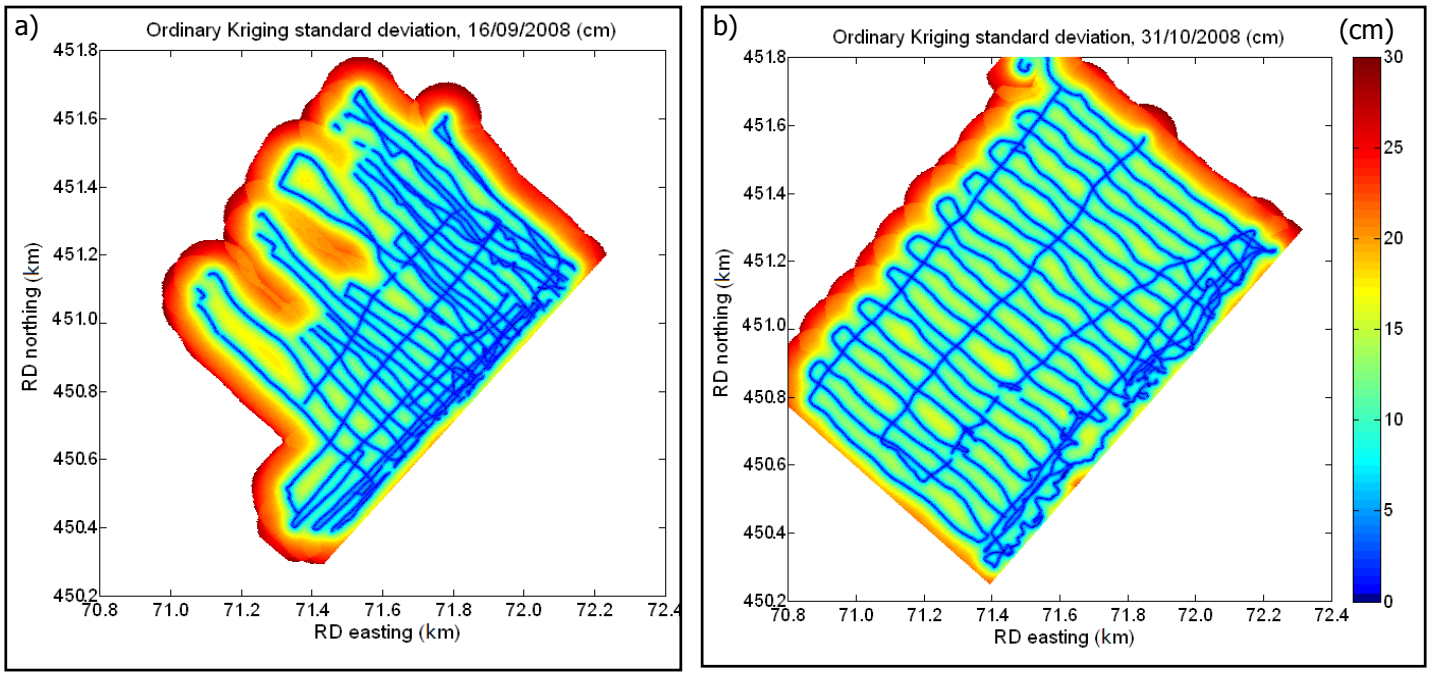

Figure 3-17: Ordinary Kriging standard deviation a) on 16/09/2008 b) on 31/10/2008

Speed of sound in water

The speed of sound in water is a required input parameter. The speed of sound depends on the depth, salinity and temperature. Their contribution to the theoretical error is described here:

Temperature

After every survey the water temperature was registered (see table 3-1 [Actuelewaterdata, 2009]). This average temperature value may in reality vary in time or with depth, for example due to the Rhine plume influence. A possible deviation from the source value is 1°C, resulting in a vertical depth error of 0.22cm per meter depth.

Salinity

The salinity has not been measured in the field; instead Rijkswaterstaat measured the salinity frequently near Ter Heijde [Waterbase, 2009]. Data is available between 1975 and 1997 from which a representative value for the salinity has been derived. In appendix D the average values for the 4-month period between September and December 1975-1997 is given. A salinity value of 28.5ppt has been chosen for all surveys. The absolute error in the salinity could be up to 5ppt. That would lead to a vertical depth error of 0.43cm per meter depth.

Note that the river Rhine discharges fresh water into the North Sea near Hoek van Holland. This Rhine plume extends over 100 km alongshore and has a different salinity and temperature than the surrounding North Sea water. From low water to high water the surface currents are directed offshore, so the plume is located furthest offshore around high water [de Boer, 2007]. The plume may affect the speed of sound in water near Ter Heijde. However, surveys are performed mainly during high tide and preferably with offshore wind (driving the plume offshore) so the Rhine plume influence will be rather low.

Depth

The depth contribution in the relation of Mackenzie is very small. The absolute error due to the difference in measured depth ranging from 1m to 10m is therefore negligible.

A table with a sensitivity analysis and salinity values is given in appendix D.

Offset between the GPS receiver and the SBES transducer

The vertical distance between the GPS antenna and the SBES transducer is 1.136m. When the GPS and the SBES are mounted on the Jetski, their vertical distance may change slightly from survey to survey. The expected order of the vertical bias in the measurements will be around 1cm.

The horizontal offset (L_{hor}) in figure 3-14 causes a horizontal error with a maximum of 0.25m, varying with the sailing direction. For this study, this error is of minor importance; therefore it is accepted and not corrected for the sailing direction.

Overview of theoretical errors

All errors mentioned in the previous section are summarized in the following table, divided into random errors, systematic errors and a contribution of the interpolation error. For every contribution the vertical (displayed bold) and horizontal value are given in table 3-2. For the roll and pitch a maximum angle of 15° is chosen which corresponds to heavy motion experienced on the Jetski. Surveys will have to be postponed for wave conditions that cause larger roll or pitch angles due to of safety of the crew and accuracy.

Table 3-2: Overview of theoretical errors:
a) Maximum random errors b) Maximum systematic errors c) Interpolation error

a) Maximum random errors	**Vertical or horizontal error**	**Magnitude**			**Reference**
		15° motion at depth:			
		1m	5m	9m	
Pitch & roll	**Vertical**	**0.12m**	**0.20m**	**0.28m**	Figure 3-15
	Horizontal	0.5m	1.25m	2.0m	
Echo sounder	**Vertical**	**0.01m**	**0.03m**	**0.05m**	Ch. 3.3.1 (5)
	Horizontal	-			
Heave	**Vertical**	**0.01m**			Ch. 3.5.2
	Horizontal	-			
GPS accuracy	**Vertical**	**0.034m**			Ch. 3.5.2
	Horizontal	0.017m			
Seafloor shape	**Vertical**	**0.01m**			Figure 3-16
	Horizontal	0.1m			
GPS/SBES offset	Horizontal	0.25m			
b) Maximum systematic bias		Depth (m)			
		1m	5m	9m	
Speed of sound	**Vertical**	**0.01m**	**0.05m**	**0.09m**	Ch. 3.5.2
	Horizontal	-	-	-	
GPS/SBES offset	**Vertical**	**0.01m**			Ch. 3.5.2
c) Interpolation	**Vertical**	**0.15m**			Figure 3-17
	Horizontal	-			

The total error is a combination of separate error contributions. Since not all random errors will occur at the same time they can be combined using the "propagation law of errors" (see section 3.5.4).

3.5.3 Empirical error

Field data is analyzed and the empirically calculated random error is estimated for different survey conditions. This has been done in three ways: First of all some available motion sensor data is used to get an idea of the platform motions during a survey. Secondly the deviation is calculated of the calculated depth relative to the smoothed (filtered) depth. This is done for different sailing directions and for different water depths. Thirdly the resulting depth values are compared for one single transect that is sailed multiple times.

1. Platform motion during a survey

Although no motion sensor has been applied during the surveys in 2008, one has been installed on the Jetski during an extra survey on the 27th of January 2009 to get an idea of the platform motion and the applicability of such a device. The device used is called an Xsens, which is a direction and rotation reference system [Xsens, 2008]. Data is available from the Jetski motion while sailing 1km seawards and back towards the shore. Appendix E shows the results for this day. It turns out that the tilt angle remains within -4° and +4°. The vertical error due to platform motions can be read from figure 3-15a and will not have exceeded a value of 0.02m.

2a. Calculation of the noise in the measured signal

The noise in the measured signal is not constant over the whole survey area. The relation with the sailing direction and water depth are compared with each other. The following actions are performed before a comparison can be made:

1. Calculate the depth values as shown earlier in this chapter (a sample is shown in figure 3-18.
2. Smoothen the bottom using the moving average filter (see equation 3-6).
3. Subtract the measured bottom from the smoothed bottom.
4. Calculate the mean of the obtained signal; the mean should be close to 0m.
5. Compute the standard deviation and the skewness for several shoreward and seaward sailed tracks and for measurements in shallow, medium and deep water (see table 3-3).
6. Perform these actions for all five surveys and compare the standard deviation values for different sailing conditions.

The values in table 3-3 are assumed to correspond to a standard normal distribution. The asymmetry of the data around the mean (skewness) is very small (<0.5). Considering outliers in the dataset (kurtosis) this dataset is relatively outlier-prone with kurtosis values up to 10. A normal distribution has a kurtosis value of 3 [MathWorks, 2005]. The normal distribution does not completely fit to the dataset, but for the sake of simplicity it is used here.

Table 3-3 shows that the overall standard deviation of the measurements is in the order of 10cm ($\sigma_{\text{all data}}$).

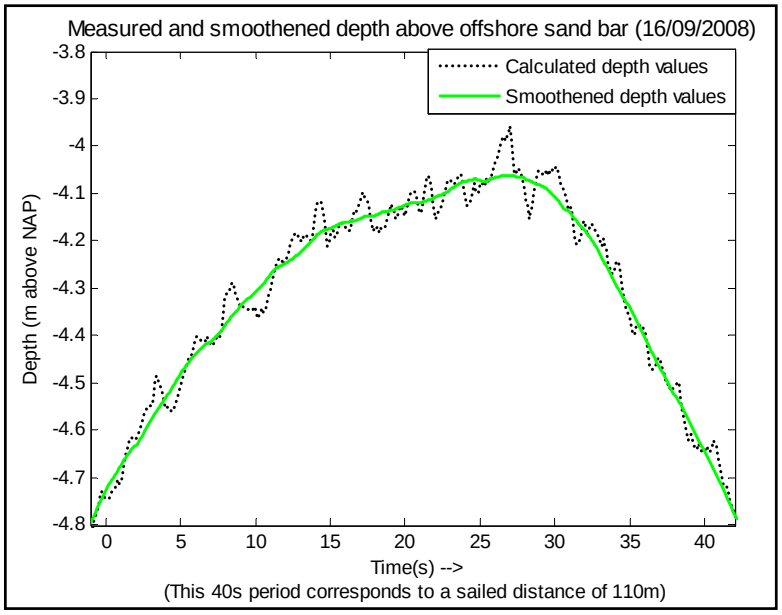

Figure 3-18: Measured and smoothed depth

2b. Effect of the sailing direction on the random error contribution

The difference in sailing direction is shown schematically in figure 3-19. Fewer waves are encountered when sailing in landward direction compared to seaward sailing. The most platform motion and thus the largest deviation from the filtered signal are expected for seaward sailed tracks. Indeed this relation is observed in the calculation of the noise in the measured signal. The standard deviation of sailing seawards, $\sigma_{seawards}$ (7.6cm) is higher than $\sigma_{landwards}$ (4.3cm). The difference of 3.3cm in standard deviation is thus fully due to wave motion. It cannot be proved here that the remaining 4.3cm of $\sigma_{landwards}$ is also fully due to wave motion. Part of this value will be the result of the platform motion on the waves and some part will be due to small-scale morphological features that are smoothed by the filter. It is thus concluded that sailing in landward direction results in a smaller error contribution than seaward sailing.

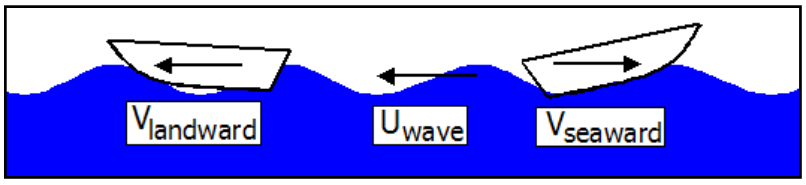

Figure 3-19: Jetski sailing direction and speed relative to the wave propagation

2c. Effect of different water depths on the random error contribution

Another notable aspect derived from table 3-3 is the fact that the standard deviation in medium water depth (6.4cm) is smaller than in deep (8.5cm) or shallow water (9.7cm). The main cause lies in the fact that the most SBES outliers (described in appendix C as occasional errors) occur near shore and in deeper water. Filtering those errors could therefore improve the shallow and deep-water measurement up to the level of the medium depth standard deviation of 6.4cm (which would be a 20% to 30% reduction of the random error).

Table 3-3: Standard deviation from smoothed signal

Survey → **Date →**	**1** 16/09/'08	**2** 23/10/'08	**3** 31/10/'08	**4** 01/12/'08	**5** 12/12/'08	**Average**
$\sigma_{all\ data}$ (cm)	8.8	9.1	6.5	5.5	10.5	**8.1 cm**
$\sigma_{landwards}$ (cm)	5.6	4.2	3.7	2.4	5.7	**4.3 cm**
$\sigma_{seawards}$ (cm)	9.6	9.9	4.8	5.3	8.4	**7.6 cm**
$\sigma_{shallow}$ (cm)	8.6	11.5	8.6	7.6	12.1	**9.7 cm**
σ_{medium} (cm)	8.1	7.5	4.7	4.3	7.2	**6.4 cm**
σ_{deep} (cm)	11.0	8.5	5.2	5.4	12.2	**8.5 cm**

Note for table 3-3: *All data* refers to a complete survey, *landwards* refers to tracks that have been sailed towards land, *seawards* refers to tracks that have been sailed towards sea, *Shallow* = 0 to –3.5m NAP, *Medium* = –3.5 to –6m NAP, *Deep* = –6 to –10m NAP.

3. Comparing one specific transect that is sailed multiple times
During survey 5 on the 12th of December 2008 one single transect has been sailed five times. Wave heights and thus flow velocities during the survey were rather high. A sample (A-A') of these measurements is shown in figure 3-20. The Jetski was sailing over the bar and the distance between tracks of the sample is 20m. The figure shows that the sailing lines are bound within 0.1m from each other. The black line corresponds to an offshore sailed track and shows the largest deviation. Either this difference is due to the morphology underneath the black track, or it is due to the error in the measured signal itself.

Note that the difference between the measurements may be a result of morphological features since the sailing lines do not cover exactly the same track (target is the vertical dashed line in figure 3-20b). The variation of morphology within a longshore distance of 20m however is in order of 0.1m. This means that the difference in depth between lines in figure 3-20 could be entirely due to the bottom topography and does not indicate the error in the measurements.

An empirical value for the deviation from the calculated mean cross-section (consisting of all these surveyed tracks) is still calculated. Next, the standard deviation is calculated with respect to the mean. The result is: $\sigma_{empirical}$ = 0.10m.
Again part of this standard deviation is a result of morphological features and part of it is due to the error in the measured signal itself.
To find that out in more detail it is recommended to perform this test more often during different environmental conditions.

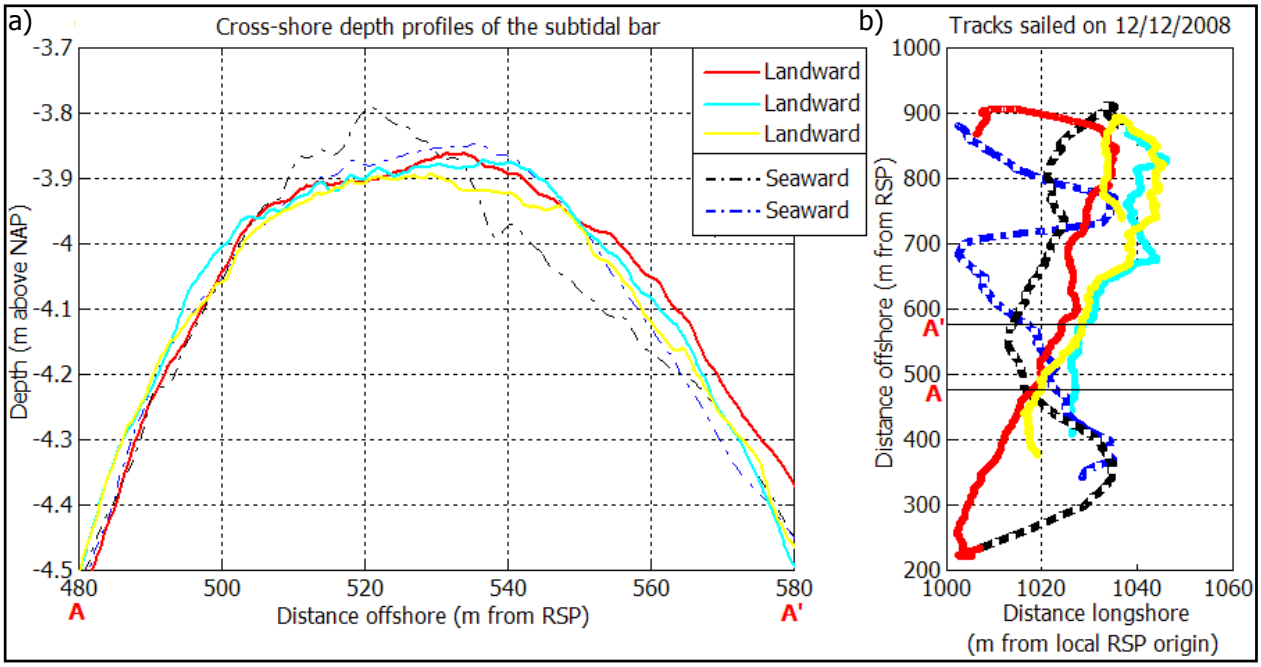

Figure 3-20: One single transect surveyed multiple times (on 12/12/2008, H_s=1.5m)
a) Cross-shore depth profiles of the offshore bar; b) Tracks sailed

3.5.4 Empirical error versus theoretical errors

The theoretical and empirical error are compared to each other in this section. A very calm day (survey 4) and a rougher day (survey 5) are compared with respect to measurement errors in 5m water depth. The theoretical random errors are summed using the propagation law of error [Mechanical Lab Manual, 2008]; the systematic error is added separately (equation 3-10). The contribution of interpolation on the error is not included here, because the focus is on the error of the measured signal and not on the bathymetric map.

$$\varepsilon_{total} = \sqrt{\varepsilon_a^{\,2} + \varepsilon_b^{\,2} + \ldots + \varepsilon_z^{\,2}} + \varepsilon_{sys}$$

$\varepsilon_{a\ldots z}$ = theoretical random error contributions

ε_{sys} = theoretical systematic bias contributions (3-10)

For survey 4 and 5 the total theoretical error is calculated. The magnitude of each separate error contribution was given in table 3-2. The only value that differs between the calm and rough condition-calculation is the error contribution due to roll and pitch.

Calm sailing conditions

On the 1st of December (survey 4) conditions were calm: H_s=0.7m with some weak offshore wind (1-2 Beaufort). For this day the total theoretical error is calculated, assuming that roll and pitch motions remained below +6° and -6°. The vertical error belonging to this value is 0.04m, derived from figure 3-15.

The assumption of the degree of pitch and roll is made on the basis of available motion sensor data as shown in Appendix E for a comparable, but somewhat calmer day in January: H_s=0.3m and weak offshore wind (2 Beaufort). The motion sensor sample shows that the roll and pitch motions remained within +4° and -4° that day.

Rough sailing conditions

On the 12th of December (survey 5) conditions were rather rough for surveying. No motion sensor data is available for any rough day. A motion of 20° will almost make the Jetski roll over; such large motions were not encountered. A value of +/-12° is assumed for the rough conditions. The vertical error belonging to this value is 0.12m, derived from figure 3-15.

Error comparison

Table 3-4 shows the total theoretical and empirical error as determined in this chapter. Only the random error contribution can be compared, since all calculated empirical errors are a result of random errors. For calculating the systematic bias, a comparison has to be made with a different measurement method (e.g. a survey on foot).

Table 3-4 shows that the random errors are all around 0.1m, somewhat higher for rough conditions, somewhat lower for calm condition. The maximum systematic bias is 0.06m.

When some of the error contributions are decreased as a result of the improvement of the survey platform, the new theoretical error can be calculated. Improvements could lead to an error that is about half of the current value. The largest vertical random error contribution is the platform motion and the largest systematic bias is due to the speed of sound in water.

Table 3-4: Theoretical and empirical error in the vertical seafloor position compared

	Calculation method	Calm conditions (Survey 4) Random ± bias	Rough conditions (Survey 5) Random ± bias
Theoretical error	Equation 3-10	0.062m ± 0.06m	0.129m ± 0.06m
Empirical error	Standard deviation from smoothed signal (table 3-3)	0.055m	0.105m
	Comparison of one transect sailed multiple times (figure 3-20)	-	0.100m

3.6 Representation of bathymetric data

Erosion-sedimentation plots and cross-sections are derived from the bathymetry in this section. The calculation method and features like artifacts in the plots are discussed.

3.6.1 Artifacts in the erosion and sedimentation plot

Morphological changes are presented in erosion-sedimentation plots in which the difference in bed level between two surveys (on the same grid) is visualized (figure 3-21). Distinction is made between artifacts and bathymetric features.

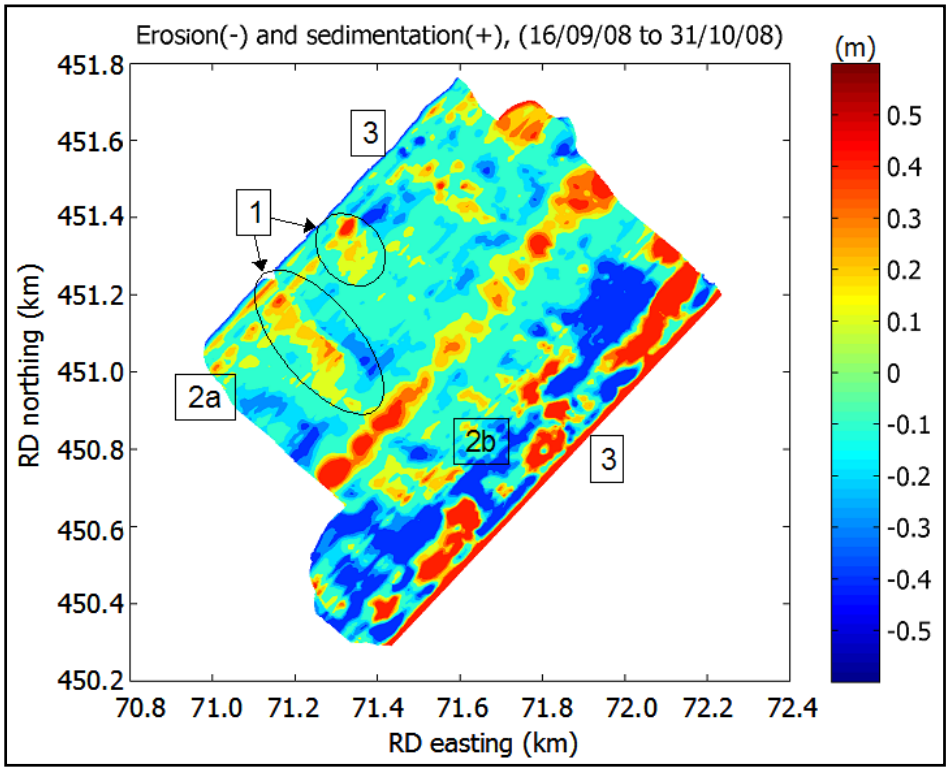

Figure 3-21: Erosion and sedimentation plot including the artifacts

Artifacts
The erosion-sedimentation plots show bathymetric changes as well as some artifacts as a result of errors in the measurements or errors introduced by interpolation. The large difference in spatial resolution plays an overall role in the introduction of shore-parallel lines, visible in figure 3-21. The average distance between the SBES measurements (spatial resolution) is 30m to 50m in the longshore direction and 0.25m in the cross-shore direction. This large difference arises from the fact that most tracks have been sailed in cross-shore direction. The consequence is that the distance between two consecutive measurements is much smaller than the distance between tracks.
Several types of artifacts in the bathymetry are numbered in figure 3-21 and their origin is discussed below:

1. The first artifact [1] is a result of bathymetric depth interpolation. During the survey on 16/09/2008 the area has not been covered completely. Some tracks lie so far from each other (>100m) that the interpolation error in the bathymetric map of 16/09/2008 can grow rather large (the growth of this error was calculated before and is shown in figure 3-17).
2. The second artifact consists of longshore lines in the erosion/sedimentation plots. This type of artifact appears in deep water [2a] and in shallow water [2b] where the Jetski rolls and pitches much while turning and manoeuvring. A second cause of these artifacts arises from occasional errors in the shallow and deep-water measurements; those errors are explained in detail in appendix C.
3. The third artifact [3] is a result of extrapolation of the boundaries. Beyond the seaward boundary there is no depth information, still some depth values are given. The calculated interpolation standard deviation (as was shown in figure 3-17) increases rapidly near the boundaries.

Artifact nr. 1 is present only during the inexperienced first survey (16/09/2008), where the mutual track distance has exceeded 60m. During later surveys tracks have been sailed with a maximal mutual distance of 60m (see figure 3-3 and table 3-1) to restrain the error due to bathymetric depth interpolation.
Other artifacts can be avoided or decreased by increasing the accuracy, by filtering inaccurate data points or by cropping the interpolation area near the boundaries. One way to increase the accuracy is by installing a motion sensor, a second option is to make sure that only those data points are included that are recorded while sailing in a straight line (i.e. not during the turning of the Jetski).

Bathymetric features
Real bathymetric features remain when the defined artifacts in the erosion-sedimentation plots are neglected. These features are discussed in the synthesis in chapter 5.

3.6.2 Cross-shore profiles

Bathymetric differences (e.g. between surveys) can also be investigated by comparing cross-shore profiles. All cross-shore profiles are given relative to the RSP line (RijksStrandPalen) in order to perform mutual comparison as well as comparison with JARKUS profiles. Since the original reference system is RD the following transformation needs to be performed:

1. Define the origin of the local (RSP) coordinate system:
   RD: X = 71422m, Y = 450183m
2. Translate the bathymetry using equation 3-11 (*XYZ* is a matrix consisting of the horizontal position of an observation in RD and the vertical position in NAP):

$$XYZ_{RSP} = \begin{bmatrix} X_{RD} - 71422 & Y_{RD} - 450183 & Z \end{bmatrix} \quad (3\text{-}11)$$

3. Define a shoreline angle: $\alpha = 48.6^{\circ}$ N, this is the shoreline angle of JARKUS transect 110.34, defined by Rijkswaterstaat.
4. Rotate the translated XYZ-file around the local origin using a rotation matrix (equation 3-12):

$$R = \begin{bmatrix} \cos(\alpha) & -\sin(\alpha) & 0 \\ \sin(\alpha) & \cos(\alpha) & 0 \\ 0 & 0 & 1 \end{bmatrix} \quad (3\text{-}12)$$

An example of a cross-shore profile has been plotted in figure 3-22.
Further zooming in to interesting parts of the cross-shore profiles is worked out in the next paragraph. Besides looking at the monitored sea floor shape also the modeled seafloor that will be investigated in chapter 5.

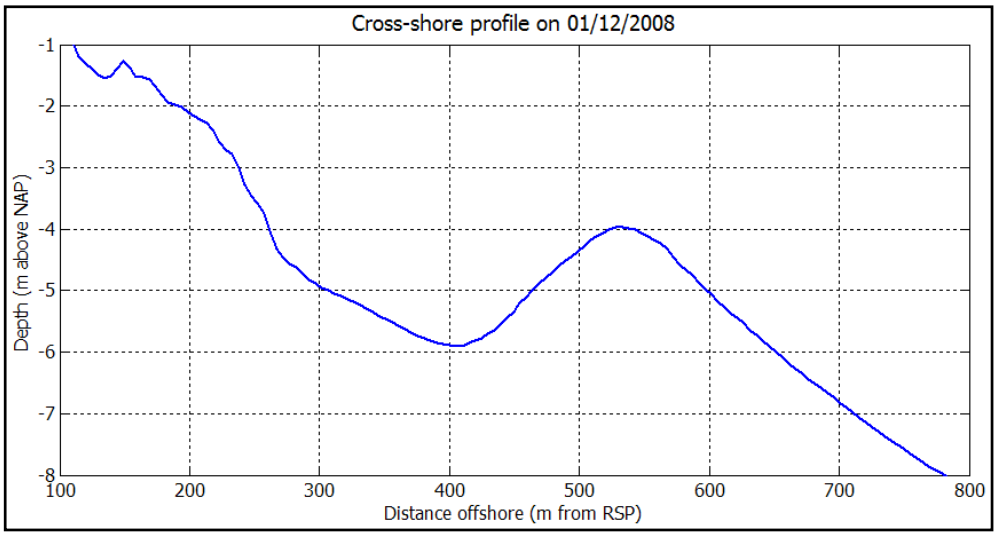

Figure 3-22: Average cross-shore profile on 01/12/2008 (averaged over area between JARKUS 110.72 and 110.34)

3.7 Interpretation of morphological results

The morphological changes as observed in the survey area between different days are presented. The attendant environmental conditions in between these survey days are related to these changes.

3.7.1 Morphodynamic behaviour observed during monitoring

The morphological changes inside the survey area as they have been monitored in the field are visualized in several ways:
First of all two erosion and sedimentation plots are given, showing the change over a calm weather period (figure 3-23) and a stormy period (figure 3-24). Some artifacts in these graphs were defined and indicated (see figure 3-21). Those artifacts are no real bathymetric features and can therefore be neglected in these figures.
Secondly the position of the subtidal bar crest is indicated as monitored on three different survey days (figure 3-25). Finally the bar-cross-sections of the North, middle and South-section of the survey area are shown in figure 3-26 and 3-27. Special attention is paid to the visualization of the subtidal bar.
All these figures give a clear idea of the morphodynamic behaviour within the survey area in time; a description of the most important aspects is given for the subtidal bar on the shoreface as well as for the foreshore:

Bar migration

- First of all onshore bar migration is observed in the calm weather period A+B (from 16/09/2008 until 31/10/2008). Erosion takes place on the seaside of the bar and sedimentation on its landside, which causes the bar to migrate onshore.
- Secondly offshore bar migration is observed in the stormy period C (from 31/10/2008 until 01/12/2008). Rather uniform sedimentation takes place on the seaside of the bar and erosion can be observed on the landside.
- Note that the offshore bar migration in the South section is more pronounced than on the North side (table 3-5 and figure 3-25 to 3-27). The bar also is higher and steeper in the South section. For the onshore migration the opposite is observed. The migration is somewhat larger in the North than in the South section. However this onshore migration difference is not so pronounced that conclusions will be drawn from it.

Table 3-5: Bar migration averaged over North, middle and South sections of survey area

Period	**Section**	**Horizontal displacement (m)** → Offshore migration ← Onshore migration	**Vertical displacement (m)** Plus (+) is upwards Minus (-) is downwards
A	North	← 12m	+0.2
	Middle	← 10m	+0.1
	South	← 7	+0.2
B	North	← <5	~0
	Middle	<5 →	-0.1
	South	← <5	~0
C	North	25 →	-0.1
	Middle	23 →	+0.1
	South	30 →	-0.1

Morphological behaviour of the foreshore

- On the foreshore near the groins the bottom topography is highly changeable. The morphological changes are given by the erosion and sedimentation plots (figure 3-23 and 3-24). Near the groins a notable opposite behaviour is observed after a calm and a stormy period, qualified in table 3-6.

Table 3-6: Erosion and sedimentation as monitored in the foreshore

	Period A + B (calm)	**Period C (stormy)**
South of the groins	Sedimentation	Erosion
North of the groins	Erosion	Sedimentation
At the tip of the groins	Sedimentation	Erosion
Seaward of the foreshore (beginning of shoreface)	Erosion	Sedimentation

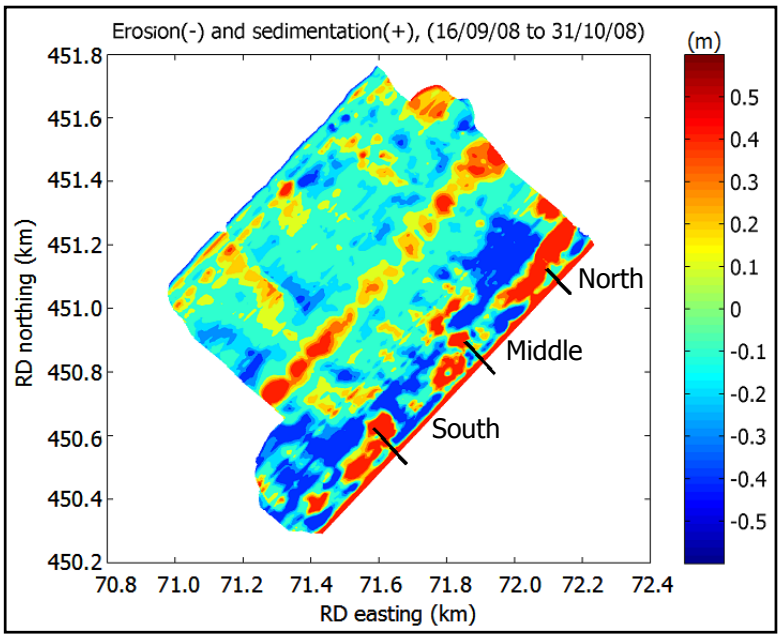

Figure 3-23: Erosion and sedimentation within period A+B: 16th of September until the 31st of October (Top view)

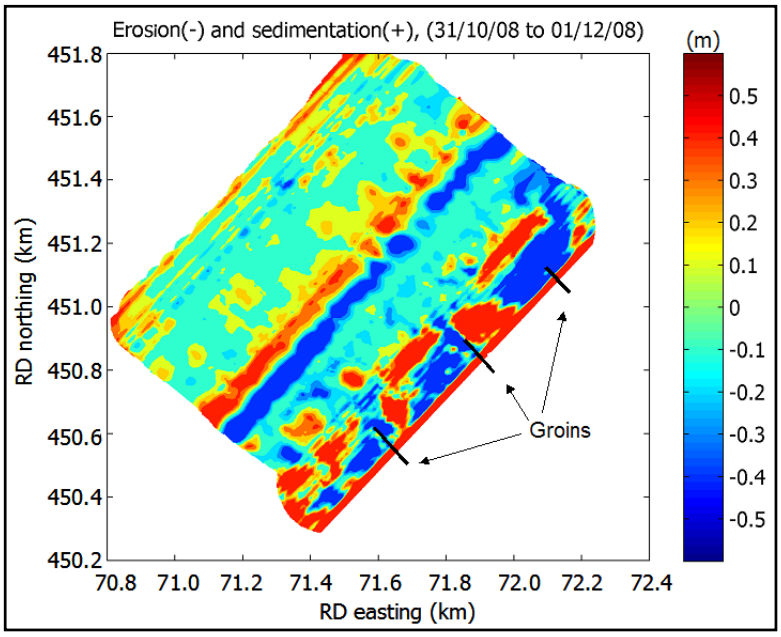

Figure 3-24: Erosion and sedimentation within period C: 31st of October until the 1st of December (Top view)

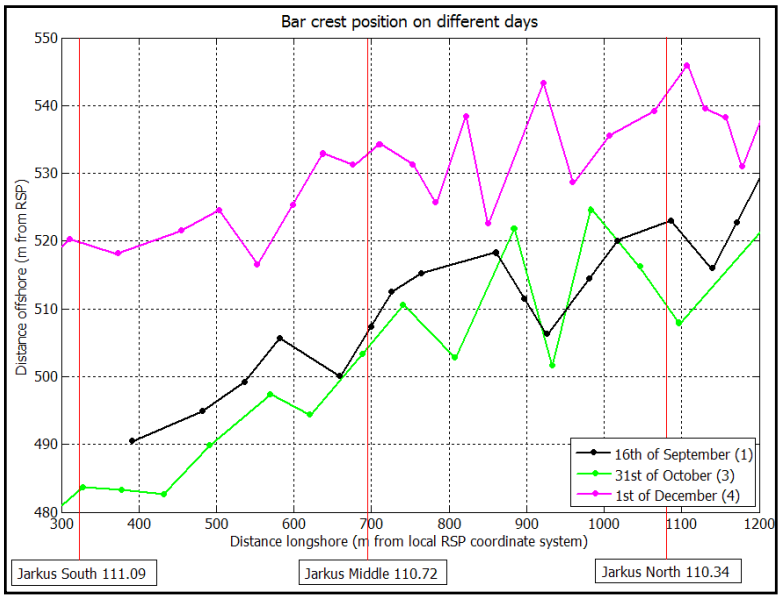

Figure 3-25: Position of the subtidal bar crest on:
- 16th of September
- 31st of October
- 1st of December
(Top View)

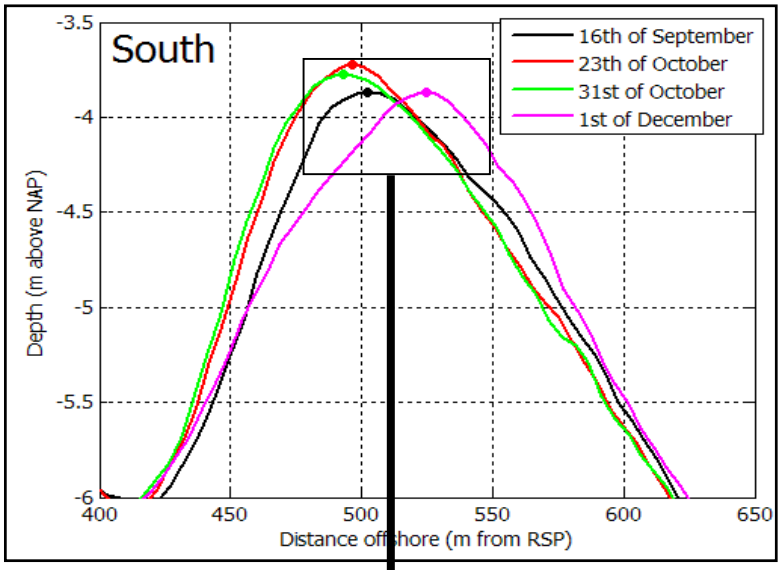

Figure 3-26: Cross-shore profiles of subtidal bar on:
- 16th of September
- 23rd of October
- 31st of October
- 1st of December
(Cross-sectional view)

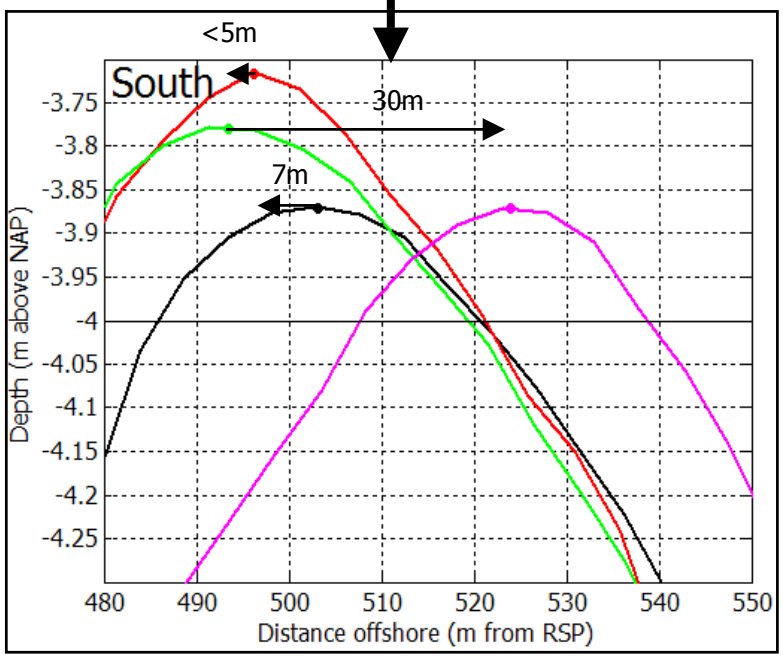

Figure 3-27: Zoomed area of the cross-shore profiles of subtidal bar.
(Cross-sectional view)

3.8 Conclusions

Surveying, processing and interpreting data obtained in the field results in a progression of the understanding of operating procedures and observed processes. The new insights that are described below can be used in future surveys and data handling.

Applicability of the survey platform
The Jetski can be used for surveys in the coastal zone of the North Sea. The small, light, fast and manoeuvrable survey platform is able to measure depths in the coastal area up 1.2m water depth inside the intertidal area. As the crew is flexible it can perform measurements within some days before and after storm events. The minimum number of days between a storm and a survey greatly depends on the environmental conditions.

Quality of the survey platform
The Jetski survey vertical accuracy is approximately 0.1m and the horizontal accuracy is approximately 0.5m, depending mostly on the sea state. Bed forms with wavelengths of order (1m) and heights of order (0.1m) cannot be monitored in a normal survey; those features will be filtered out in the smoothing process.

Jetski-accuracy improvement
The vertical accuracy could be improved about half of the current value by means of the following actions:

- Install a motion sensor and filter measurements for moments that the Jetski tilts more than allowed (e.g. 8 degrees to both sides).
- Measure the speed of sound in water more accurately. This should be done by a bar-check before, during and after the survey.
- Improve the quality of the Single Beam Echo Sounder.
- Only include measurements from tracks sailed in landward direction since those are more accurate than tracks sailed in seaward direction.
- Only include depth measurements while sailing in a straight line. Inaccuracy grows due to the platform motion while making turns.

The horizontal accuracy can also be reduced considerably by installing the motion sensor and by correcting the data for the sailing direction.

The actual surveying

- Cross-shore tracks are sailed. Some longshore tracks should also be sailed.
- A trade-off should be made between the survey area covered and information about the features of interest. The larger the distance between tracks the more uncertainty about the intermediate morphology.
- The beach area can be included by means of a walking survey. Overlap is realized by a high water Jetski survey and low water walking survey (spring tide is needed for overlap).

Additional data gathering

- Bathymetric data of more periods of storms and calms would be valuable for relating environmental conditions to the movement of the subtidal bar.
- During future surveys it is worth sailing one single track more than once before covering the area.
- Compare the Jetski survey with a walking survey: On the 28th of January a Jetski survey has been performed at Scheveningen during high water together with a walking survey during low water showing overlap.

- Compare the Jetski measurements with an existing survey platform (e.g. from Rijkswaterstaat) on the same day.

Most important aspects of the coastal monitoring

Five field surveys were performed on the foreshore and shoreface near Ter Heijde. The obtained raw data has been processed into depth values. Those values are interpolated in order to obtain a bathymetric map of the area. Besides, the data is visualized in cross-shore profiles and erosion/sedimentation plots.
The quality of the data has been assessed and it turns out that the accuracy is of order 0.1m for the vertical depth values and 0.5m for the horizontal position.
Finally several field experiments are compared to each other, they show that the subtidal bar migrates onshore during fair weather conditions and offshore in more stormy periods.

4 Coastal modeling

4.1 Introduction

A numerical model is set up for two purposes. On one hand the model is used to provide quantitative and qualitative information about hydrodynamic processes that are not measured in the survey area (e.g. flow velocities or wave heights). On the other hand an attempt is made to reproduce the morphological changes as observed in the field (figure 4-1).

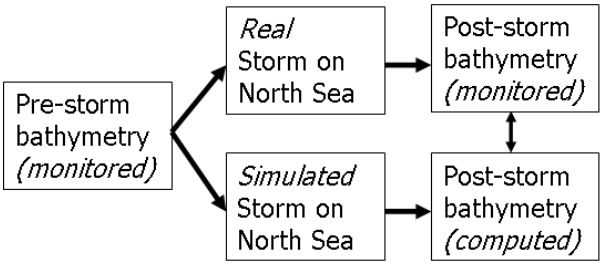

Figure 4-1: Modeling versus monitoring

First of all the propagation of offshore wave conditions (as recorded by a buoy) towards the shore is simulated. Accordingly the wave and tide driven flow velocities are computed for several environmental conditions. Finally the morphological changes due to these currents are computed.
Note: In many graphs the North (green lines), middle (blue lines) and South (red lines) sections are presented; these sections were classified earlier in figure 3-2.

Numerical models are generally divided into three types [Van Rijn, 2002]:

- Coastline models (CL);
- Coastal Profile (CP) Models, suitable for 2D coasts;
- Coastal Area (CA) Models, suitable for 3D coasts, with certain variants of both being applicable to 2.5D coasts.

The survey area has been monitored with great detail showing the non-uniform bar crest as well as the non-uniformity of the foreshore. In chapter 2 the shoreface of Ter Heijde was therefore classified as a 2.5D coast. The area model Delft3D is chosen for the Ter Heijde coast because of these non-uniformities and because of the fact that an area was monitored instead of only transects. The application of a 2D Coastal Profile or Coastline Model for the Ter Heijde coast would imply that the coastal system is simplified to a 2D system, thereby assuming uniformity in the longshore direction and thus neglecting the existence of the longshore variability of the subtidal bar crest (see bathymetric map in figure 3-10).

4.2 Model set-up and schematization

4.2.1 Delft3D

Delft3D is a process-based morphodynamic area model developed by WL|Delft Hydraulics (now called Deltares). With this software package it is possible to combine tides, waves and morphology on both the short and the long term [WL|Delft Hydraulics, 2005] and [Lesser et al., 2004]. For this study only the processes are modeled on the time scale of storms, which corresponds to short-term modeling.
A more detailed description of Delft3D is given in appendix F. For the following paragraphs of this chapter the reader is assumed to have some general knowledge about the Delft3D model.

4.2.2 Computational grid

For the Delft3D-FLOW as well as for the Delft3D-WAVE module, computational grids are created. Wave data from the time intervals between successive field surveys is recorded by the Europlatform buoy[3] (see figure 4-2). In order to translate those wave characteristics from offshore towards the survey area a number of WAVE-grids is used. Four grids (A to D in figure 4-2) with different cell sizes (quantified in table 4-1) are nested in each other to save computation time. FLOW computations are performed only on grid D.

Table 4-1: Computational grid properties

Grid	Grid size (km)	Grid cell size (m)	n.o. grid cells	Used for:
A	70 x 50	800 x 800	1650	WAVE
B	15 x 12	200 x 200	6800	WAVE
C	4 x 3	75 x 35	3700	WAVE
D	1.2 x 0.8	10 x 10	10400	WAVE & FLOW

4.2.3 Bathymetry

A bathymetric file in RD and NAP with a resolution of 3x3m has resulted from Ordinary Kriging interpolation (Chapter 3.4). The Delft3D grid (D) is 10x10m, which means that there is redundancy of data within each Delft-3D grid cell. The interpolation method "grid cell averaging" is used to define the depth-values on the corner points of the grid cells. This results in a depth-file on which Delft3D can perform its computations.
Note: For future computations it is recommended to create a bathymetric depth file for Delft3D directly from Ordinary Kriging, one interpolation step can then be omitted.

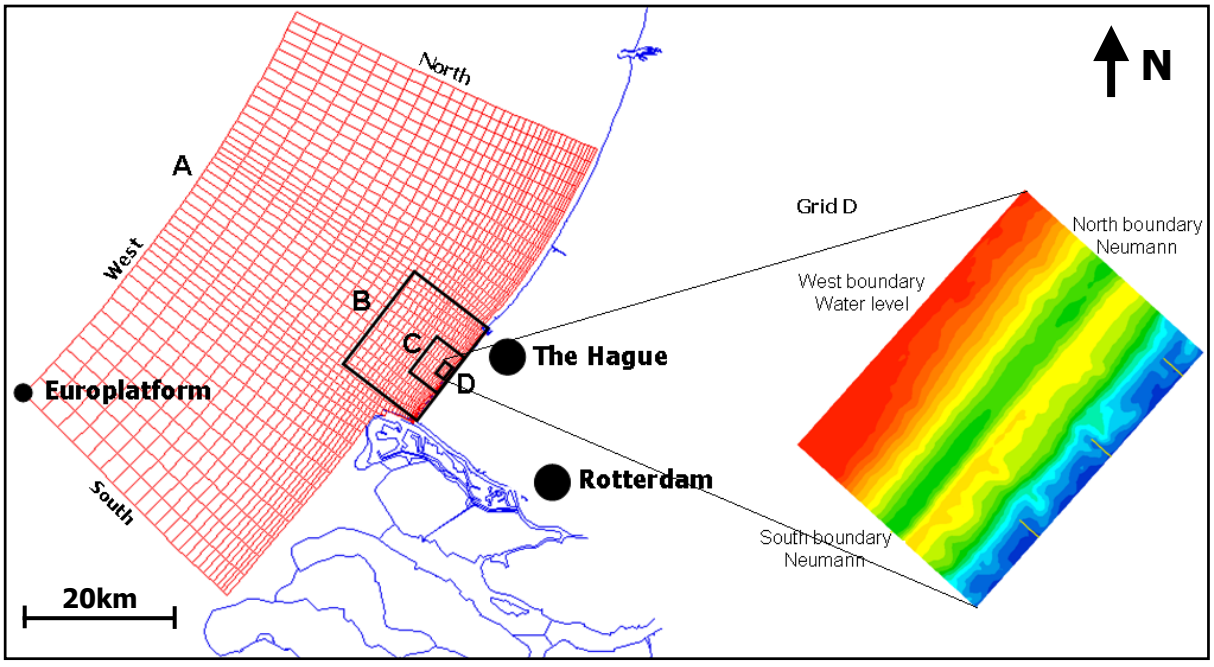

Figure 4-2: Computational WAVE grids (A to D) and FLOW grid (D) including FLOW boundaries

[3] Located 50km West of Hoek van Holland in 30m water depth.
Coordinates: RD easting = 9.963km, RD northing = 447.601km

4.2.4 Boundary conditions

Wave boundaries
All wave conditions recorded by the Europlatform buoy (figure 3-6) are assumed to be representative for the North, West and South boundaries of the coarsest WAVE grid (grid A in figure 4-2).
Waves are enforced to these boundaries in two ways. The first one is to simulate a real storm by using the recorded buoy data as a boundary condition on the North, West and East boundaries. The second manner is the enforcement of a constant wave height, wave period and wave direction. These constant wave conditions are also based on buoy data, but will be used to assess the effects of specific wave conditions. The Delft3D-WAVE module translates all wave conditions from offshore (i.e. the boundaries of grid A) towards the shoreface where they will serve as the new boundary condition for the smallest grid (grid D).

Flow boundaries
The Delft3D-FLOW module computes the wave-induced and the tide-induced flow velocities. The tidal water level fluctuations are set at the boundaries of the FLOW-grid (D). A dataset of tidal components with their amplitude and phase is available from tidal stations in Hoek van Holland and Scheveningen (see figure 2-1a). Ter Heijde is situated between those stations, so all astronomic components are interpolated linearly to obtain values at the North, South and West boundary of the FLOW-domain.
Astronomic water levels are prescribed at the West boundary, whereas astronomic Neumann conditions are applied to the North and South boundaries [Roelvink, 2004]. Neumann conditions determine the boundary solution by imposing the longshore water level gradient.

4.2.5 Model parameters

Numerical stability
The Courant number gives an indication of the numerical stability and accuracy. In models that have large differences in the geometry or coastline, the Courant number should not exceed a value of 10 [WL|Delft Hydraulics, 2005]. By means of adjusting the time step the Courant number is set. For accuracy the time step should be as small as possible, however to reduce computational time a larger time step is more efficient. The Courant analysis together with sensitivity runs for some different time steps shows that a time step of 12s satisfies. Unfortunately the computational time is rather long, but it is still acceptable for this study.

Parameter settings
Most parameter settings in the FLOW and WAVE module are kept at their default value. Some parameters have been changed; their values are given in table 4-2, the default values are given in appendix F.

Table 4-2: Model parameter settings

Parameter	Value	Unit	Description
Δt	12	s	Computational time step
D_{50}	300	μm	Median sediment diameter
ρ	1025	kg/m^3	Water density
Others	Roller (Yes), Snelli (No), Gamdis(-1), Gamma(0.6), Betaro(0.05)		

Other settings of importance are the horizontal viscosity (ν_H) and the horizontal diffusivity (D_H). They are kept at their default value, though it may me worth to alter them for specific cases.

4.2.6 Sediment transport

The sediment transport model uses the sediment-online version of Delft3D. Flow and transport of sediments are computed at the same time and both are fed back for bottom updating simultaneously. In this study the sediment-online version is used in combination with the transport relation (TRANSPOR2004) formulated by Van Rijn [2004].

For the transport formulations the transport parameters as used for the Egmond model were taken [Walstra, 2004]. This model showed good results and the situation is typical for the Holland coast as it is schematized in this study. Initially the same factors, given in table 4-3, were used for this study. Finally the computations were performed with the values shown in the 3rd column (an extensive sensitivity analysis is not performed for these parameters). The parameters describe the behaviour of transport in a quantitative sense, making distinction between bed-load and suspended load transport and wave related and current related transport. Accordingly Delft3D computes the total change in sediment by summation of the change of the suspended load and the change due to bed-load [Lesser et al., 2004].

Table 4-3: Model transport parameters

	Egmond	Ter Heijde	Description
Sus	1	1	Multiplication factor for suspended sediment
Bed	1	1	Multiplication factor for bed load transport
Susw	0.2	0.1	Wave-related suspended sediment transport factor
Bedw	1	0.1	Wave-related bed-load sediment transport factor

4.3 Quasi-3D model approach

A quasi-three-dimensional model approach was chosen for this study. The reasons for this choice and a short description of the principals of this approach are treated.

4.3.1 Choice of model approach

Three different approaches can be used for FLOW computations in Delft3D [Henrotte, 2008], though not all of them are appropriate for this study:

1. Depth-averaged model approach (2DH). With depth averaged modeling (2DH) the onshore transport quantities are far overestimated, as there are no components compensating the onshore drift. For this study the 2DH approach did not give satisfactory results considering offshore bar migration.
2. Three-dimensional approach (3D). This model consists of multiple layers in the vertical water column, enabling undertow as a compensating component for the onshore drift. Offshore sediment transport will be simulated well with this approach. However, the 3D-computation times are very high, making this approach very unpractical for this study.
3. Quasi-three-dimensional approach (Q3D). A Q3D approach has a computation time that of the same order as the 2DH approach (up to a factor 6 shorter than 3D computations). Besides it is able to simulate undertow and thus offshore sediment transport. Henrotte [2008] proved for several practical cases that the offshore migration of an outer breaker bar of the Q3D model show much agreement with the 3D model results.

For the reasons mentioned above the quasi-three-dimensional approach was chosen for this study.

4.3.2 Model principals

The Q3D model solves the vertical velocity distribution in the cross-shore and longshore direction accounting for tidal forcing, wind, breaking waves and dissipation due to bottom friction [Reiniers et al, 2004].

What makes the model quasi-three-dimensional?
Q3D models of nearshore currents are developed on the basis of existing concepts of 2DH (horizontal plane) and 1DV (vertical plane) current models. The result is a combination of a depth-integrated model and a vertical profile technique. Instead of using the logarithmic velocity distribution in case of 2DH modeling, the Q3D velocity distribution is used to compute the sediment transport (equation 4-1):

$$\int_{z=a}^{z=z_t} u_{q3d}(z)c_{q3d}(z)dz = S_{q3d} \qquad (4\text{-}1)$$

In this equation the quasi-three dimensional sediment transport (S_{q3d}) is calculated by multiplying the Q3D velocity u_{q3d} by the Q3D concentration rates c_{q3d} and integrated over the vertical (from the Van Rijn reference height a near the bed to the wave trough level z_t, see figure A-3 in appendix A).

Suspended load transport is computed by solving the depth-integrated advection-diffusion equation. This means that a reference concentration profile is needed. The computed Q3D transport is divided by the depth-averaged velocity and the depth to obtain the Q3D reference concentration for suspended load computations (equation 4-2).

$$\frac{S_{q3d}}{\overline{uh}} = c_{rep,q3d} \qquad (4\text{-}2)$$

Bed load transport is computed with the Q3D velocity and concentration at the Van Rijn reference height.

In short the only difference compared with 2DH is the reference concentration and the bed-load transports. All other values are 2DH values and are not influenced by the Q3D implementation [Henrotte, 2008].

4.4 Model computations

The numerical model is used for the computation of number of hydrodynamic conditions. This has resulted in the definition of three cases for which several input variables have been defined.

4.4.1 Definition of computational cases

The quantitative values of the wave conditions are derived from the buoy data (figure 3-6). In November 2008 a storm with wave heights of 4 to 5m and with periods from 8 to 9 seconds approached the coast from the Northwest. This storm has served as for the definition of the cases in table 4-4.
Each case serves a different purpose: First the wave propagation from offshore towards the shoreface is computed. Accordingly the wave propagation inside the survey area is assessed for various circumstances. Next the wave- and tide induced flow velocities in longshore and cross-shore direction are defined. Last, an attempt is made to reproduce the morphological changes as observed in the field. In all cases, except from case 3C, storm conditions are schematized as block functions, where the storm is present from the start of the computation.

Table 4-4: Computational cases for the Q3D model runs

Case	Wave height H_s (m)	Wave period T_p (s)	Wave direction (-)	Water level NAP (m)	Duration (days)
Case 1: Wave propagation					
A	4m	9s	N, NW, W, SW	0m	-
B	4m	9s	West	-1m, +1m	-
C	4m	9s	NW / SW	-1m, +1m	-
Case 2: Flow velocities					
A	4m	9s	NW / SW	0m	-
B	0m	0s	-	-	-
Case 3: Morphological change					
A	4m	9s	N, NW, W, SW	Astronomical tide	1 day
B	1, 2, 3, 4, 5	9s	North	Astronomical tide	1 day
C	Buoy data	Buoy data	Buoy data	Astronomical tide	2 days[4]

4.4.2 Case 1: Wave propagation

Wave propagation in the offshore domain. From offshore towards shallow water (Case 1A)
Figure 4-3 shows the development of an offshore wave field coming from the Northwest (H_s=4m, T_p=9s) and traveling towards the survey area near shore. Computations of wave fields approaching from different directions show that waves from the North, Northwest and West have lost about 40% of their offshore wave height; waves from the Southwest have lost about 55% of their offshore wave height when entering the survey area (grid D). Mainly bottom friction and refraction causes the loss of energy and thus a reduction of the wave height in shoreward direction.

[4] For this case the storm on the 22nd and 23rd of November 2008 was simulated.

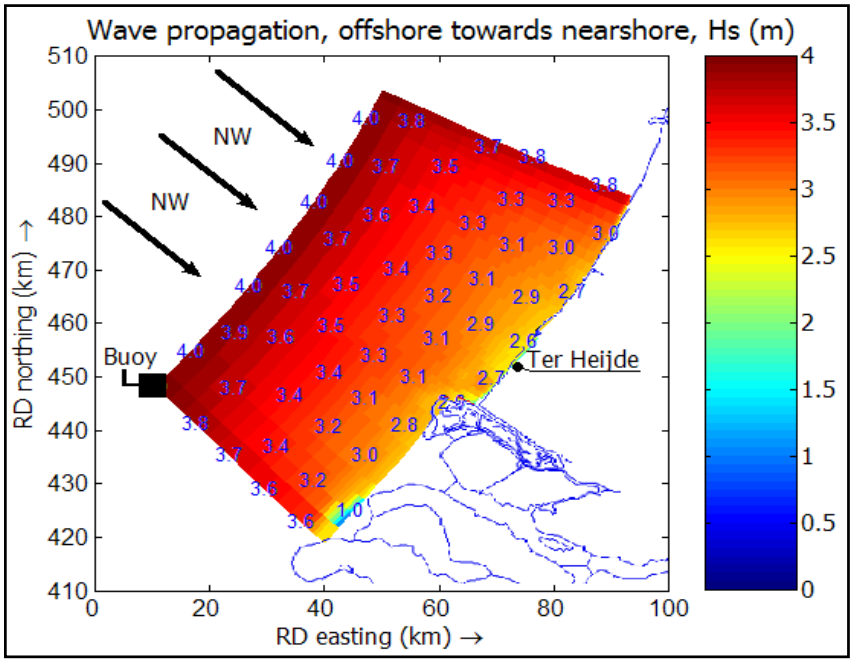

Figure 4-3: Model results: Wave propagation from offshore towards the survey area.
Case 1A:
H_s=4m (in blue)
T_p=9s
Direction = Northwest

Wave propagation near shore: Inside the survey area (Case 1B & 1C)
Figure 4-4 shows the position of the outer bar for three sections within the survey area. In the following the dissipation of energy in all three sections is discussed as well as the development of the wave height inside the survey area.

Energy dissipation
The increase of energy dissipation between 500m and 600m offshore (figure 4-5) indicates that waves break over the subtidal bar. The figure shows that the dissipation of energy is strongly related to the water level. This can be observed by considering the tidal influence (range of +/- 2m) as well as the bar crest height:
On average the bar crest in the South section of the survey area is higher than in the Middle and North sections. The water depth above the crest is only 5% to 10% higher in the South section whereas 20% more dissipation of energy is observed in South section compared to the Middle and North section.
The tidal influence on the dissipation of energy is even more outstanding. During high water conditions (dashed lines) the rate of dissipation of energy has dropped considerably compared to low water conditions (normal lines). This means that waves break more frequently over the bar during low water and thereby dissipating energy.

Wave height reduction on the shoreface
A consequence of dissipation of energy is a decrease of wave height. Figure 4-6 shows the evolution of the wave height inside the survey area. All lines correspond to an offshore wave height of 4m and a period of 9s (case 1C). Only the wave direction is different: the two upper lines (magenta) correspond to a storm from the Northwest, whereas the lower lines (cyan) correspond to a storm from the Southwest. The effect of the presence of the subtidal bar on the wave height is the most outstanding for the Northwest storm during low tide. In the other three cases the breaker function of the offshore bar is relatively small. The same relation is derived from the breaker parameter in table 4-5: for the case 1C-conditions, waves clearly break for waves from the Northwest and during low water. No breaking occurs for waves from the Southwest during high water.

This corresponds to what is expected from the breaker parameter (equation 4-3 and appendix A):

$$\gamma = \frac{H_{\max}}{h} \qquad (4\text{-}3)$$

H_{max} is the wave height where waves tend to break; h is the water depth at which that happens. In table 4-5 the breaker conditions are given for case 1C. The difference in nearshore wave height is due to the direction from which the offshore waves approach.

As a concluding remark it can be said that the water level difference of almost 2m has a significant effect on the dissipation of wave energy and thus on the breaker function of the bar.

Table 4-5: Wave breaking above the bar (for case 1C)

Direction	**Breaker parameter γ**	**Water depth h(m)**	**H_{max} (m)**	**Nearshore wave height**	**Breaking wave?**
Northwest	0.5	3m (LW)	1.5	2.5	Yes
Northwest	0.5	5m (HW)	2.5	2.5	Some
Southwest	0.5	3m (LW)	1.5	1.5	Some
Southwest	0.5	5m (HW)	2.5	1.5	No

Wave height reduction on the foreshore

Further note that on the foreshore (<200m from RSP) there is a difference in wave height evolution between waves from the Northwest and waves from the Southwest. This is due to the existence of near shore bars. Although the same cross-section is compared, the waves from the Northwest have encountered a bar in the foreshore, where they will first shoal and then break. On the other hand waves from the Southwest have not encountered that bar, their wave height reduction in the surf zone is more constant.

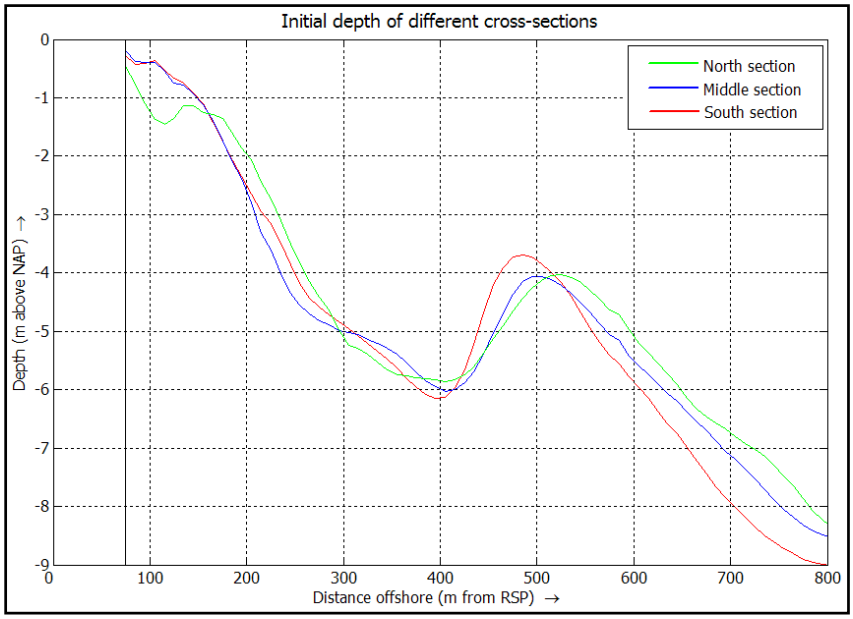

Figure 4-4: Cross-shore profiles within the survey area
(Monitored in the field)

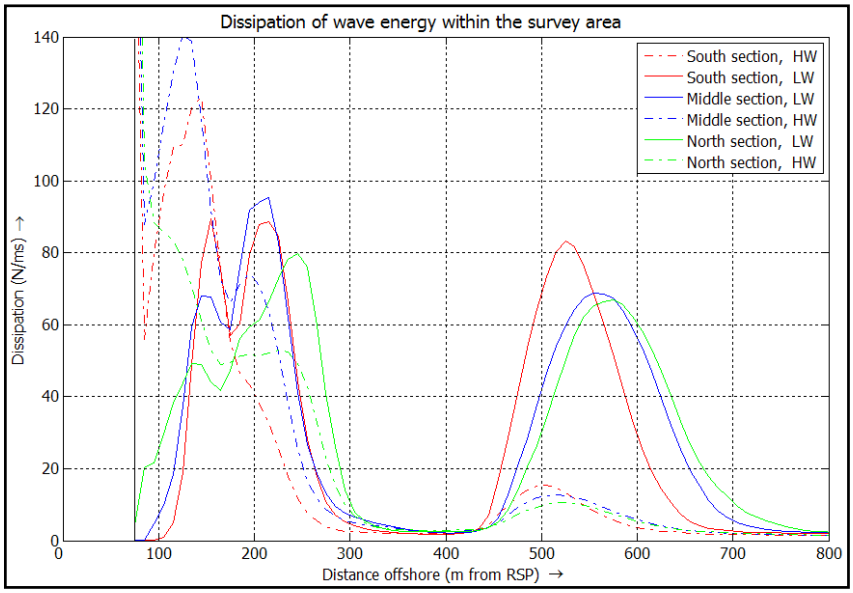

Figure 4-5: Model results: dissipation of wave energy inside the survey area.
Case 1B:
H_s=4m
T_p=9s
Direction=West

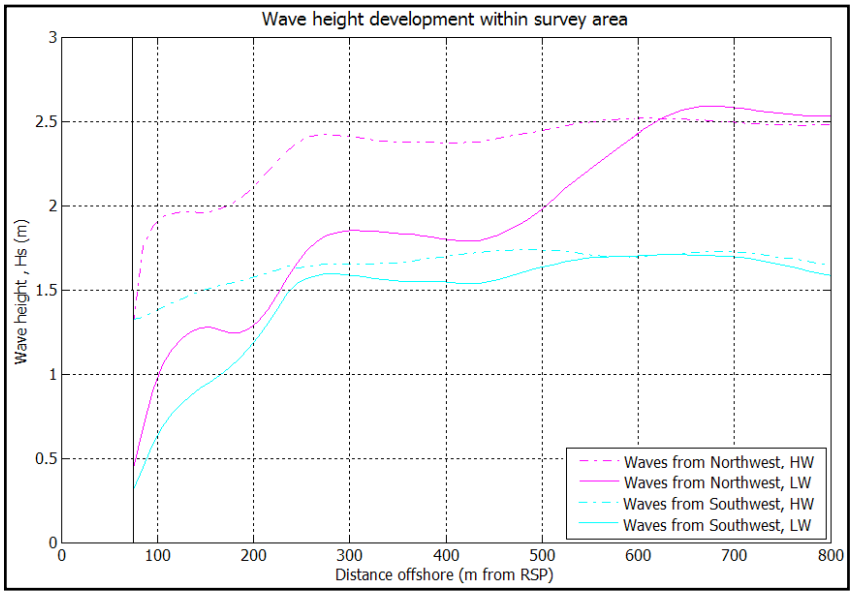

Figure 4-6: Model results: Wave height development inside the survey area
Case 1C:
H_s=4m
T_p=9s
Direction=NW / SW

4.4.3 Case 2: Flow velocities

Both tide and waves generate currents. Currents will eventually transport sediment. The objective of this case is to determine the magnitude of both flow contributions. A distinction is therefore made between tide induced currents and wave-induced currents.

Wave induced flow velocities (depth averaged)
Wave induced flow velocities inside the survey area are shown in figure 4-7. The white-colored arrows indicate the depth-averaged velocities; the color bar indicates their magnitude.
All longshore velocities are Southward directed. The largest current velocities can be found above the bar and in the foreshore, where the most wave energy is dissipated due to wave breaking.

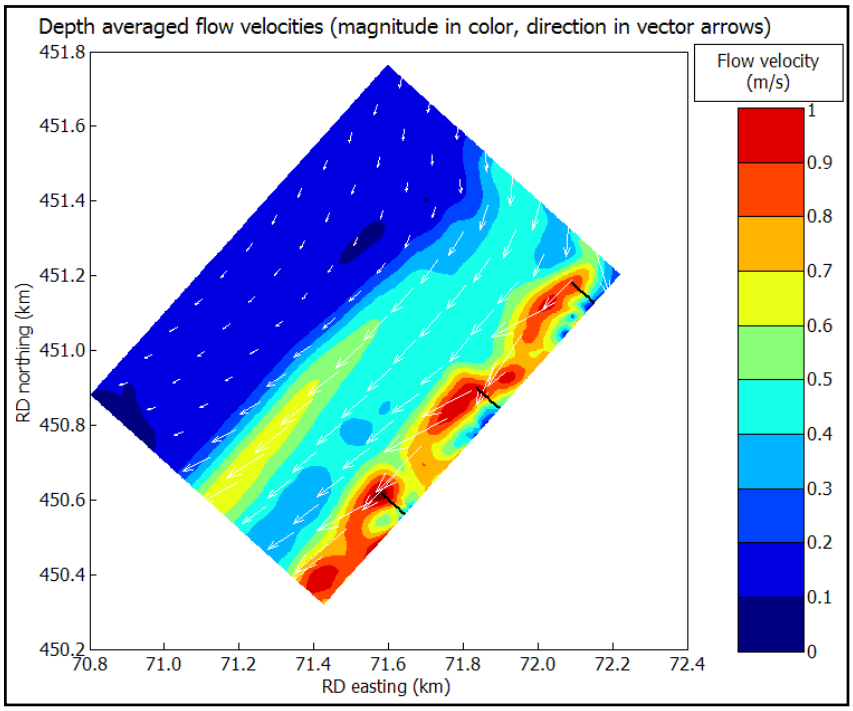

Figure 4-7: Model results: Depth averaged flow velocities
Case 2A:
H_s=4m
T_p=9s
Direction=Northwest
Water level: 0m NAP
No tidal current
Groins submerged

Wave-induced longshore currents above the bar are generally up to 0.6m/s for offshore wave heights up to 4m (from Southwest). Storms from the Northwest show the opposite behaviour; maximum longshore current velocities are up to 1.0m/s in Southward direction above the bar for offshore wave heights up to 4m (the peak longshore velocities are present during low tide).

Wave induced flow velocities (Quasi-three-dimensional)

Figure 4-8 shows the cross-shore velocity profile over the depth at a two points above the bar. An overall offshore-directed flow is observed, mainly due to undertow that is an important factor under these storm conditions (from case2A with waves from the Northwest).

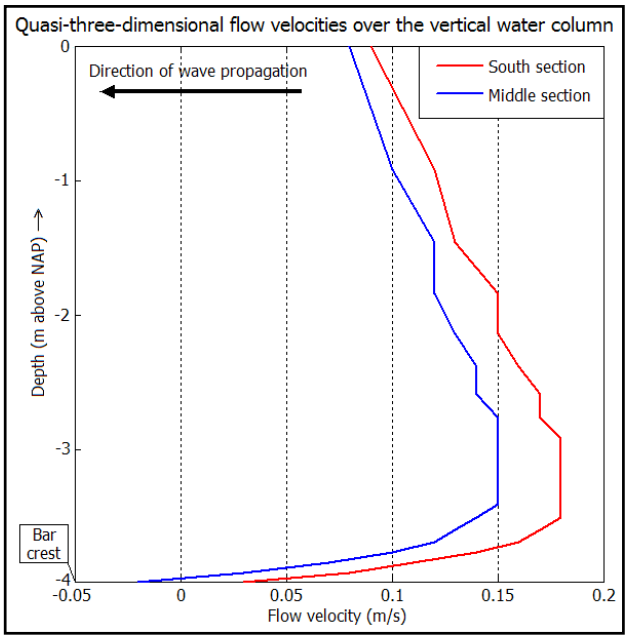

Figure 4-8: Model result: Quasi-three-dimensional cross-shore velocity profile in the vertical above the bar.
Case 2A:
H_s=4m
T_p=9s
Direction=Northwest

Tidal flow velocities

Results from case 2B show that the maximum tidal longshore current velocities (depth averaged) in the foreshore vary in the range of 0.3m/s to 0.6m/s. Storms from the Southwest strongly enhance the flood currents to the North, but reduce the ebb currents to the South whereas storms from the Northwest enhance the ebb currents to the South.

4.4.4 Case 3: Morphological behaviour

Morphological behaviour of the survey area under different wave fields is simulated. For sediment transport the online version is used that continuously updates transport of sediments. Bed level changes during the computations and feedback is given to the hydrodynamic processes.

Sedimentation and erosion

Case 3A and 3B are used to compute the sedimentation and erosion rates inside the survey area for specific wave conditions. Depending on the wave height and wave direction the magnitude and pattern of the changes varies.

<u>Wave direction dependency:</u>

The most severe erosion occurs when waves approach the shore from the Northwest and the West (figure 4-9). During those storms most sedimentation occurs on the seaside of the bar, less sediment is deposited on the landside of the bar.
During storms from the Southwest and the North the bar is eroded and sediment is spread more evenly to both the landside and the seaside of the bar.

Wave height dependency:
Figure 4-10 shows the erosion and sedimentation for different wave heights. The stronger the storm, the higher is the impact on the bottom topography. A notable observation is that a heavy storm (Case 3B with H_s=5m) moves the sediment much further offshore than calmer conditions (Case 3B with H_s≤4m).

Bar migration
As a result of the simulated storms of case 3A and 3B the bar migrates offshore and the top of the bar is flattened. Erosion of the bar crest and sedimentation on the land and seaside of the bar is observed in the simulated bottom change (figure 4-9 to 4-11). These cases contained constant storm conditions during the simulation period of a day.

Real simulated storm on the North Sea:
On the other hand, case 3C uses the real data of a storm as it was measured by the Europlatform buoy. Not the full November month was simulated, only the peak storm on the 22nd and 23rd were used for the boundary conditions (figure 3-6). The erosion and sedimentation pattern due to that storm simulation is given in figure 4-12. The figure clearly shows that the bar crest is eroded and that most sediment is deposited in the seaside of the bar, indicating offshore bar migration. Sedimentation is also observed in the trough (between the bar and the foreshore), which indicates flattening of the bar (indicated by the black arrows in the figure 4-12).

Note that there is more sedimentation and erosion on the South side of the area compared to the North side. Some differences between the South and North side were already identified: The bar is higher, the most wave energy is dissipated and the flow velocities above the bar are the highest on the South side of the survey area. Those aspects are in agreement with the simulated erosion and sedimentation pattern in figure 4-12.

Morphology of the foreshore
A clear erosion pattern around the groins and sedimentation on the seaside of the groins is observed in figure 4-12.

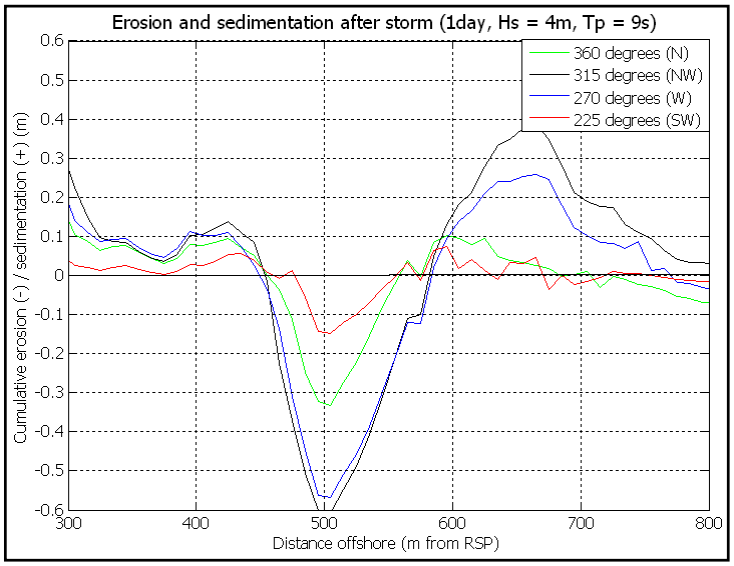

Figure 4-9: Model results: Erosion and sedimentation after storms.
Case 3A:
H_s=4m
T_p=9s
Direction=N, NW, W, SW
Duration=1 day

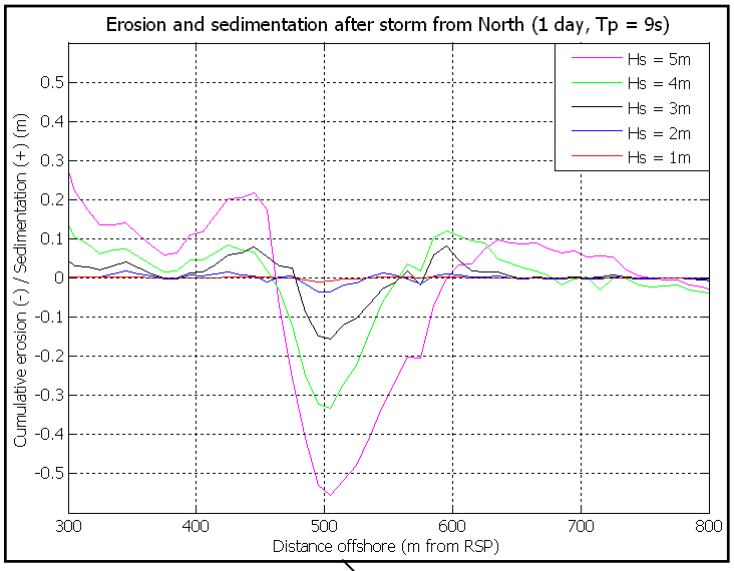

Figure 4-10: Model results: Erosion and sedimentation after storms.
Case 3B:
H_s=1, 2, 3, 4, 5m
T_p=9s
Direction=North
Duration=1 day

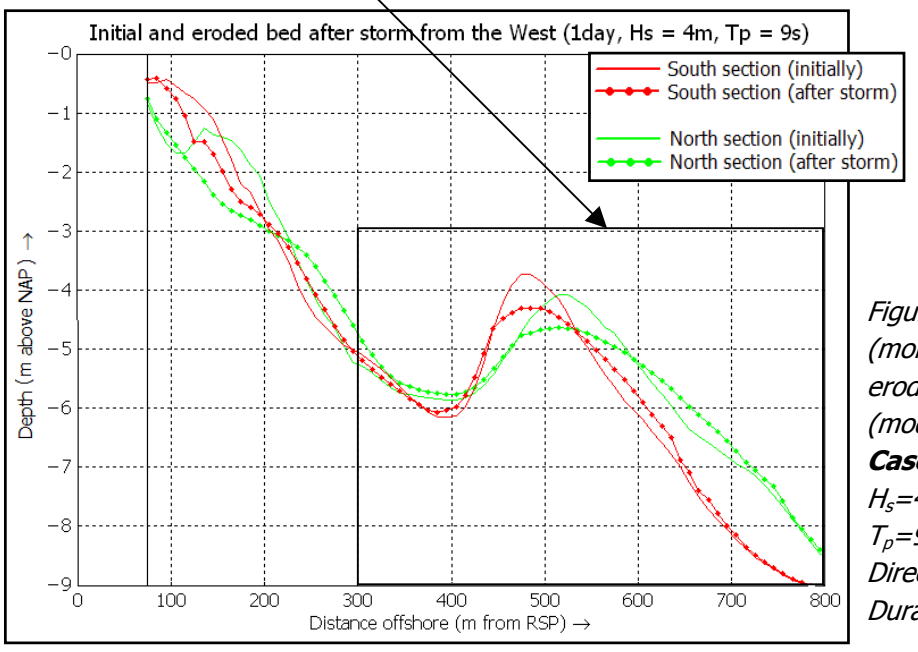

Figure 4-11: Initial bed (monitored) and eroded bed after storm (modeled)
Case 3A:
H_s=4m
T_p=9s
Direction=West
Duration=1 day

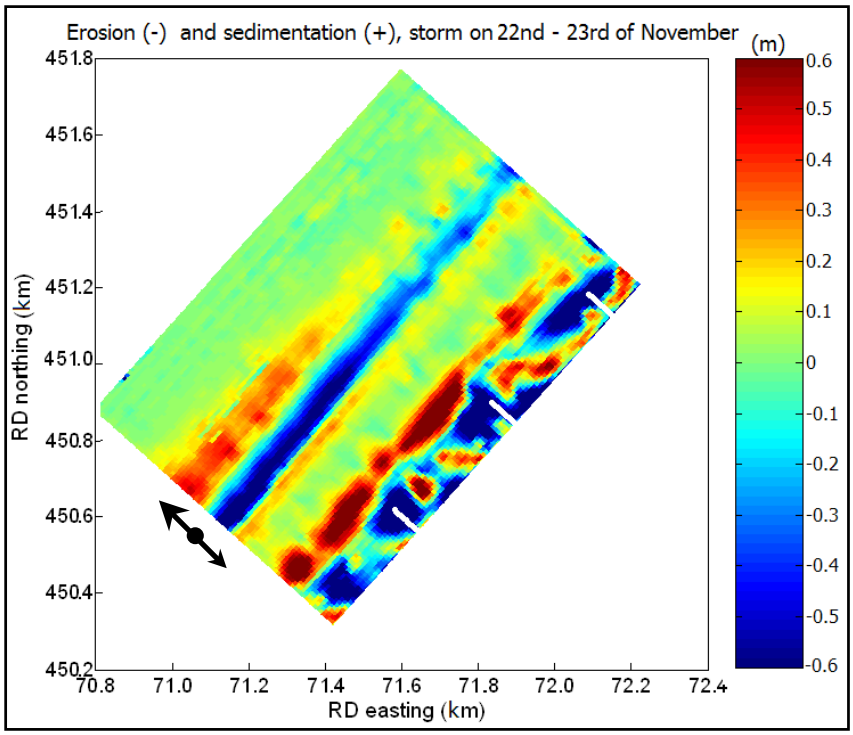

Figure 4-12: Model result: Erosion and sedimentation after storm. `

Case 3C:

Buoy data of the storm on the 22nd and 23rd of November

4.5 Conclusions

4.5.1 Conclusions

Numerical model applicability

The numerical area model Delft3D is tested for predicting coastal sand transport and morphodynamics against monitored field data. The model is useful for describing the hydrodynamic processes in the nearshore zone. Quantitative values for processes that have not been monitored in the survey area (e.g. flow velocities and wave heights) are derived from the model. Changes observed in the field can thus be related to quantitative and qualitative values of the processes that cause the morphological changes.

A simulated storm in the Quasi3D module of Delft3D does simulate offshore bar migration. The bar migrates offshore, but the bar crest is flattened considerably during a storm. Foreshore behaviour in the morphodynamic modeling gives an idea where sedimentation or erosion takes place. During a storm, erosion is mainly observed around the groins and sedimentation further seawards.

Water level dependence

The water level is an important factor concerning the energy dissipation of an offshore breaker bar. During high water the offshore bar dissipates far less energy and the wave height is not reduced so much by the presence of the bar than during low water. The water level thus influences the effectiveness of an offshore sandbar as a natural breakwater.

Morphological change

In the area where the offshore bar is higher, the most wave energy is dissipated, the flow velocities above this bar are higher and the most sediment transport takes place.

Roughly it can be said that peak tidal flood or ebb currents are increased by a factor 2 to 3 due to wave-driven processes during major storm events from Southwest or Northwest direction.

Most important aspects of the coastal modeling

In this chapter the numerical model Delft3D has been set up. The waves propagating from the deep-water buoy towards the shore are simulated. Wave propagation, wave and tide induced currents and morphological change inside the survey area are computed for several scenarios.

The model is capable of simulating offshore migration of the subtidal bar. The foreshore behaviour is highly changeable, but gives an idea where erosion and where sedimentation takes place.

5 Synthesis

5.1 Introduction

In this synthesis several aspects from previous chapters are brought together. It is analyzed to what extent the results from the field experiments (chapter 3) agree with existing theory and observations from literature (chapter 2) and results from the numerical model (chapter 4). Schematically the synthesis is set-up as shown in figure 5-1.

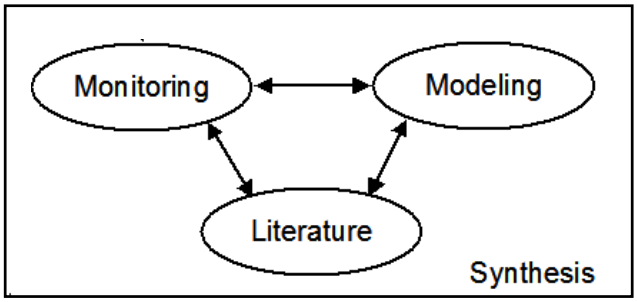

Figure 5-1: Synthesis set-up

First a recollection of the morphodynamics from these previous chapters is given.

5.1.1 Morphodynamic behaviour observed in the field

The subtidal bar migrated onshore during fair weather conditions and offshore during the stormy month (November 2008). Most sediment transport is observed where the bar is the highest.
On the foreshore near the groins the bottom topography is highly changeable. When comparing a calm period with a stormy period, an opposite pattern of erosion and sedimentation is observed.

5.1.2 Morphodynamic behaviour described in literature

Bar migration
In paragraph 2.4.4 the findings from literature stated that storm waves cause sediment to move offshore, while fair-weather waves return the sediment shoreward. Offshore-directed transport is mainly due to the generation of undertow. Net onshore-directed transport is due to the asymmetry of the near-bed orbital velocities and the generation of onshore streaming.

Morphological behaviour of the foreshore
In TAW [1995] a description is given of the effect of groins along the Dutch coast. Around low water the currents and thus the sediment transport will be blocked due to the presence of the groins. Besides, the flow is pressed in seaward direction and seaward-directed rip currents along the groins can develop.
Around high water the groins are completely submerged. In comparison with a situation without groins the flow resistance is now increased, thereby decreasing the flow velocities.

5.1.3 Morphodynamic behaviour computed by the model

Bar migration
The bar behaviour under storm conditions as computed by the model shows an overall offshore migration. Most of the sediment is deposited on the seaside of the bar after a storm situation. The bar crest however is eroded considerably and lowered by more than 0.5m after a day. The crest is very much flattened after a storm simulated by the model.

Morphological behaviour of the foreshore
During a storm, erosion is mainly observed around the groins and sedimentation further seawards.

5.2 Comparing monitoring, literature and modeling

This paragraph compares data obtained during the field experiments with theories and observations from literature and with results from the Delft3D model computations.

5.2.1 Off- and onshore bar migration

The wave conditions in figure 3-6 show a rather calm period A+B, whereas period C is dominated by storms (mainly coming from the Northwest and North).

Offshore bar migration
The field observations correspond with the expected offshore migration pattern as described in literature. The model results from chapter 4 also show offshore bar migration as a result of a storm, which is also in agreement with literature and field observations. The bar migration computed with the Delft3D model (figure 5-2) is compared to the migration as observed in the field (figure 5-3). A comparison of the sedimentation and erosion in a cross-section above the bar is shown in (figure 5-4). The model tends to flatten the bar during storm instead of shifting the bar offshore. The model results are therefore satisfying to a certain extent. When longer storms are simulated, the bar flattens more, in some cases the model computations were aborted due to high erosion rates near the groins.

Onshore bar migration
The field observations correspond with the expected onshore migration pattern as described in literature. For this study the model limitations restricted the simulation of onshore bar migration: in the first place because of the long computational time to simulate a calm weather period, in which the bar should move onshore. Secondly due to the fact that areas near the boundaries and near the groins cause the model to behave abnormally after long period calculations due to the high local erosion or sedimentation rates. All data is available to run the model this way, but first some schematizations and assumptions need to be changed. Moreover a computer that is faster than a normal PC would also be helpful for these computations.
A different type of model (e.g. the profile model UNIBEST) could also be used to describe the behaviour of the bar under these conditions. It could be found out which model suits best for this dataset.

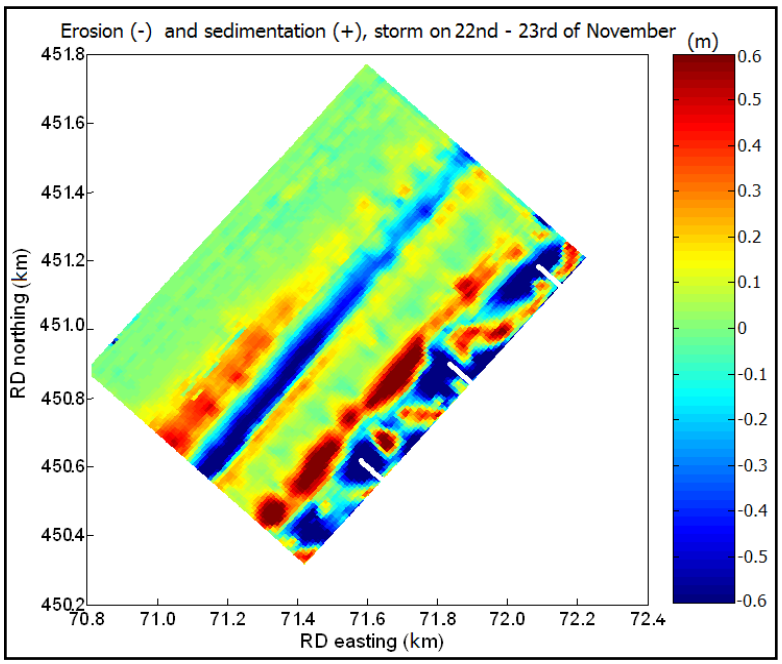

*Figure 5-2: **Model result** Erosion and sedimentation after storm on the 22nd and 23rd of November in period C (Top view)*

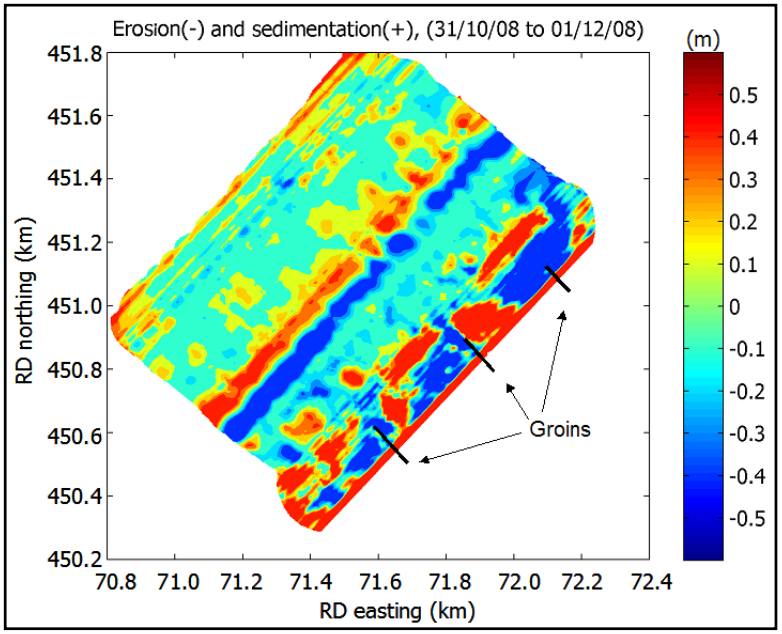

*Figure 5-3: **Monitored result** Erosion and sedimentation within period C: 31st of October until the 1st of December (Top view)*

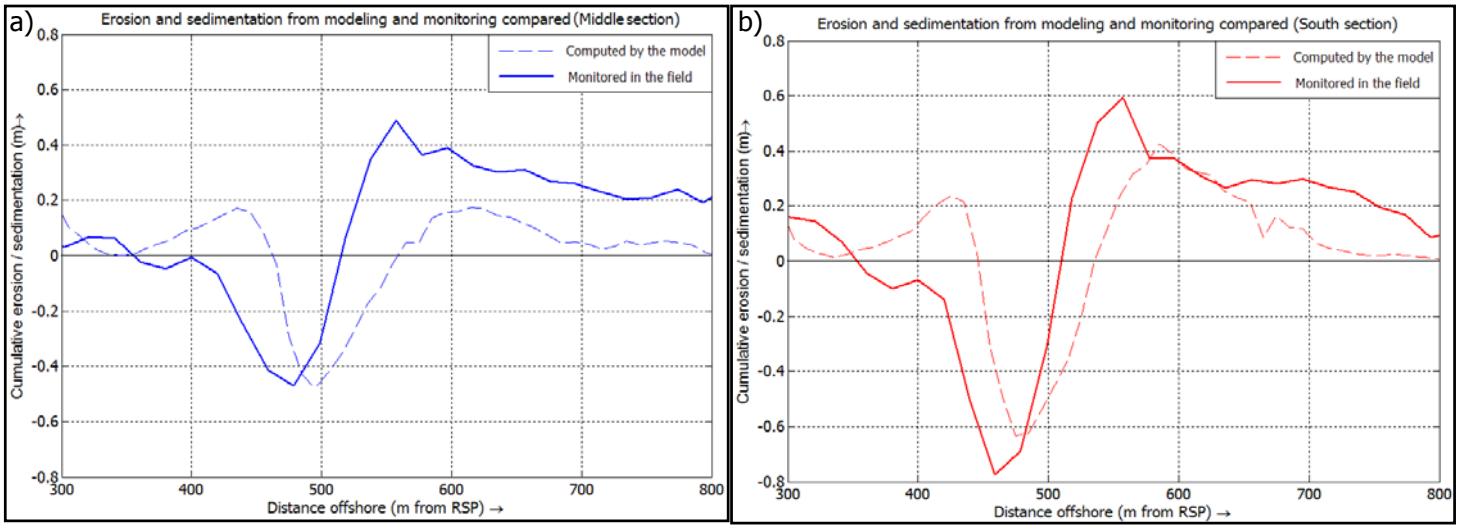

Figure 5-4: Modeled (case 3C) and monitored erosion and sedimentation (Cross-section view of the area above the bar). a) Middle section b) South section

Bar migration in relation to the incoming wave field

Figure 5-5 gives the quantity of the bar migration related to the incoming wave field from the North Sea. The blue line indicates the wave height in between the four surveys. The red and green line shows in which direction the bar has migrated in between the surveys. Only straight lines are drawn in between. In practice the bar will not have migrated linearly from one survey moment to another. The black dashed line in the figure shows how the bar in the North section may have moved within these periods. This possible line is based on the fact that on short time scales, the bar reacts directly on the incident wave conditions. Storm waves move sediment offshore whereas calm period waves gradually move sediment onshore.

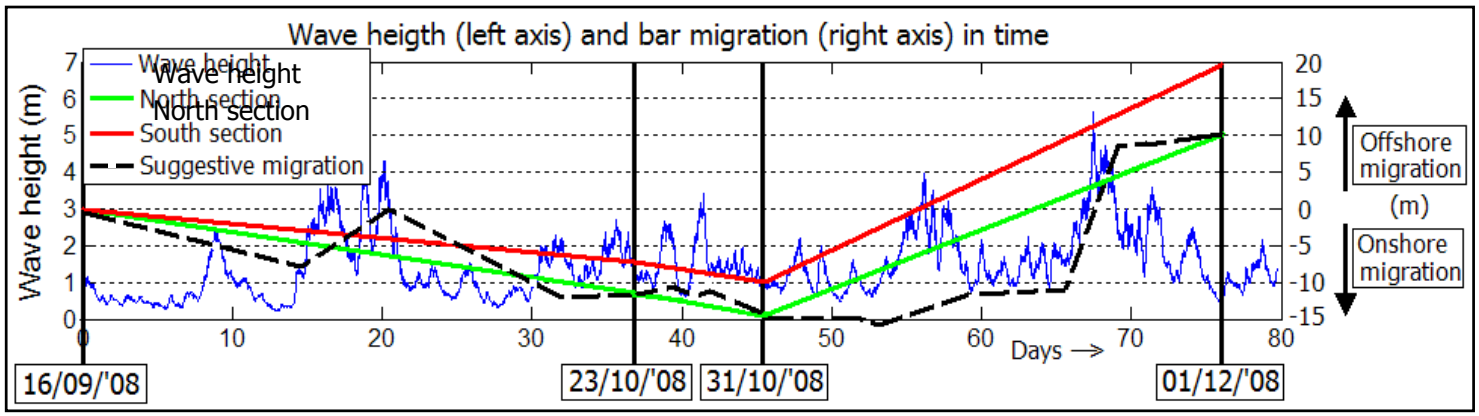

Figure 5-5: Wave height (left axis) and bar migration (right axis) in time

5.2.2 Morphological behaviour of the foreshore

Near the groins a notable opposite behaviour between the calm period A and the stormy period C was observed, as qualified in table 5-1. Some speculative remarks can be made about this foreshore behaviour. On one hand one could say that storms may move sediment locally from one place to another, whereas a calm period that follows takes care of the recovery of the storm impact. The erosion around the groins could be due to the described seaward-directed rip-current along the groins.

Table 5-1: Erosion and sedimentation of the foreshore near the groins

	Monitored	**Modeled**
Time period in between	Period C completely	November 22nd & 23rd
South of the groins	Erosion	Erosion
North of the groins	Sedimentation	Erosion/sedimentation
At the tip of the groins	Erosion	Erosion
Seaward of the foreshore (beginning of shoreface)	Sedimentation	Sedimentation

Considering the fact that the foreshore is highly changeable, it is worth looking at wave conditions in the last days of period A+B and of period C (table 5-2).

Table 5-2: Wave conditions on the days before field surveys

Last days of period	Wave height (m)	Wave period (s)	Wave direction (-)
A+B	1.5m	6s	North-Northwest
C	1-2m	5s	Southwest

The wave conditions in the week before the surveys look very similar. The only real difference is the wave direction. However, the wave height is very low and it is not likely that large amount of sand are transported during these calm conditions. The great change of the foreshore is therefore more likely due to storm impact.

5.2.3 Jetski surveys versus JARKUS measurements

JARKUS measurements are performed on a yearly basis. When considering the bar migration near Ter Heijde, the differences between successive JARKUS measurements show cross-shore movements in the order of 20 to 50 meters. JARKUS 110.34, which lies inside the survey area, has been plotted in figure 5-6 for two different years.
On the other hand Jetski surveys have been performed on a storm time scale, in practice they were performed on a monthly basis, showing the inter-annual variability. Differences between successive Jetski measurements show cross-shore movements in the order of 5 to 30 meters. Bar-migration on a yearly interval could therefore be of the same order as the storm time scale changes. Between two JARKUS profiles more morphological changes may thus have occurred than visualized. Even between two Jetski measurements morphological changes may have occurred that cannot be seen because of the interval of the measurements (as suggested by the black dash-dotted lines in figure 5-5).

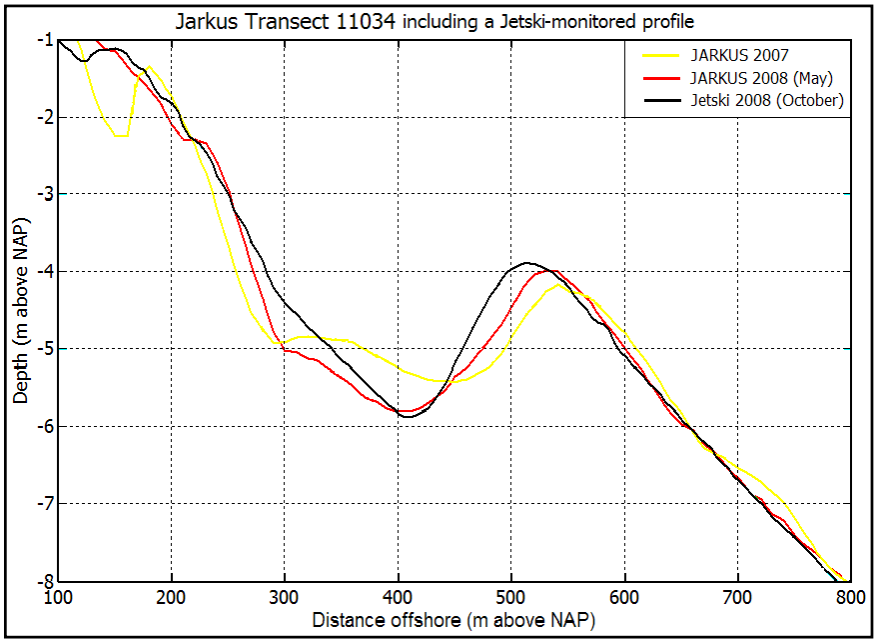

Figure 5-6: Cross-shore profiles from JARKUS, including a cross-shore profile as measured by the Jetski

5.3 Conclusions

The two and three-dimensional morphological behaviour of the nearshore sandbar system in relation to the characteristics of the incoming wave and flow field has been evaluated.

Two dimensional bar behaviour
Literature, model results and the performed field observations show that the subtidal bar off the Ter Heijde coast moves seaward during high energetic environmental conditions at sea. During calms the bar migrates in shoreward direction. These calms have not been modeled, but literature as well as the monitored field data shows this onshore movement.

Three dimensional bar behaviour
The subtidal bar is a few decimeters higher, the slope is slightly steeper and the trough is a few decimeters deeper on the Southside of the survey area compared to the North side. Storm-energy dissipation rates and flow velocities above the bar are the highest on the Southside. Since flow velocities are related to the sediment transport, there will be more transport of sediment during storm where the bar is higher.

For this study the Delft3D model is restricted to the simulation of morphological change due to a storm with a duration of maximal a few days. The storm is schematised by applying constant conditions on one hand and time-varying buoy data on the other. More agreement with the monitored morphological changes is found for the latter case.

JARKUS measurements
Bar migration resulting from successive JARKUS measurements show that the displacement of the bar observed in monthly Jetski surveys is of the same order of magnitude. Annual trends of JARKUS can thus be analysed relative to monthly trends using the Jetski measurements on a storm time scale.

Most important aspects of the synthesis
Observed morphological changes in the field are tested on their agreement with existing theory and observations from literature. Besides, the results from the numerical model are also compared to the field experiment results and to literature. All three components of the synthesis are in agreement with each other. Only the model shows results that deviate from the expected morphological change (the subtidal bar flattens more during a storm than it is expected to do).

6 Conclusions and recommendations

An overview of the most important conclusions and recommendations resulting from this study is presented in this chapter. Two aspects were present in the main objective: one regarding the survey platform and the other concerning the coastal morphological processes. More detailed conclusions can be found at the end of each separate chapter.

6.1 Survey platform

CONCLUSIONS

The quality and applicability of the TUDelft Jetski as a platform for bathymetric surveys in the coastal zone of the North Sea is assessed.

- The platform accuracy turns out to be of order 0.1m in the vertical; the horizontal accuracy is of order 0.5m.
- The small, light, fast and manoeuvrable Jetski is able to perform bathymetric measurements in the shoreface up to 1.2m water depth in the foreshore. As the crew is flexible it can perform measurements within some days before and after storm events, depending on the environmental conditions.

RECOMMENDATIONS

The vertical accuracy could be improved about half of the current value by means of the following actions:

- Install a motion sensor and filter measurements from moments where the Jetski tilts more than allowed;
- Measure the speed of sound in water more accurately;
- Improve the quality of the Single Beam Echo Sounder;
- Only include measurements from tracks sailed in landward direction;
- Only include depth measurements while sailing in a straight line.

The horizontal accuracy can also be improved considerably by installing the motion sensor and by correcting the data for the sailing direction.

Besides, it is recommended to compare the Jetski measurement with existing survey platforms (e.g. from Rijkswaterstaat) and to analyze other reference measurements. An available dataset of a survey on foot and a Jetski survey performed on the foreshore near Scheveningen shows an overlapping area. The differences between these areas provide an extra reference for the quality assessment.

6.2 Coastal morphology

CONCLUSIONS

The two and three-dimensional morphological behaviour of the nearshore bar system is related to the characteristics of the incoming wave and flow field. It turns out that:

- Storm waves move the subtidal shore-parallel bar offshore;
- Calm weather wave conditions move the bar onshore;
- More cross-shore sediment transport takes place during storm in the area where the bar is higher.

The offshore bar migration as computed by the numerical area model Delft3D is compared to the seabed evolution as monitored in the field. The results show that:

- Delft3D is capable of simulating offshore bar migration during a storm, however the model tends to flatten the bar crest much more than is observed in the field;
- The breaker function of the subtidal shore-parallel sandbar greatly depends on the water level during storm. Storm upset is therefore a very important parameter in numerical models regarding the impact of a storm on the coastal area.
- The best morphological simulation is performed for time varying wave conditions from buoy data compared to a highly schematized constant wave field.

Other conclusions that are drawn on basis of this study:

- Bar-migration monitored on a yearly interval (JARKUS) could be of the same order as changes monitored on a storm time scale.
- Annual trends of JARKUS can be analysed relative to monthly trends using the Jetski measurements on a storm time scale.

RECOMMENDATIONS

Model related recommendations:

- Longer period model runs (i.e. order of a month) with calm period wave conditions could be executed to test whether the model simulates onshore bar migration correctly. The same could be done for longer storm periods and offshore migration;
- The monitored bathymetry at Ter Heijde could be used in models where behaviour of several types of nourishments are tested on their effectiveness (e.g. on the model of Koster [2006]);
- Test whether other types of models (e.g. profile model UNIBEST) describe the behaviour of the bar under these conditions and find out which model suits best for this dataset;
- Investigate when and why the model flattens the top of the bar. Perform a sensitivity analysis to investigate the impact of input parameters on the model results.
- An interesting case study could be to include the Ter Heijde beach and dune profile in the model schematization and to simulate effect of the most extreme storm that this part of the coast needs to withstand.

Recommendations concerning coastal monitoring:

- Monitor the morphological changes of the foreshore on an even smaller time scale (of days) instead of only monthly;
- Collect data of the bar position from many periods of storms and calms. The aim would be to obtain an empirical relation between the bar migration in relation to the incoming wave field for this area.
- Appoint some representative locations along the Dutch coast that are monitored on a storm time scale (e.g. at least monthly) to observe the inter-annual coastal behaviour. When monthly monitoring is not feasible, JARKUS measurements could be performed at least twice per year. Once after the storm season and one after the calm summer season.

Bibliography

Aubrey, D., 1979. Seasonal patterns of onshore/offshore sediment movement, *Journal of Geophysical Research,* 84, 6347-6354.

Augustijn, B., Daan, J., Mourik, B., Messerschmidt, D. and Zwart B., 1990. Stormenkalender; chronologisch overzicht van alle stormen langs de Nederlandse kust voor het tijdvak 1964-1990., *Technisch Rapport, T.R.-2*, KNMI De Bilt.

Augustijn, B., and Zwart B., 1996. Stormenkalender; chronologisch overzicht van alle stormen (windkracht 8 en hoger) langs de Nederlandse kust voor het tijdvak 1990-1996, *KNMI publicatie; 176*, KNMI De Bilt.

Battjes, J.A., 2006. Developments in coastal engineering research, *Journal of Coastal Engineering,* 53(2-3), 121-132.

Davis, R.A. and Hayes M.O., 1984. What is a wave-dominated coast? *Marine Geology* 60, 313-329.

De Boer, G., 2007. SST observations of upwelling induced by tidal straining in the Rhine ROFI. *Continental shelf research,* 29(1), 1-3.

Carter, R.W.G., and Balsillie J.H., 1983. A note on the amount of wave energy transmitted over nearshore sandbars, *Earth Surface Processes and Landforms,* 8, 213-222.

CERC, 1984. Coastal engineering Research Center, Department of the Army, Waterways Experiment Station, "*Shore protection manual*".

Gallagher, E.L., Elgar S., and Guza, R.T., 1998. Observations of sand bar evolution on a natural beach, *Journal of Geophysical Research,* 103 (C2), 3203-3215.

Gallappatti, R., 1983. A depth integrated model for suspended transport, *Delft University of Technology Report* 83-7, Delft, The Netherlands.

Henrotte, J., 2008. Implementation, validation and evaluation of a Quasi-3D model in Delft3D, *Master of Science Thesis report*, Delft University of Technology.

Holthuijsen, L.H., 2007. Waves in Oceanic and Coastal waters, *Cambridge University Press.*

Koster, L., 2006. Humplike nourishing of the shoreface. A study on more efficient nourishing of the shoreface. *Master of science Thesis report*, Delft University of Technology.

Lesser, G.R., Roelvink, J.A., Van Kester, J.A.T.M., Stelling, G.S., 2004. Development and validation of a three dimensional morphological model. *Coastal Engineering,* 51: 883-915.

Mackenzie, K. V., 1981. Nine-term equation for sound speed in the ocean. *Journal of the Acoustical Society of America*, 70(3), 807-812.

MacMahan, J., 2001. Hydrographic Surveying from Personal Watercraft. *Journal of surveying engineering,* 127(1).

Orfanidis, S.J., 1996. Optimum Signal Processing. An Introduction. 2nd Edition, Prentice-Hall, Englewood Cliffs, NJ.

Plant, N.G., Holland, K.T., Puleo, J.A., 2002. Analysis of the scale errors in nearshore bathymetric data, *Marine Geology, 191*, 71-86.

Reiniers, A.J.H.M., Thornton, E.B., Stanton, T.P., and Roelvink, J.A., 2004. Vertical flow structure during Sandy Duck: observations and modeling. *Coastal Engineering* 51, 237-260.

Roelvink, J.A. and Walstra, D.J.R., 2004. Keeping it simple by using complex models. 6th International Conference on Hydroscience and Engineering (ICHE-2004), Brisbane, Australia.

Sistermans, P., and Nieuwenhuis, O., 2007. Case study: Holland Coast (The Netherlands). *Technical report, EUROSION.*

Stive, M.J.F., de Vriend, H.J., Dronker, J., van Dongeren, A. and Wang, Z.B., 2006. Coastal inlets and tidal basins, *Lecture notes*, Delft University of Technology.

Stolk, A., 1989. Zandsysteem kust- een morphologische karakterisering. Kustverdediging na 1990, *Report GEOPRO* 1989-02, Department of Physical Geography, Utrecht University, 97.

Sun, B., 2004. Verification of Hydrodynamic and Morphodynamic Modeling on a Shoreface Nourishment at Egmond, The Netherlands. *WL-report Z3624.*

TAW, 1995. Technische Adviescommissie voor Waterkeringen, Basisrapport zandige kust, Behorend bij de Leidraad Zandige Kust.

Van de Graaff, J., 2006. Coastal Morphology and Coastal Protection. *Lecture notes,* Delft University of Technology.

Van Dongeren, A.R. et al., 1995. SHORECIRC: a quasi 3-D nearshore model, *Coastal Engineering*, 3, 2741-2754.

Van Rijn, L.C., 1997. Sediment transport and budget of the central coastal zone of Holland. *Coastal Engineering,* 32(1997), 61-90.

Van Rijn, L.C., and Walstra, D.J., 2002. Basic features of morphodynamics at the Egmond site on the short-term time scale of storms, *Coast3D-Egmond*, I1-I16.

Van Rijn et al., 2002. COAST3D-Egmond. The behaviour of a straight sandy coast on the time scale of storms and seasons, *Aqua publications.*

Van Rijn, L.C., Walstra D.J.R., Van Ormondt, M., 2004. Description of TRANSPOR2004 and Implementation in Delft3D-ONLINE. *WL|Delft Hydraulics report Z3748.*

Taylor, J.R., 1999. An Introduction to Error Analysis: The Study of Uncertainties in Physical Measurements. *University Science Books.* p. 94, §4.1.

Thornton E.B., and Humiston, R.T., 1996. Bar/trough generation on a natural beach, *Journal of Geophysical Research, 101* (C5), 12097-12110.

Wackernagel, H., 2003. Multivariate Geostatistics, Springer.

Walstra, D.J.R., Roelvink, J.A. and Groeneweg, J., 2000. Calculation of wave-driven currents in a 3D mean flow model. *Coastal Engineering, 2*, ASCE, New York, 1050-1063.

Walstra, D.J.R., Van Ormondt, M., and Roelvink, J.A., 2004. Shoreface nourishment scenarios. WL|Delft *Hydraulics report Z3748.21*.

Wiegmann, N., 2002. Onderzoek naar efficiency verbetering kustlodingen Rijkswaterstaat Meetkundige Dienst, *rapport MD-GAM-2002-49.*

Wijnberg, K.M., 1995. Extracting decadal morphological behaviour from high-resolution, long-term bathymetric surveys along the Holland coast using eigenfunction analysis. *Marine Geology,* 126: 301-330.

Wright, L.D., and Short A.D., 1984. Morphodynamics variability of surf zones and beaches: a synthesis, *Marine Geology, 26,* 93-118.

WL|Delft Hydraulics, 2006. Onderwatersuppleties Ontwerprichtlijnen. *Report Z4099*.

Websites and manuals

- Actuele waterdata, 2009. www.actuelewaterdata.nl
- Dutch Cadastre, 2008. Coordinate Calculator v4.1, www.rdnap.nl
- HYPACK Hydrographic Survey Software, 2008. www.Hypack.com
- Hydrobox Hydrographic Echo Sounder, 2008. www.syqwestinc.com/hydrobox
- LNR, 2008. Globalcom GPS Reference Station – Hoek van Holland. www.lnrglobal.com
- Leica SR530 Geodetic RTK Receiver Brochure, 2001. Leica Geosystems
- MathWorks, 2005. The language of technical computing. www.mathworks .com
- Mechanics Lab Manual, 2008. Uncertainties and Error Propagation, Appendix V from the Mechanics Lab Manual, Case Western Reserve University.
- Rijkswaterstaat, 2009. Rijkswaterstaat Dienst Noordzee. www.hmc-noordzee.nl
- Waterbase, 2009. www.waterbase.nl, Ministerie van verkeer en waterstaat
- Watermarkt, 2009. www.watermarkt.nl/kustenzeebodem, Ministerie van verkeer en waterstaat
- WL|Delft Hydraulics, 2005. Delft3D-FLOW / Delft3D WAVE User manual
- Waternormalen, 2008. www.waternormalen.nl. Rijkswaterstaat, Tidal water levels
- Xsens, 2008. www.xsens.com, 3D inertial motion tracking

Appendix A Coastal Morphology

A short description derived from Van de Graaf [2006] of important processes concerning hydrodynamics and morphodynamics is given in this appendix.

Hydrodynamics
Hydrodynamics describes the motion of fluids. When waves travel from deep water into shallow water, many processes start playing a role. In shallow nearshore areas the characteristic of waves change rapidly due to the decreasing water depth and the interaction with the seabed.

Morphodynamics
Morphodynamics describes processes determining the coupled evolution of seabed topography and the wave–current field.

Refraction
When waves approach water that is gradually becoming shallower (e.g. a sandy coast), and the wave crests make an angle to the depth contours, the waves will refract. The part of the wave crest, which is already in shallower water, will travel more slowly and therefore the wave crest will bend towards the coast, diminishing the angle between the wave crest and the depth contours.
When assuming that no wave energy moves laterally along the wave crest (i.e. energy remains constant between orthogonals normal to the wave crest), the local value of the wave direction can be computed with the Snell's law (equation A-1):

$$\frac{\sin(\theta)}{c} = \text{constant along a ray} \qquad \text{(A-1)}$$

In which θ is the wave angle and c the wave celerity.

Shoaling
The sea floor will affect an approaching wave when the water depth becomes less than about half the wavelength. Near the breaker line, shoaling occurs. This means that the wave celerity and therefore the wavelength decrease due to the decreasing water depth.
Because no energy is dissipated the wave height increases. The shoaling factor k_s (equation A-2) is defined as the root of the ratio of wave celerity in deep water (c_{g0}) and wave group celerity at a certain point (c_g).

$$k_s = \left(\frac{c_{g0}}{c_g} \right)^{0.5} \qquad \text{(A-2)}$$

Wave Breaking
At a certain point, the wave height (or in some cases the steepness of the wave) becomes too high and the waves will break. In the shoreface and foreshore wave energy is finally dissipated during the wave breaking processes. Several formulations are available to compute the depth where waves tend to break. The ratio between the depth and the wave height is called the breaker parameter (equation A-3).

$$\gamma = \frac{H_{\max}}{h} \qquad \text{(A-3)}$$

The value of this parameter is generally around 0.5 meaning that waves break in water depth of approximately half their wave height.

Radiation stress

Propagating waves exert a net horizontal force. Additionally to the hydrostatic force, this force (called radiation stress) is always present when waves migrate through a body of water. However, its effect is most eminent in the nearshore zone, where relatively strong longshore currents can be generated by changes in the magnitude of the radiation stresses.
In deep water, it can be argued that this net effect will be very small (pressure fluctuations occur over a relatively small portion of the water column). Therefore, in deep water the pressure contribution to the radiation stress is often neglected.

In shallow water the pressure fluctuations due to wave action are felt over the entire water column and are even felt at the bottom, both under a wave crest and under a wave trough, hydrostatic pressures can be assumed to occur. Under these conditions the net effect over a wave period results in a net force (contribution to the radiation stress) in the direction of wave propagation equation A-4.

$$S_{xx} = \int (p + \rho u^2) dz - \int p_0 dz \qquad \text{(A-4)}$$

In which S_{xx} is defined as the radiation stress normal to the coast, p is the pressure, p_o the

$$S_{xx} = \left[\frac{1}{2} + \frac{2kh}{\sinh 2kh} \right] E \qquad \text{(A-5)}$$

hydrostatic pressure and integration is done over the vertical dz.
The magnitude of the radiation stress depends mainly on the wave height, via the wave energy (equation A-5).
In here k is the wave number, h the water depth and E the wave energy (equation A-6).

$$E = \frac{1}{8} \rho g H^2 \qquad \text{(A-6)}$$

With ρ defined as the water density and H the wave height.

Wave set-up and set-down

The magnitude of the radiation stress depends on the water depth, the wave number and the wave height (equation A-5 and A-6). If dissipation of wave energy can be neglected outside the breaker zone, then in this area the energy flux (Ec_g) is constant. With linear wave theory it can be shown that the radiation stress increases with decreasing depth in the region outside the breaker zone.

An increasing radiation stress S_{xx} in landward direction means that at a water column a resulting force is acting in seaward direction equation A-7.

$$\frac{dS_{xx}}{dx} = -\rho g (h + h') \frac{dh'}{dx} \qquad \text{(A-7)}$$

In which h' is the average water level change at point x.
Equilibrium of forces can be achieved again with a (small) difference in water level at both sides of the water column (Figure A-1). This is called wave set-down, which means that outside the breaker zone in intermediate depths, the water level at the landward side of a water column is a little lower at the seaward side.

Inside the surf zone the magnitude of the radiation stress S_{xx} decreases rapidly due to wave breaking while moving towards the coast. A resulting force is now acting in shoreward direction. To achieve equilibrium again, the water level at the landward side of the column should be higher than the water level at the seaward side resulting in a wave set-up.

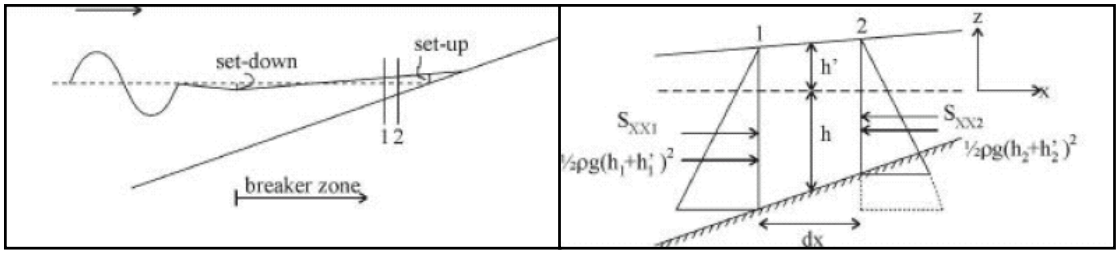

Figure A-1: Wave set-up and set-down

Longshore current

Inside the breaker zone a gradient in the radiation stress S_{yx} occurs due to changes in wave height due to wave breaking. This results in a force in longshore direction dependent on the cross-shore gradient of S_{yx}. This longshore current leads to a bottom shear stress, which counter-acts the driving force. Equilibrium is reached once the bottom shear stress equals the cross-shore gradient in S_{yx}. The longshore current depends on the angle between the wave direction and the shore. By increasing the angle, the longshore currents increases until a maximum at an angle of 45 degrees.

Cross-shore current

Breaking waves cause a net shoreward momentum transport, which results in a wave set-up shoreward of the breaker zone. Looking at a vertical plane, a mass of water transport towards the coast occurs in the part between wave crest and wave trough. In the lower part of the water column (in a two dimensional case) the same mass of water has to return seawards again. This results in a so-called undertow or return flow (Figure A-2). In case of non-breaking waves the undertow is rather small, in breaking waves the transport of momentum towards the coast may become quite large, resulting in significant undertow velocities.

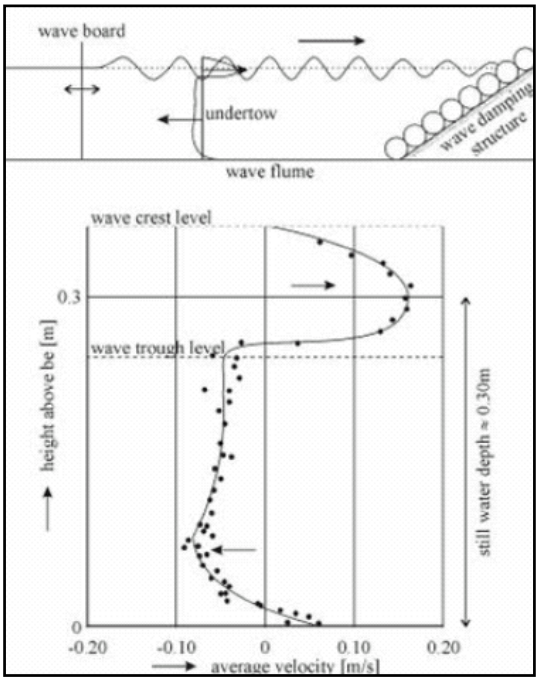

Figure A-2: Velocities under a propagating wave

Sediment transport
Sediment transport can be defined as the movement of sediment particles through a well-defined plane over a certain period of time. The transport rate depends on the characteristics of the transported material and on the forces, which induce such a transport. The primary force behind sediment transport is the bed shear stress exerted by the water motion at the bed. Sediment particles will tend to move when a certain critical bed shear stress is exceeded. The local bed shear stress can be induced by wind, wave, tide and density driven currents, by the oscillatory water motion itself (wave-related transport) or by a combination of currents and waves.

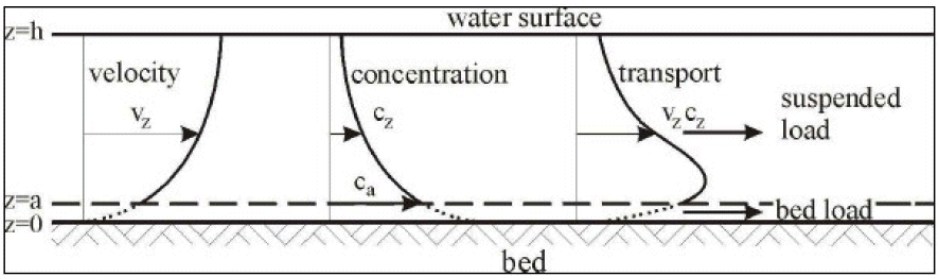

Figure A-3: Principle of (suspended) sediment transport computation

Sediment transport is generally split into two modes of transport: bed load and suspended load. To compute sediment transport it is first necessary to determine the velocity distribution *u(z)* and the sediment concentration distribution *c(z),* figure A-3.
Basically, sediment transport can be defined as a quantity of sediment that is moving with a specific velocity through a well-defined plane. The total depth-integrated transport (from bottom till surface level) at a point is defined (equation A-8):

$$\vec{S} = \int_{z=-d}^{z=\eta} c(z) \cdot \vec{u}(z) dz \qquad \text{(A-8)}$$

When considering sediment transport in the coastal zone, sediment transport normal to the coast (cross-shore transport) and sediment transport parallel to the coast (longshore transport) are distinguished. Cross-shore transport is generally caused by a combined effect of the orbital velocities in case of wave asymmetry and in case of breaking waves by the undertow. Gravity along the slope also plays a role. Longshore transport is usually caused by the longshore current that is driven by radiation stress of waves approaching under an angle.

Morphology
Sediment transport itself does not cause any changes in the topography of the coastline. Only when there are gradients in the transport rate, there will be erosion or sedimentation. Gradients in the cross-shore direction lead to a realignment of the profile. Gradients in the longshore direction will lead to systematic erosion or sedimentation along the coastline.

Appendix B Ordinary Kriging

This appendix describes the theory behind the Ordinary Kriging interpolation method used for creating bathymetric maps in this study. This method can be used for interpolation to estimate values in a regular grid using irregularly spaced data [Wackernagel, 2003].

Kriging weights

Kriging determines weights w_i for the prediction of a depth $\check{z}_0 = w_1z_1+...w_nz_n$ at location p_0, given depth observations $z_1,...,z_n$ at locations $p_1,...,p_n$ (figure B-1) and given a covariance function that returns a covariance value as a function of horizontal distance between the observations (isotropic case). First we discuss theoretical and empirical covariance functions, then we show how Kriging uses a covariance function to determine the weights in an optimal way.

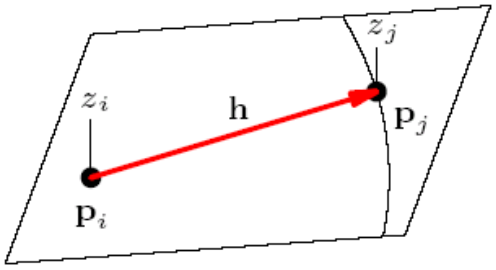

Figure B-1: Measured point and predicted point

The covariance function

The theoretical covariance function or second moment of a stationary random function $Z(x)$ is defined as $Cov(s) = E\{Z(x)-m\}\{Z(x+s)-m\}$, where $m=E\{Z(x)\}$ denotes the mean or first moment of $Z(x)$. Given some observations a discrete experimental covariance function can be determined by computing experimental covariances between any two observations and by grouping the obtained outcomes according to some distance interval. A continuous covariance function is obtained from the experimental values by fitting them into a covariance model. One can also take a covariance function that is suited to perform some special task. For example, a Gaussian covariance model without nugget effect but with a long range drops relatively slow and therefore has a smoothing effect on the data interpolation.

Ordinary Kriging

Suppose that, as above, we are given height measurements $z_1,...,z_n$ and want to predict a height $\check{z}_0 = w_1z_1+...w_nz_n$ at position (x_0, y_0). Assume moreover that we are given a covariance function $Cov(.)$ producing a covariance value C_{ij} between two positions (x_i, y_i) and (x_i, y_j). The Ordinary Kriging system consists of n+1 equations:

$$\begin{aligned} &w_1C_{i1} + w_1C_{i1} + ... + w_1C_{i1} + \mu = C_{i0} \text{ for all } i = 1,...,n \\ &w_1 + w_2 + ... + w_n = 1 \end{aligned} \qquad \text{(B-1)}$$

This implies that the weights can be found by:

$$\begin{pmatrix} w_1 \\ \vdots \\ w_n \\ \mu \end{pmatrix} = \begin{pmatrix} C_{11} & \cdots & C_{1n} & 1 \\ \vdots & \ddots & \vdots & \vdots \\ C_{n1} & \cdots & C_{nn} & 1 \\ 1 & \cdots & 1 & 0 \end{pmatrix}^{-1} \cdot \begin{pmatrix} C_{10} \\ \vdots \\ C_{1n} \\ 1 \end{pmatrix} \qquad \text{(B-2)}$$

The μ is a so-called Lagrange multiplier and is an extra variable added to make the system solvable. The Ordinary Kriging system is obtained within a random function model. This means that with every position a random variable is associated.
In the case of Ordinary Kriging it is assumed that the expected height is independent of the location and that the mean of the heights is unknown. Ordinary Kriging aims at optimizing two parameters and this optimization results in Equations (B.1) and (B.2).
First of all the expected error $r_0 = \check{z}_0 - z_0$ in the height prediction should be unbiased.
It can be shown that this condition $E\{r_0\} = 0$ leads to the equation $w_1 + \ldots + w_n = 1$. The other aim is to minimize the error variance $Var\{r_0\}$. Looking for the best solution for the weights under this condition gives the other Ordinary Kriging equations. Moreover, one obtains a formula for the error variance $\sigma^2_{prediction} = Var\{r_0\}$:

$$\sigma^2_{prediction} = \sigma^2 - \sum_{i=1}^{n} w_i C_{i0} - \mu \qquad \text{(B-3)}$$

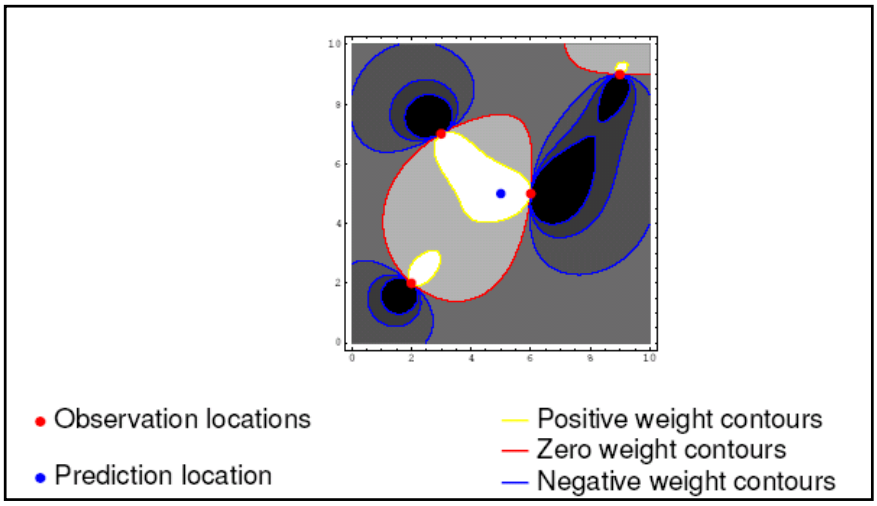

Figure B-2: Weight contours

Appendix C Occasional errors

The raw dataset shows some occasional errors that occur only in specific situations. In this appendix two types of errors are given together with an example from the dataset. Deleting part of the data filters out most errors. Filtering the data would be less time consuming and in this appendix some suggestions are given for the construction of those filters. In table C-1 the error types are given together with the depth at which they occur.

Table C-1: Types of occasional errors

Error type	SBES	GPS	Error occurs where:
1a	Sticks to one depth value	Logs normally	Depth < 1.5m
1b	Sticks to one depth value	Logs normally	Depth > 9m
2	Logs normally	No GPS signal	Any depth

C.1 Error definition and treatment

Error type 1

Error type 1a (figure C-1) occurs when below a certain depth (at least <1.5m) the SBES cannot distinguish the reflected sound pulse from the distortion in the water column (as explained in chapter 3). Error type 1b (figure C-2) could appear above some depth (at least >9m) where the Hydrobox cannot properly detect the reflected pulse from the SBES. Either the receiver cannot pick up the reflected pulse (Jetski sailing speed too high) or the sound pulse that returns to the receiver has become too weak. In these situations Hydrobox will return a constant depth value, which is not a real measured value. An error occurs when the GPS still logs its position, resulting in a GPS value that is coupled to an artificial constant depth value.

Error removal

Some ways to prevent this error may be to:

1. Manually look for these points and delete the time intervals where they occur (laborious work).
2. Delete data where at least three successive SBES values have exactly the same decimal value.
3. Change the settings in Hydrobox in such a way that no depth value will be returned when the reflected pulse is not properly detected.

Error type 2

Errors are introduced when the SBES logs normally but the GPS signal is absent or gives a wrong position. Since the GPS values are interpolated by using cubic spline interpolation these outliers may be even more exaggerated, as shown in an example (figure C-3).

Error removal

Some ways to prevent this error may be to:

1. Manually look for these intervals and delete the time intervals where they occur (laborious work).
2. Remove all depth points at times where there is no GPS position
3. Delete all GPS values that have unrealistic gradients between two successive records

C.2 Error examples

In figure C-1 to C-3 examples of the errors as discussed in this sections are shown. An overall cause of these errors occurs when the Jeski fully hits a wave. Due to abrupt accelerations of the Jetski, the GPS and the echosounder will not be able to function properly and errors of both types may occur in these situations.

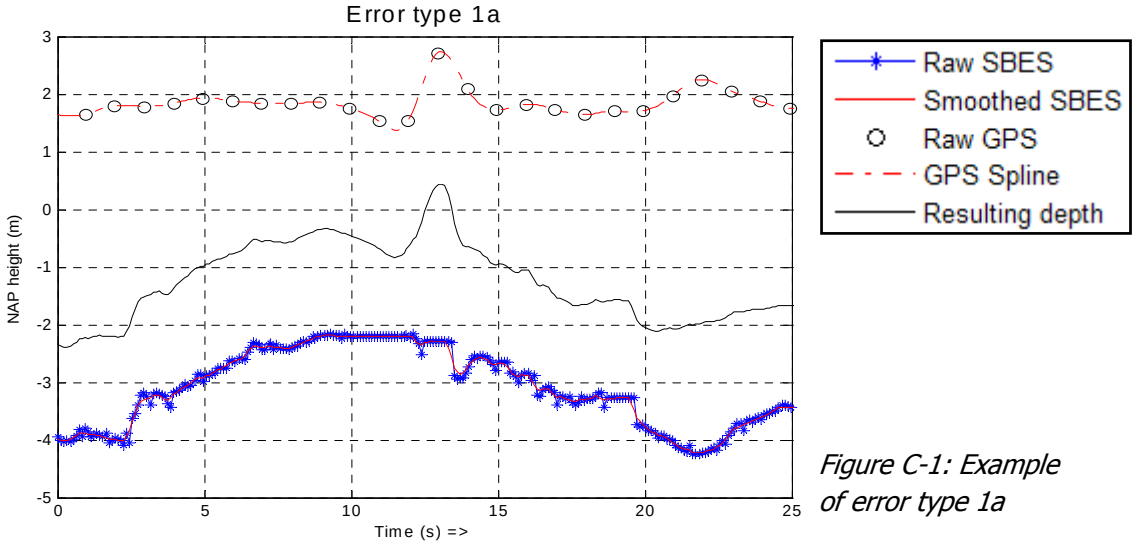

Figure C-1: Example of error type 1a

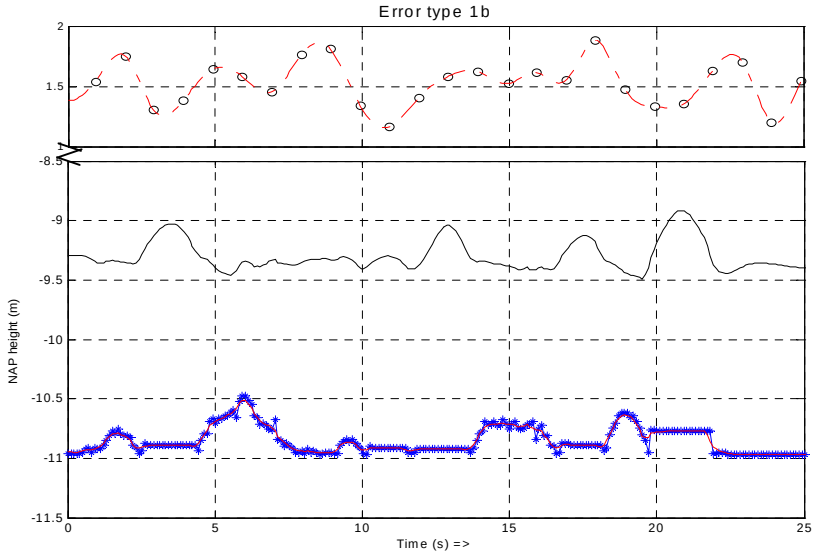

Figure C-2: Example of error type 1b

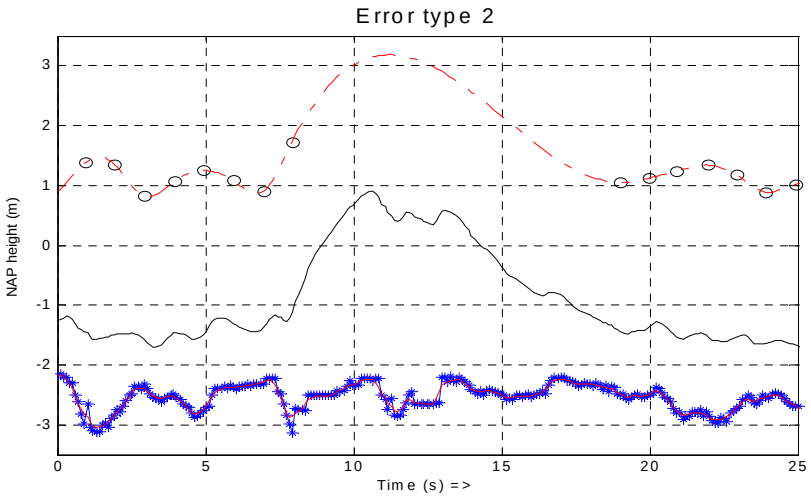

Figure C-3: Example of error type 2

Appendix D Survey data

In this chapter tables are given of data that was collected from Rijkswaterstaat on environmental conditions in the survey area. Next, the measured signals of the GPS, the SBES and the calculated seafloor position are given for several different survey conditions.

D.1 Data processing

The parameters influencing the speed of sound in water are given in the tables D-1 and D-2.

Table D-1: Salinity near Ter Heijde between September and December (1975 to 1997) Source: [Waterbase, 2009]

	Salinity near shore (ppt)	**Salinity 1km off shore (ppt)**
Mean	28.9	28.5
Standard dev.	2.1	1.8
Skewness	-1.0	-0.3
Minimum	24.0	22.8
Maximum	33.4	31.7

Table D-2: Sensitivity of the parameters contributing to the speed of sound in water

Error source	**Temperature (°C)**	**Salinity (ppt.)**	**Depth (m)**	**Speed of sound (m/s)**	**Relative error (%)**	**Absolute error (per m depth)**
Depth	15	28.5	1	1499,0		
	15	28.5	10	1499,1	0,01%	Negligible
Salinity	15	23	5	1492,5	0,36%	0,36cm
	15	28.5	5	1499,0		
	15	33	5	1504,4	0,43%	0,43cm
Temperature	14	28.5	5	1495,8	0,22%	0,22cm
	15	28.5	5	1499,1		
TOTAL						1,01cm

D.2 Measured signal

The measured signal from the GPS, the SBES and the resulting bottom derived from these signals is shown here for two different surveys: a calm day and a rougher day (see table D-3 for the details and conditions during those surveys. Next, figure D-1 to D-4 show the actual measured signal during those surveys for tracks sailed landwards as well as tracks sailed seaward.

Table D-3: Details and conditions of displayed survey-signals

Wave conditions	**Survey**	**Sailing direction**	**Figure**
Calm (H_s = 0.7m)	4 (12/01/2008)	Landward	D-1
		Seawards	D-2
Rough (H_s = 1.5m)	5 (12/12/2008)	Landward	D-3
		Seawards	D-4

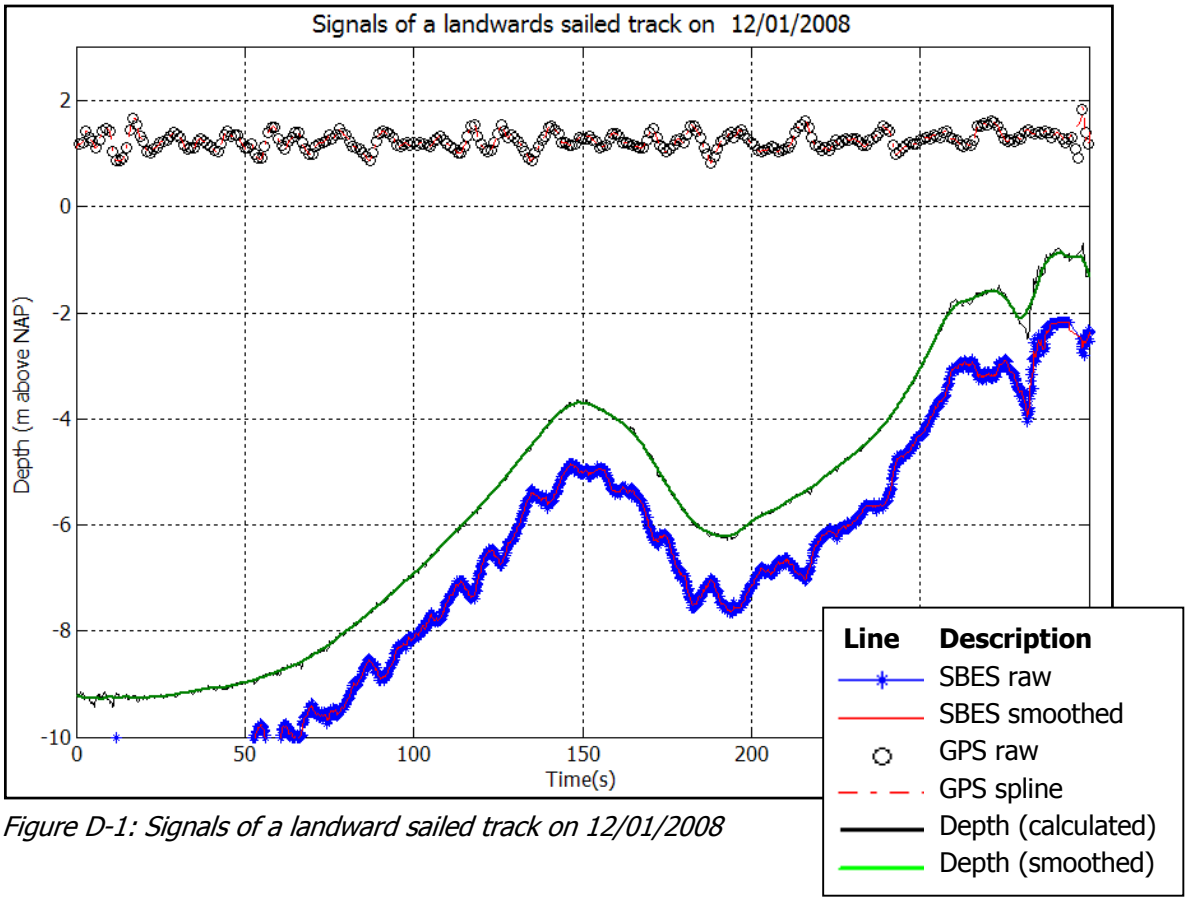

Figure D-1: Signals of a landward sailed track on 12/01/2008

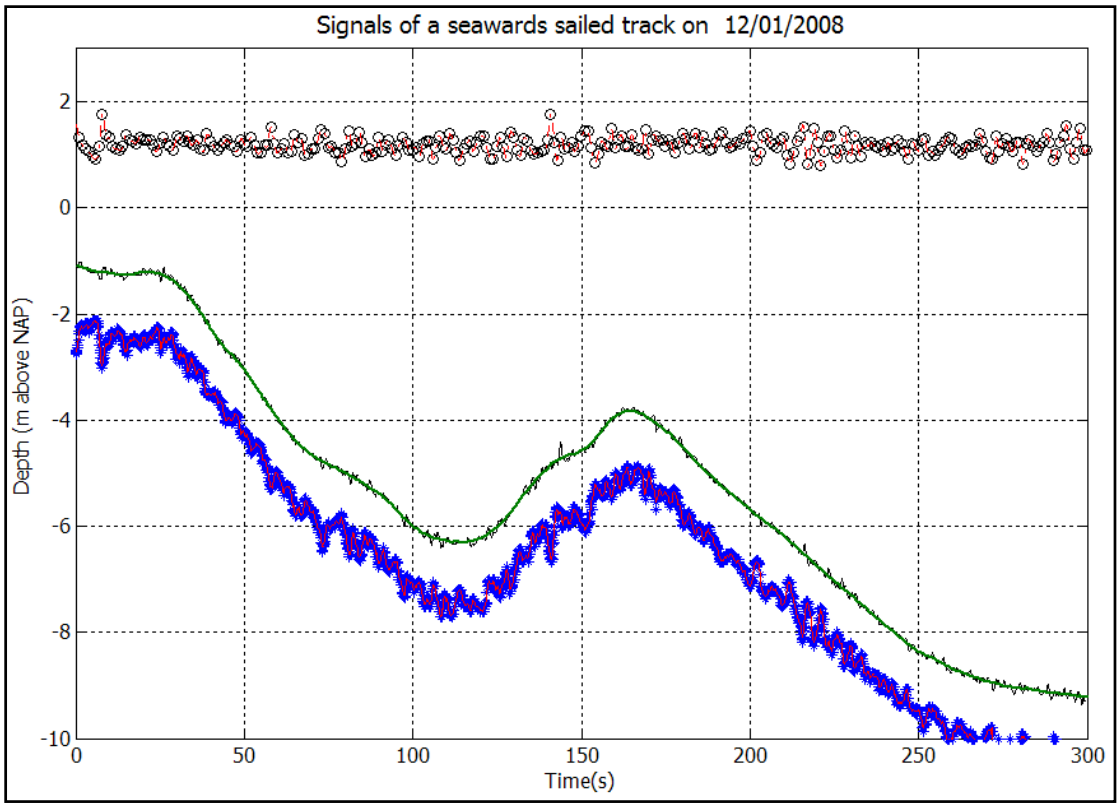

Figure D-2: Signals of a seaward sailed track on 12/01/2008

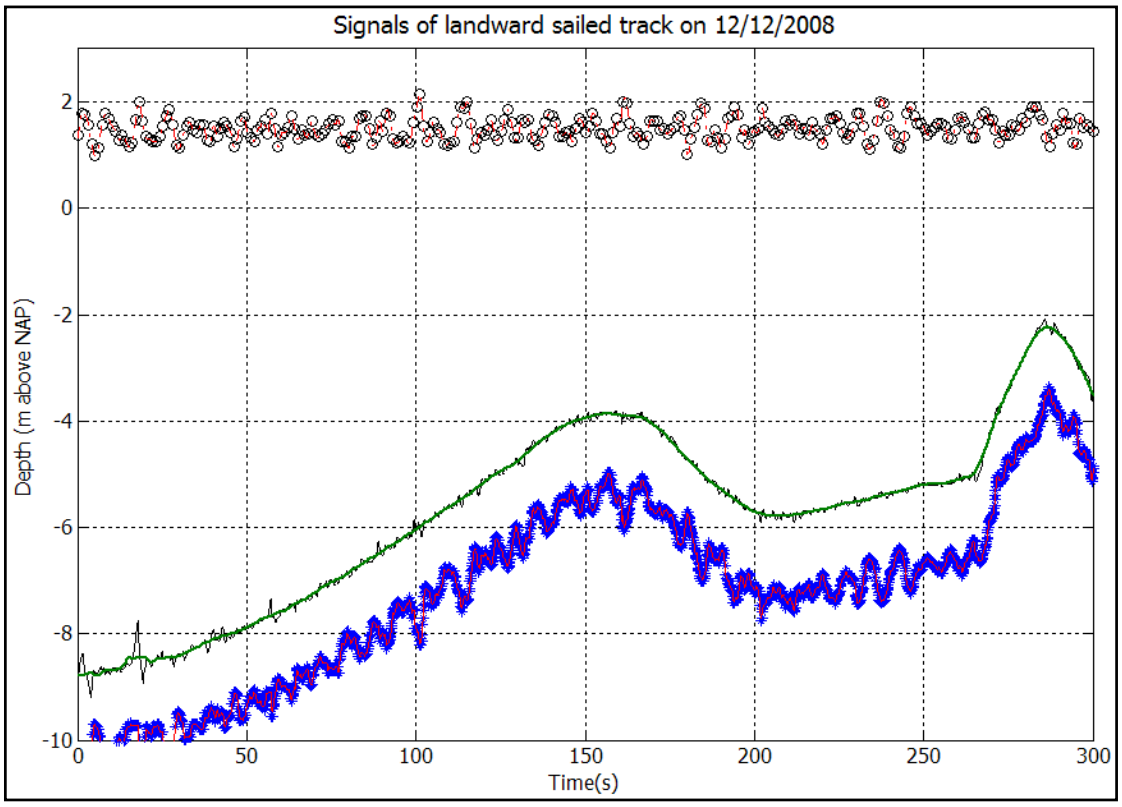

Figure D-3: Signals of a landward sailed track on 12/12/2008

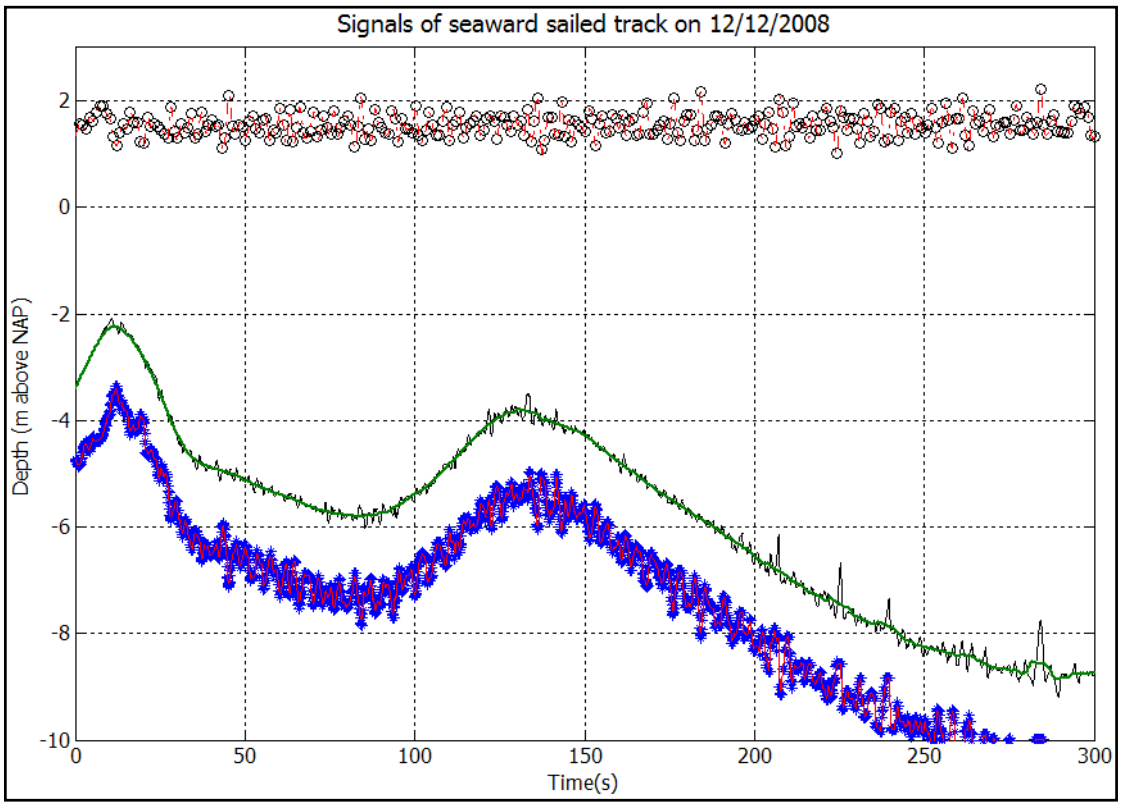

Figure D-4: Signals of a seaward sailed track on 12/12/2008

Appendix E Motion sensor data

a)

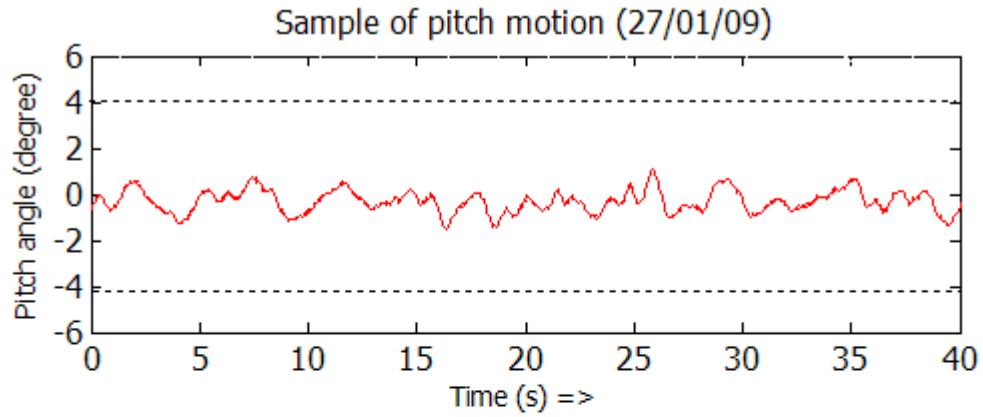

b)

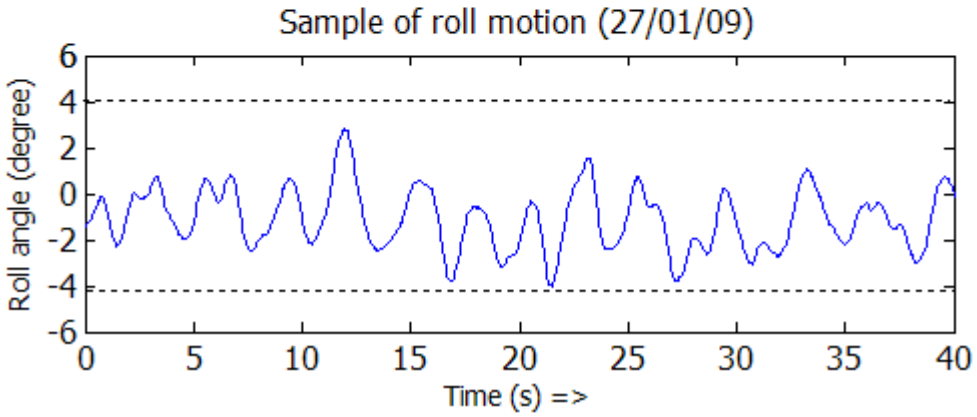

Figure E-1: Samples of platform motion, a) Pitch angle, b) Roll angle

Figure E-1 shows a short sample of the motion sensor output, obtained on the 27th of January 2009. The upper graph shows the roll motion and the lower graph the pitch motion for a 40s period in which the Jetski sailed offshore. Waves were extremely low that day (Hs<0.3m), which explains the small motions.
Some speculative remarks can be made about the obtained motion data:
At all times in the dataset the roll motion amplitude is larger than the pitch motion amplitude despite the fact that the sailing direction was perpendicular to the waves. An explanation can be found in the shape of the Jetski; First of all the length is larger than the width; secondly the rounded keel shaped does not give much resistance against the roll motion.

Both the roll and the pitch data show a signal consisting of two different frequencies. The first signal is a motion with a period that is smaller than 1s. The amplitude of this signal is in the order of a few degrees. A possible explanation (also considering experience) of this motion would be the Jetski bouncing on small wind induced waves or waves induced by the Jetski itself.
The second signal has a larger period. In this dataset the roll motion period is of order 2s, being slightly above 2s for offshore sailing and slightly below 2s for onshore sailed tracks. The pitch motion has a period of order 3s for offshore sailing and 5s for onshore sailed tracks. Altogether some remarks that can be made about the platform motion are as follow.

Pitch - Small fluctuations from small local wind waves or Jetski-induced waves (order <1s)
- Larger fluctuations showing the longer waves/swell corrected with the sailing speed
The order is a few seconds depending on wave period and sailing direction (on- or offshore).

Roll - Small fluctuations from small local wind waves or Jetski-induced waves (order <1s)
- Larger fluctuations when the Jetski moves over a wave. The order is 2s, which is about half of the relative wave period, meaning that the Jekski rolls twice while sailing over 1 wave.

The motion sensor could be used to filter or correct the SBES data that were recorded at moments where the Jetski angle exceeds a certain value. For example, if the maximum tilt angle may not exceed 4°, then all SBES values with corresponding Jetski angle above the dashed line in figure E-1 are removed. When the tilt angle of the Jetski on a certain moment is known, then a correction as given in equation E-1 can be applied. The assumption is made that the sea floor within a radius of a few meters below the Jetski is flat.

$$d = d' \cdot \cos(\varphi_{roll}) \cdot \cos(\varphi_{pitch}) \qquad \text{(E-1)}$$

Where:

d' = Measured depth

d = Corrected depth

φ = Tilt angle

Note that the tilt angle is always a combination from roll and pitch on a certain moment.

In both graphs (figure E-1) the mean angle is around zero, this is not necessarily the case for all circumstances. Note that the position of the driver and distribution of load on the Jetski can create a bias in either positive or negative roll or pitch angle.

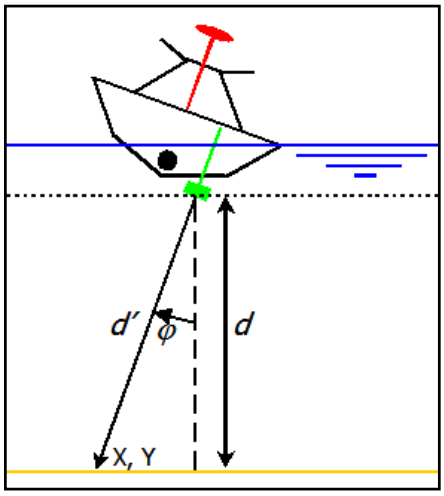

Figure E-2: Depth measurement under a 20º roll motion.

Appendix F Delft 3D

Delft3D is a process-based morphodynamic model based on a description of relevant processes like waves, tide, currents and sediment transport. Delft3D solves the Reynolds-averaged Navier-Stokes equations. This set of equations is applicable in shallow water where the length scales are much larger than the depth scales.

F.1 Model principles

Delft3D WAVE and FLOW
Two modules are used here: Delft3D FLOW and Delft3D WAVE. The former is the central module that provides the hydrodynamic basis for other Delft3D modules. Flow, transport and bottom changes are computed simultaneously. Delft3D WAVE is based on the spectral wave model SWAN and simulates the evolution of wind-generated waves in coastal waters. SWAN is a third generation wave model, using an Eulerian approach. At each location the spectral energy balance of the waves is resolved simultaneously. The model includes wave propagation, wave generation by wind, non-linear wave-wave interactions and wave energy dissipation for a given topography, wind field, water level and current field [Holthuijsen, 2007b]. The wave conditions calculated in Delft3D-WAVE are used as input for the Delft3D-FLOW module to compute wave driven currents, enhanced turbulence, bed-shear stress and stirring up by wave breaking. A more detailed description of Delft3D and the underlying formulas can be found in Lesser et al. [2004] and in the Delft3D manuals [WL|Delft Hydraulics, 2005a/b].

F.2 Default model parameters

The default parameters used in the model are given in table F-1. Table F-2 contains additional parameter settings.

Table F-1: Default parameter settings in Delft3D

Parameter	**Value**
Co-ordinate system	Cartesian
Latitude	52.02°
Computational time step	12s
Median sediment diameter	300µm
Water density	1025 kg/m^3
Horizontal eddy viscosity	0.1m^2/s
Horizontal eddy diffusivity	10m^2/s
Reference density for hindered settling	1600kg/m^3
Specific density	2650kg/m^3
Dry bed density	1600kg/m^3
Morphological scale factor	1
Spin-up interval before morphological changes	720min
Minimum depth for sediment calculation	0.1m
Van Rijn's reference height factor	1
Treshold sediment thickness	0.05m
Estimated ripple height factor	2

Factor for erosion of adjacent dry cells	0
Treshold depth	0.1m
Smooting time	60min
Store communication file	20 min
Restart interval	1440 min

Table F-2: Additional parameter settings in Delft3D

Additional parameters	**Value**	**Additional parameters**	**Value**
Cstbnd	Yes	Roller	Yes
TraFrm	Vrijn2004.frm	Snelli	No
Trtrou	Y	Gamdis	-1
Trtdef	Vrijn04.frm	Gamma	0.6
Trtu	Trtuv.inp	Betaro	0.05
Trtv	Trtuv.inp	DzMax	0.05
TrtDt	2		
Sus	1		
Bed	1		
Susw	0.1		
Bedw	0.1		

F.3 Computational procedure

The FLOW module performs the hydrodynamic computations and simultaneously ("online") calculates waves, transport of sediments and an update of the bathymetry. Figure F-1 shows a schematization of the online Delft3D approach used for this study. A communication file is written and data is exchanged after running the WAVE and FLOW computations.

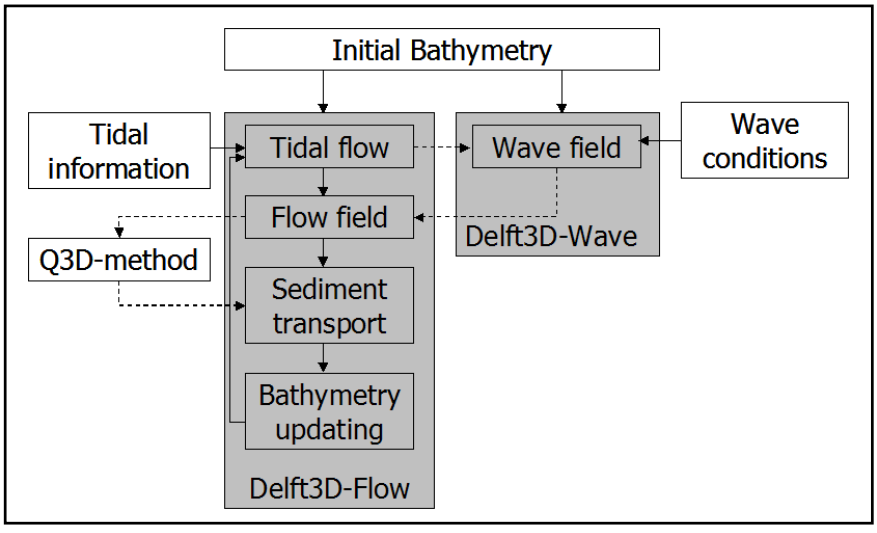

Figure F-1: Computational procedure Delft3D [Sun, 2004] with implemented Q3D mode

F.4 Q3D model principals

Sediment transport

The transport of sediment is determined with access to a variety of semi-empirical formulae and a depth integrated advection-diffusion solver for suspended sediment. The transport computation is based on time-dependent current fields.

For depth-averaged applications the 3D advection-diffusion equation is approximated by the depth-integrated advection-diffusion equation (Gallappatti, 1983), see equation F-1. The depth-averaged concentrations are computed by dividing the total sediment transport by the depth-averaged velocity and the depth.

$$\frac{\partial \overline{hc}}{\partial t} + \overline{u}\frac{\partial \overline{hc}}{\partial x} + \overline{v}\frac{\partial \overline{hc}}{\partial y} - D_H\frac{\partial^2 \overline{hc}}{\partial x^2} - D_H\frac{\partial^2 \overline{hc}}{\partial y^2} = \frac{\overline{c}_{eq} - \overline{c}}{T_s} \qquad \text{(F-1)}$$

In which h is the water depth, u and v are the velocities in x- and y- direction. D_h is the horizontal dispersion coefficient, c the sediment concentration, c_{eq} the equilibrium concentration and T_s an adaptation time scale.

Morphology

The seabed changes due to gradients in sediment transport fields. The determination of bed evolution is based on the conservation of sediment mass. Bed level changes due to bed-load transport are computed by equation F-2:

$$\frac{\partial hc}{\partial t} + (1 - \varepsilon_{por})\frac{\partial z_a}{\partial t} + \left(\frac{\partial S_x}{\partial x} + \frac{\partial S_y}{\partial y}\right) = 0 \qquad \text{(F-2)}$$

In which z_a is the bed level, S_x and S_y the sediment transport in x- and y-directions and ε_{por} the bed porosity.

Appendix G JARKUS description

Organisation

Rijkswaterstaat performs JAaRlijkse KUStmetingen (JARKUS) since 1963. Height measurements of the dunes and beaches as well as depth measurements in the nearshore zone are performed on yearly basis. By coupling both height and depth measurements a cross-shore profile of the coastal zone is constructed.

The coastal measurements comprise depth and height readings along imaginary lines perpendicular to the coast (transects). The distance between these lines is 200 to 250 meters. The complete Dutch coastline is covered by almost 2,000 lines.
Depth-sounding grids start in the foreshore and continue up to the edge of the coastal shelf, which coincides approximately with the NAP -20 meter line. The measurements are carried out in phases. The frequency of readings varies from once per year to once per six years, depending on the dynamics of the area.

The complex morphology of the coastal area requires measurements on different scales. Extra measurements produce supplementary knowledge of the processes involved, such as the behaviour of sand waves, the effect of rising sea levels and the steepening of the shoreface. Collecting such information is an additional activity to the standard monitoring program of Rijkswaterstaat.

Monitoring techniques and precision

Depth measurements are carried out annually from ships using an automatic depth-sounding system in combination with global positioning system (figure G-1). Research of the accuracy of these soundings has been performed by Wiegmann [2002]. The resulting precision of the sea floor height relative to NAP is 0.14m for multi-beam echo sounder (MBES) measurement and 0.34m for single beam (SBES) measurements.
Height measurements of the beach and dunes are carried out every second year using laser altimetry.
Depth measurements are performed during high water whereas height measurements are performed during low water. This method gives the most complete profile along a direction-line. By post-processing, the direction-line data from the depth-soundings are interpolated towards an area-covering grid containing 20m x 20m cells.

Use of JARKUS data

For each transect the so-called Momentary Coastline (MKL) and the Test Coastline (TKL) are calculated. Both are compared with the Basal Coastline (BKL). An interpretation of the outcome is used to decide where supplementary sand is needed.

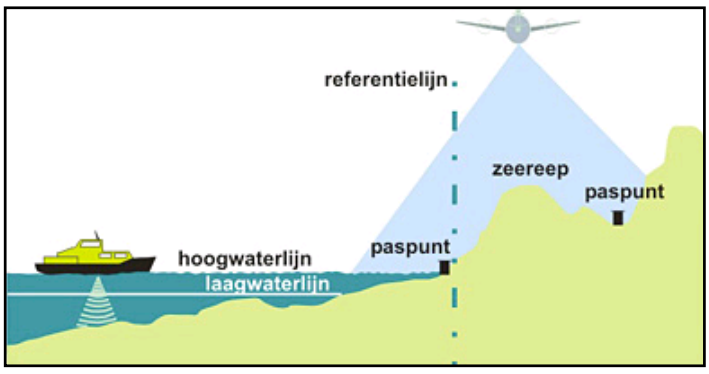

Figure G-1: JARKUS height and depth measurements, source: Rijkswaterstaat